THE QUADRUPOLAR INTERACTION IN VANADIUM-OXYGEN COMPOUNDS

A STUDY OF THE QUADRUPOLAR INTERACTION

IN

IN VANADIUM OXYGEN COMPOUNDS

By

SHAUL DAVID GORNOSTANSKY, B.Sc.

A Thesis

Submitted to the Faculty of Graduate Studies

in Partial Fulfilment of the Requirements

for the Degree

Doctor of Philosophy

McMaster University

May 1968

DOCTOR OF PHILOSOPHY (1968)
(Physics)

McMASTER UNIVERSITY
Hamilton, Ontario.

TITLE: A Study of the Quadrupolar Interaction in Vanadium-Oxygen Compounds

AUTHOR: Shaul David Gornostansky, B.Sc. (Bar-Ilan Univ.)

SUPERVISOR: Dr. C. V. Stager

NUMBER OF PAGES: viii, 147

SCOPE AND CONTENTS:

Pentavalent vanadium, in vanadium-oxygen compounds, shows a large variety of structures for the nearest neighbour environment of the vanadium ion. Properties of the charge distribution in this environment were studied by observing the nuclear magnetic resonance of the V^{51} nucleus. In addition, a point multipole model and a covalent model were used to correlate the experimental results with bond parameters.

ABSTRACT

The quadrupolar interaction in sodium orthovanadate dodecahydrate, calcium orthovanadate, vanadinite, descloizite, zirconium divanadate, cadmium divanadate, potassium metavanadate and vanadium pentoxide, was studied by nuclear magnetic resonance. The V^{51} quadrupole coupling constants in these compounds show a strong correlation with the distortion of the tetrahedral symmetry around the vanadium ion. Vanadium pentoxide is an exception and shows a surprisingly small coupling constant. The point multipole model was found to be inadequate for the calculations of the electric field gradients in these compounds. A covalent model provides an explanation of the small magnitude of the coupling constant of vanadium pentoxide. However, because of the numbers of approximations in this model, only a qualitative correlation with the experimental results was achieved. In addition, the chemical shift tensor of the V^{51} resonance line in a single crystal of vanadium pentoxide was measured to be very large. This result was correlated with a large Van Vleck term in the magnetic susceptibility of vanadium pentoxide.

ACKNOWLEDGEMENTS

Dedicated to Limor and Sagiv

I express my deep appreciation to my supervisor, Dr. C. V. Stager, for his continued guidance and patience. I want also to thank Dr. C. Calvo for stimulating discussions and his valuable help in orienting the crystals.

I want to thank my fellow students, Mr. R. Atkinson, Mr. Z. Melkvi and Mr. C. Fowlis for their help in the laboratory.

I am most grateful to the Government of Ontario for the award of an Ontario Graduate Fellowship and to the Defence Research Board for their financial support of this project.

Mrs. H. Kennelly has typed this work in a record breaking time.

My deepest appreciation is given to my parents, who always taught me how sweet it is to learn and to know.

Last, but not least, I thank my wife, Sara, for her patience, love and encouragement. Without it, this work could not have been finished.

TABLE OF CONTENTS

LIST OF FIGURES

LIST OF FIGURES (continued)

LIST OF TABLES

CHAPTER I

INTRODUCTION

This thesis is divided into six chapters. Chapter I summarizes previous work about the interpretation of the quadrupolar interaction in crystals and the correlation with different models for the charge distribution. In addition, this chapter includes reasons for studying vanadium oxygen compounds in general, and the particular compounds that were studied in this work. Also included, in tabular form, are some of the crystallographic data available on these compounds. Chapter II gives the theory of the quadrupolar interaction in crystals and discusses the two models that were used in this work. Also included is a discussion on chemical shifts. Chapter III gives the preparation of the samples and the methods by which the data were obtained. Chapter IV gives the results of the experiments and the calculations. Chapters V and VI contain, respectively, a discussion of the results and the conclusions.

Nuclear magnetic resonance techniques are very useful for studying structural and bonding aspects of the solid state. In particular nuclear magnetic resonance can be used to study internal electric and magnetic fields at the site of

various nuclei in different compounds. Although much information can be obtained from a polycrystalline sample, a single crystal is preferable because it permits the determination of many more parameters. In this work the additional parameters are the anisotropy of the quadrupole coupling and chemical shift tensors and the orientation of the principal axes. The principal axes define the co-ordinate system in which the tensor is diagonal.

The quadrupole coupling tensor and the chemical shift tensor are symmetric second rank tensors. The number of independent components depends on the point symmetry group at the site of the nucleus. The quadrupole coupling tensor is traceless and therefore has one less independent component than a general symmetric second rank tensor. If the point group contains a three or four fold axis, the second rank tensor is said to be in axial symmetry and the number of independent components is two. If the point group is cubic, the number of independent components is one. For any other point group the number of independent components is three.

The orientation of some or all of the principal axes is often determined by symmetry. If the point group contains a two or three fold rotation axis, one of the principal axes is constrained to be along the rotation axis. If the point group contains a mirror plane, one of the principal axes is perpendicular to the mirror plane.

Equivalent sites in a crystal are those sites that

are related by a symmetry operation of the space group. The tensor properties of equivalent sites are identical, but the principal axes are not necessarily parallel. However, they are related by the symmetry element. The nuclear magnetic resonance spectra depend on the orientation of the magnetic field relative to the principal axes. Therefore in an external magnetic field two crystallographically equivalent sites can give rise to inequivalent spectra. However, the spectra are related by the symmetry element that relates the equivalent sites. Crystallographically equivalent sites that give rise to inequivalent spectra in the presence of a magnetic field are called magnetic sites.

The quadrupolar interaction is an electric interaction between the nucleus and the charge distribution of the environment. This interaction can be written as $\bar{Q}.\bar{\bar{\nabla E}}$, which is the scalar product between $\bar{Q}$, the quadrupole tensor of the nucleus, and $\bar{\bar{\nabla E}}$, the electric field gradient tensor at the nuclear site caused by the charge distribution of the nuclear environment.

Early studies of the quadrupole resonance interaction were done by Pound[1,2] in the U.S.A. and by Dehmlet and Kruger[3,4] in Europe. However they limited their studies to crystals having nuclei in environments with axial symmetry. Carr and Kikuchi[5] derived the angular dependence of the quadrupolar energy for crystals having nuclei in such an environment. Volkoff, Petch and Smellie[6]

generalized these results to crystals having nuclei in an environment of arbitrary symmetry, but discussed only the first order effect. This effect comes from treating the quadrupolar interaction by perturbation theory and taking only the first term. Bersohn[7] gave the general expression for the quadrupolar interaction in crystals having nuclei in an environment of arbitrary symmetry, but did not give explicit expressions for the angular dependence of the interaction. Volkoff[8] used Bersohn's results to obtain explicit expressions for the angular dependence of the first and second order terms of the interaction energy. Petch, Cranna and Volkoff[9] analyzed the spectra of Spodumene using these expressions.

The quadrupolar interaction in a crystal depends on the field gradient at the nuclear site, which in turn depends on the charge distribution around the nucleus. Therefore, a study of the quadrupolar interaction in a crystal should provide valuable information about the bonding of the crystal. Townes and Dailey[10] derived an analytical expression for the quadrupole coupling constant of an atom in a diatomic molecule, with an unfilled p-shell, in terms of the free atom quadrupole coupling constant, the coefficients of the orbitals in the hybridized wavefunctions and the ionic character. The ionic character, in turn, was related[11] to the electronegativity difference between the two constituents of the molecule. Although

this theory can only be applied directly to diatomic molecules, much data that was obtained for polyatomic molecules was interpreted by an extension of the Townes and Dailey theory[12-15].

Another way of interpreting the experimental data was suggested by Bersohn[16]. He used a point charge model, in which every ion is considered as a point charge for the purpose of calculating the electric field gradient, but with effective charges on the ions, as opposed to the formal valence charges. He then derived an expression for the quadrupole coupling constant caused by these effective charges. His results confirmed Pauling's charge neutrality principal[17].

Sharma and Das[18] tried to improve Bersohn's calculations by allowing the charges to spread in space, but not to overlap. In first order this is equivalent to the inclusion of contributions to the field gradient tensor from electric dipole moments situated at the site of the point charges. They showed that these contributions, in the spirit of Bersohn's model, are quite important and can not be neglected, particularly if highly polarizable ions are situated at sites that do not have inversion symmetry.

The chemical shift is a shift in the resonance field caused by a magnetic coupling of the electrons to the nucleus. The magnetic fields, originating from the motion of the electrons, give rise to the chemical shift. The

total magnetic field at the nuclear site can be written as $H = H_o + \Delta H$, where H_o is the applied magnetic field and ΔH is the internal magnetic field which represents the interaction between the electrons and the nucleus. ΔH can be written as $\Delta H = -\sigma \cdot H_o$ where σ is called the chemical shift tensor.

Ramsey[19-22], in an effort to explain the chemical shift tensor, considered the vector potential at the electron site caused by an external magnetic field and the magnetic moment of the nucleus. This vector potential was substituted into the Hamiltonian, and by applying perturbation theory, it was shown that there is an induced magnetic field which is proportional to the applied magnetic field. This proportionality is expressed as the chemical shift tensor and is the sum of two parts. One is the isotropic diamagnetic term which is the analog of Lenz's Law and the second part is an anisotropic paramagnetic term which arises from the external field mixing a paramagnetic excited state into the diamagnetic ground state. He also showed that electrons which are tightly bound to distant nuclei make a very small contribution to the chemical shift. For these distant electrons the diamagnetic and paramagnetic terms almost cancel one another.

The two contributions discussed above are temperature independent if there is no paramagnetic excited state within kT of the ground state. Ramsey's theory was

applied successfully to the study of the chemical shift of the F^{19} resonance line in different compounds[23,24]. The wavefunction that was chosen for the molecule was a linear combination of atomic orbitals. However, in calculating the matrix elements in Ramsey's theory only local contributions were included, i.e. contributions from the fluorine electrons. Bramey et al.[25] argued recently that nonlocal contributions must be included in calculations of the chemical shift of nuclei in compounds containing transition metal ions.

The anisotropy of the chemical shift tensor has been studied by many workers[26-28], but the only single crystal study of the chemical shift tensor was reported by Lauterbur[29]. This was a study of the chemical shift tensor of the C^{13} resonance line in calcite ($CaCO_3$) relative to the C^{13} resonance line in an aqueous solution of potassium carbonate.

A study of the anisotropy of the chemical shift tensor can be correlated with a study of the anisotropy of the Van Vleck term in the magnetic susceptibility[30]. Both involve an external magnetic field mixing a paramagnetic excited state into the diamagnetic ground state through second order perturbation theory.

Vanadium compounds are especially interesting for a nuclear magnetic resonance study. V^{51} has a spin of 7/2 and therefore, a non-vanishing electric quadrupole moment.

A value of -0.05 barns[31] has been recently determined as the quadrupole moment of V^{51}. In a magnetic field of 10 KG, the resonance frequency is approximately 11.2 MHz.

Pentavalent vanadium in the presence of oxygen shows a large variety of structures for the near neighbour environment of the vanadium ion. For example[32], if vanadium pentoxide is dissolved into a solution of potassium hydroxide, the precipitated compound depends on the pH of the solution. With high pH, the precipitated compound is an orthovanadate. By lowering the pH one gets the divanadate. Further lowering of the pH results in precipitation of the hydrated and anhydrous metavanadate. A further lowering of the pH will result in further condensation of the vanadate anions into higher molecular weight polyanions.

The orthovanadates probably have discrete VO_4^{3-} groups with nearly tetrahedral symmetry. Nearly tetrahedral coordination is also found among the near neighbour oxygen atoms of the vanadium ion in the divanadates. However, these VO_4 groups are not discrete, as two VO_4 groups share one oxygen to form a $V_2O_7^{4-}$ group.

In the anhydrous metavanadates, there is also a tetrahedral coordination of oxygens around the vanadium ion. However, the VO_4 groups share two oxygens to form a

continuous chain through the crystal.

The four fold tetrahedral oxygen coordination which appears to be characteristic of the orthovanadates, divanadates and the anhydrous metavanadates, becomes a five fold trigonal bipyramid in the hydrated metavanadates and vanadium pentoxide. Again the VO_5 groups are not discrete but share a corner oxygen and an edge of the trigonal bipyramid to form a continuous sheet through the crystal.

The only reported values of quadrupole coupling constants of orthovanadates are the vanadium and sodium quadrupole coupling constants in sodium orthovanadate tesseradecahydrate[33]. The data were obtained from a polycrystalline sample and the reported values are 3.1 MHz and 0.32 MHz respectively. The only reported value of quadrupole coupling constants of a divanadate are those of vanadium and sodium in a polycrystalline sample of hydrated sodium divanadate[33]. The reported values are 3.1 MHz and 0.75 MHz respectively. There are two reported values of quadrupole coupling constants in metavanadates. Vanadium in a polycrystalline sample of ammonium metavanadate is reported to have a quadrupole coupling constant of 3.04 MHz[33]. Vanadium and sodium in a polycrystalline sample of ferroelectric sodium metavanadate, which is not isostructural with ammonium metavanadate[34] are reported[33] to have quadrupole coupling constants of 3.4 MHz and 0.94 MHz respectively.

An accurate crystal structure of vanadium pentoxide has been recently redetermined[35]. X-ray data could not distinguish between the two space groups Pmnm and $Pmn2_1$, and refinement was carried out in both space groups. In the space group Pmnm, the vanadium ions are situated on a mirror plane perpendicular to the c axis, while in the space group $Pmn2_1$, they are not situated on a symmetry element. The trigonal bipyramid sheet is roughly perpendicular to the crystallographic b axis. The coordination number of the vanadium is sometimes considered to be six. However, the sixth oxygen is too far away from the vanadium, 2.785 Å, [35] to be considered as bonded to the vanadium.

There are three previous determinations of the quadrupole coupling constant of vanadium in polycrystalline vanadium pentoxide. The values are 0.752 MHz[36], 0.780 MHz[37] and 0.735 MHz[33]. These values were derived from the experimental data with the assumption that the quadrupole coupling tensor is axially symmetric. The first and the last references also include a point charge calculation of the electric field gradient at the vanadium site.

The chemical shift of the vanadium resonance line in a polycrystalline sample of vanadium pentoxide has been reported[37], and assuming that the chemical shift tensor is axially symmetric, the eigenvalues are $\sigma_{\parallel} = -3.5 \times 10^{-4}$ and $\sigma_{\perp} = 2.0 \times 10^{-4}$ relative to the vanadium resonance line in an aqueous solution of sodium metavanadate.

The magnetic susceptibility of a polycrystalline sample of vanadium pentoxide has been reported twice. Klemm et al.[38] found the susceptibility to be paramagnetic and temperature independent, while Kosuge et al.[39] found it to be diamagnetic.

This work is a study of the various vanadium oxygen groups mentioned above. Sodium orthovanadate dodecahydrated ($Na_3VO_4 \cdot 12H_2O$), calcium orthovanadate ($Ca_3(VO_4)_2$, and the two minerals, vanadinite ($Pb_5Cl(VO_4)_3$) and desclorzite ($Pb(Zn \cdot Cu)[OHVO_4]$) represent the orthovanadates. The crystal structures[44,45] of these minerals show discrete VO_4^{3-} groups. The divanadates are represented by zirconium divanadate (ZrV_2O_2) and cadmium divanadate ($Cd_2V_2O_2$). The metavanadate studied was potassium metavanadate (KVO_3), and vanadium pentoxide (V_2O_5) was included as a representative of five fold oxygen coordination around the vanadium. The crystallographic data for these compounds are summarized in Table 1.

Whenever the quadrupole coupling constant was found to be non-zero, two models were used to calculate the electric field gradient at the vanadium site. These models are a point multipole model, with various effective charges on the vanadium and oxygen ions, and a covalent model, which explicitly takes into account the overlap between the vanadium and oxygen wavefunctions.

TABLE 1

Summary of the crystallographic data of the compounds that were studied in this work

Compound	Unit Cell	Lattice Parameters (Å)	Z	Space Group	Ref.
$Na_3VO_4 \cdot 12H_2O$	Hexagonal	a=12.2 c=12.9	4	$P\bar{3}c1$ or P3c1	40, 41
$Ca_3(VO_4)_2$	Monoclinic	a=19.0 b=10.8 c=14.0 $\beta=116.5^{\circ}$		Cc or C2/c	42, 43
Vanadite	Hexagonal	a=10.31 c=7.34		C63/m	44
Descloizite	Orthorhombic	a=6.05 b=9.39 c=7.65	4	Pmcm	45
$Cd_2V_2O_7$	Monoclinic	a=7.088 b=9.091 c=4.963 $\beta=103^{\circ}21'$	2	C2/m	46
ZrV_2O_7	Cubic	a=8.76	4	Pa3	47
KVO_3	Orthorhombic	a=5.22 b=10.82 c=5.70	4	Pabm	34
V_2O_5	Orthorhombic	a=11.519 b=4.373 c=3.564	4	Pmnm or $Pmn2_1$	35

CHAPTER II

THEORY

This chapter contains the different aspects of theory that were used in this work. The first three sections discuss the effects of external and internal magnetic fields and an internal electric field gradient on the resonance frequency. Sections 4 and 5 give the two models that were used to calculate the electric field gradient. Section 6 gives the hybridized orbitals that are needed in the covalent model and section 7 discusses the antishielding factor.

A. The Zeeman Effect

A magnetic moment μ can be associated with the nuclear angular momenta, $\hbar I$, of a nucleus where I is the quantum spin number. In particular, when such a nucleus is placed in a magnetic field H_o, the Hamiltonian of the interaction is given by:

$$\mathcal{H}_z = - \mu \cdot H_o \qquad (2\text{-}1)$$

The magnetic moment of the nucleus is related to its spin quantum number I by

$$\mu = g\mu_N I \qquad (2\text{-}2)$$

where g is the nuclear g factor and μ_N is the nuclear magneton. The Hamiltonian can now be written

$$\mathcal{H}_z = -g\mu_N I \cdot H_o. \qquad (2\text{-}3)$$

If the direction of the applied magnetic field is chosen as the z axis , the energy of the nucleus, as a result of the magnetic field, can be written as

$$E_z = -g\mu_N m H_o = -h\nu_L m \qquad (2\text{-}4)$$

where m, the magnetic quantum number, is the projection of the spin quantum number I on the magnetic field vector, and ν_L is the Larmor frequency. At an applied magnetic field of the order of ten kilogauss the Larmor frequency is in the radio frequency range of the electromagnetic spectra. Therefore, when a radio frequency field is applied, transverse to H_o, at the Larmor frequency, a magnetic dipole transition is induced between energy levels separated by $\Delta m = \pm 1$. There are 2I+1 energy levels and 2I possible transitions between them that satisfy $\Delta m = \pm 1$. However, since all the energy levels are equally spaced, only one resonance frequency will be observed. The energy levels are shown in Figure 1 for a nucleus with spin I = 7/2.

B. Quadrupolar Interaction

The theory of the quadrupolar interaction in a single crystal, given by Volkoff[8] will be summarized here. An electric quadrupole moment of a nucleus is a measure of the deviation of its charge distribution from spherical symmetry. Therefore, every nucleus with $I \geq 1$ has a non-vanishing quadrupole moment. The Hamiltonian of the quadrupolar interaction can be written as

$$\mathcal{H}_Q = \bar{Q} \cdot \overline{\nabla E} \qquad (2\text{-}5)$$

which is the scalar product of $\bar{Q}$, the electric quadrupole tensor of the nucleus and $\overline{\nabla E}$, the electric field gradient tensor at the nuclear site.

In order to calculate the matrix elements and the energy levels of this interaction, it is convenient to distinguish between the following cases :

1. Quadrupolar interaction >> Zeeman interaction.
2. Quadrupolar interaction ≈ Zeeman interaction.
3. Quadrupolar interaction << Zeeman interaction.

The first case occurs mainly in covalent halogen compounds such as BrCN[48], CH_3I[49], AsF_3[50] and ICl[51]. These compounds contain atoms with unfilled p-shells. However, recently a very large quadrupolar interaction was observed for the Nb^{93} nucleus in ferroelectric $LiNbO_3$[52] The Nb^{93} ion does not have an unfilled p-shell. A treatment of this case is given by Das and Hahn[53]. In principal, the Zeeman interaction is treated as a small perturbation compared with the quadrupolar interaction.

In the second case, the two interactions are comparable and $\mathcal{H}_z$ and $\mathcal{H}_Q$ have to be diagonalized simultaneously.

In the third case, which is the one applicable in compounds that were studied in this work, the quadrupole interaction is treated as a small perturbation compared with the Zeeman interaction.

The matrix elements of $\bar{Q} \cdot \overline{\nabla E}$ can be separated into a

product of two factors. One depends only on the nuclear coordinates and is proportional to $3m^2 - I(I+1)$, and the second factor depends only on the environment. There is no longer only one resonance line which is characteristic of a zero quadrupolar interaction, but a resonance pattern which is split into 2I components. The spectrum is said to be composed of a central line and 2I-1 satellites in the case when I is half integer and 2I satellites when I is an integer. The effect of a small quadrupolar interaction on the Zeeman interaction is shown in Figure 1.

If a coordinate system is introduced which is fixed with respect to the crystal, then Volkoff[8] has shown that the frequency difference $\nu_m'-\nu_m''$, , between a pair of satellites corresponding to the transitions $m \longleftrightarrow m-1$ and $-m \longleftrightarrow -(m-1)$, is given by the following expression:

$$(\nu_m'-\nu_m'')_x = \tfrac{1}{2}(2m-1)(a_x+b_x\cos 2\theta_x+c_x\sin 2\theta_x)$$
$$= \tfrac{1}{2}(2m-1)(a_x+R_x\cos 2(\theta_x-\delta_x)) \qquad (2\text{-}6)$$

where θ_x is the angle between the magnetic field and the y axis when the magnetic field is perpendicular to the x axes,

$$a_x = -\frac{3eqQ}{2I(2I-1)h}\cdot\frac{\phi_{xx}}{eq}$$

$$b_x = R_x\cos 2\delta_x = \frac{3eqQ}{2I(2I-1)h}\cdot\frac{\phi_{yy}-\phi_{zz}}{eq} \qquad (2\text{-}7)$$

Figure 1

The effect of an external magnetic field and internal electric field gradient on the energy levels of a nucleus with spin 7/2 and quadrupole moment $Q>0$. The observed resonance pattern is shown at the bottom of the figure.

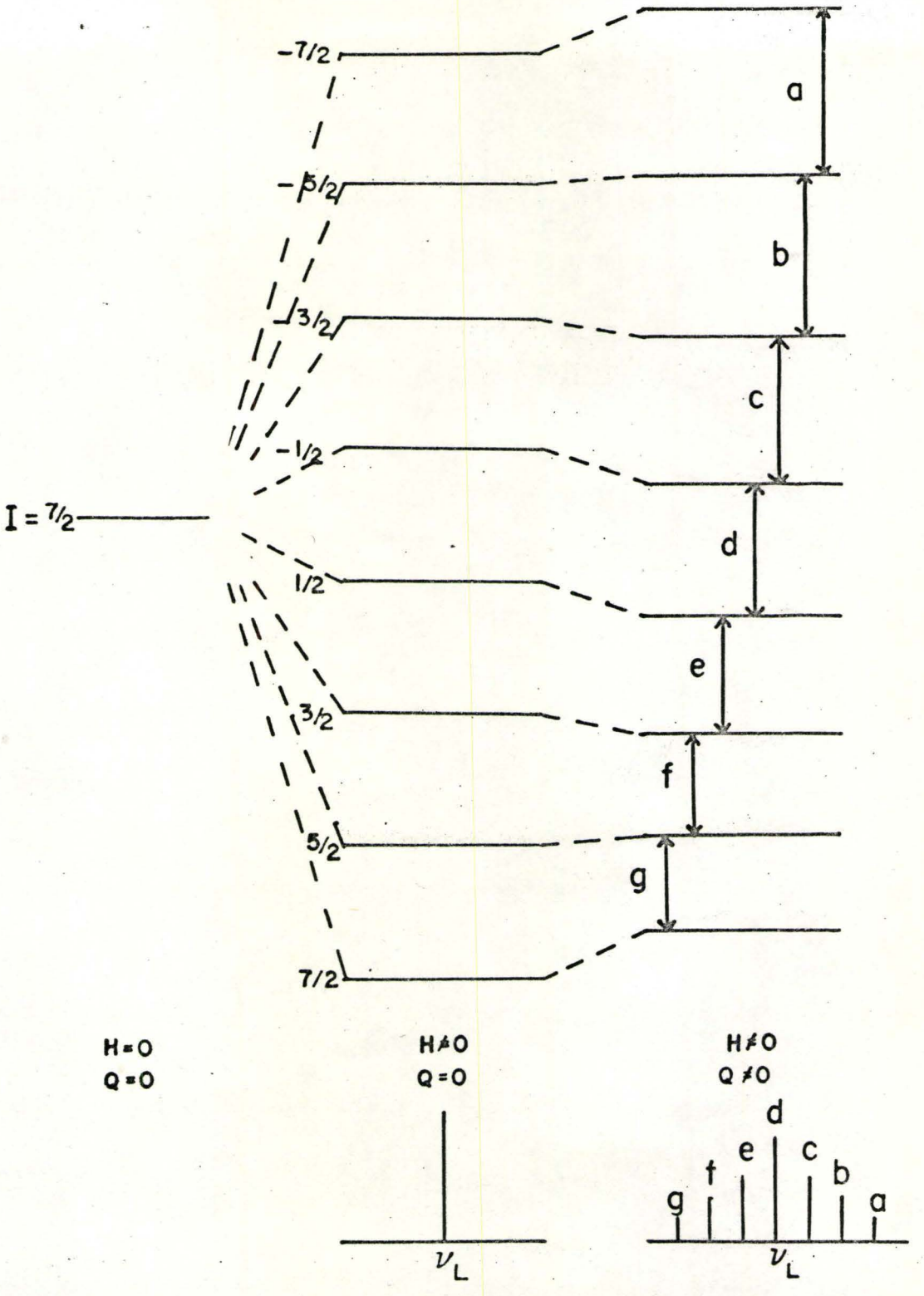

Figure 1

$$c_x = R_x \sin 2\delta_x = -\frac{3eqQ}{I(2I-1)h} \cdot \frac{\phi_{xz}}{eq}$$

$$\phi_{ij} = \frac{\partial^2 \phi}{\partial X_i \partial X_j} \qquad (2\text{-}8)$$

where ϕ is the electrostatic potential at the nuclear site and q is the largest eigenvalue of ϕ_{ij}.

Expressions for the magnetic field rotated in the xz and xy planes can be obtained by cyclic permutations of the indices.

The center of gravity of a pair of satellites which correspond to the transitions $m \longleftrightarrow m-1$ and $-m \longleftrightarrow -m-1$, is defined by

$$\bar{\nu}_m = \frac{1}{2}(\nu_m' + \nu_m'') \ . \qquad (2\text{-}9)$$

The shift of the center of gravity from the Larmor frequency, when the magnetic field is rotated in the yz plane, is given by

$$(\bar{\nu}_m - \nu_L)_x = n_x + p_x \cos 2\theta_x + r_x \sin 2\theta_x + u_x \cos 4\theta_x + v_x \sin 4\theta_x \qquad (2\text{-}10)$$

$$= n_x + P_x \cos 2(\theta_x - \gamma_x) + U_x \cos 4(\theta_x - \delta_x)$$

where

$$n_x = \frac{1}{576\nu_L}\{18C_2(m)a_x^2 + [(C_2(m) - 4C_1(m)](b_x^2 + c_x^2) + 4[C_2(m) - C_1(m)]\ (c_y^2 + c_z^2)\}$$

$$p_x = P_x \cos 2\gamma_x = \frac{1}{576\nu_L}\{-12C_2(m)a_x b_x + 4[C_2(m) + C_1(m)]\ (c_y^2 - c_z^2)\}$$

$$r_x = P_x \sin 2\gamma_x = \frac{1}{576\nu_L}\{-12C_2(m)a_x c_x + 8[C_2(m) - C_1(m)]c_y c_z\} \qquad (2\text{-}11)$$

$$u_x = U_x \cos 4\delta_x = \frac{1}{576\nu_L}\{[C_2(m) + 4C_1(m)](b_x^2 - c_x^2)\}$$

$$\nu_x = U_x \sin 4\delta_x = \frac{1}{576\nu_L} \{[C_2(m)+4C_1(m)]2b_x c_x\}$$

and

$$C_1(m) = 4[(I+\tfrac{3}{2}) - 6(m-\tfrac{1}{2})^2]$$
$$C_2(m) = 2[(I+\tfrac{3}{2})(I-\tfrac{1}{2})-3(m-\tfrac{1}{2})^2] \qquad (2\text{-}12)$$

For a nucleus with half integer spin, the shift of the central resonance line can be obtained by substituting $m = \frac{1}{2}$ in equations (2-10), (2-11) and (2-12). This shift can be used to obtain the quadrupole coupling tensor if the satellites cannot be observed.

In general, three rotations around three mutually perpendicular axes are needed to determine the parameters a_x, b_x, c_x, c_y and c_z, which are related to the five components of the quadrupole coupling tensor. This tensor can be diagonalized in order to obtain the three eigenvalues of this tensor and the orientation of the principal axes. The XYZ principal axes are defined in such a way that the three eigenvalues obey the inequality $eq = \phi_{ZZ} > \phi_{YY} > \phi_{XX}$. The anisotropy factor is defined by

$$\eta = \frac{\phi_{YY}-\phi_{XX}}{\phi_{ZZ}} \qquad (2\text{-}13)$$

In terms of the anistropy factor, the eigenvalues can be written as

$$\phi_{ZZ} = eq \ , \ \phi_{XX} = -eq\,\frac{1+\eta}{2} \ , \ \phi_{XX} = -eq\,\frac{1-\eta}{2} \qquad (2\text{-}14)$$

If the orientation of one of the principal axes is known as a result of symmetry considerations, one rotation, in which the magnetic field is rotated in a plane perpendicular

to this axis, is sufficient to obtain the three eigenvalues and the orientation of the other two principal axes. This is a result of the vanishing trace of $\emptyset_{ij}$. If the known principal axis is chosen as the X axis, the three eigenvalues are given by

$$-a_x, \frac{1}{2}(a_x+R_x), \frac{1}{2}(a_x-R_x) \qquad (2\text{-}15)$$

The eigenvalue $-a_x$ corresponds to the X principal axis. The eigenvalue $\frac{1}{2}(a_x+R_x)$ corresponds to the principal axis which coincides with the magnetic field when $\Theta_x = \delta_x$.

In some cases, the quadrupole coupling constant can be obtained from a polycrystalline sample. It is necessary that the anisotropy of the quadrupole coupling tensor be small, otherwise the orientation averaging, that takes place when a polycrystalline sample is used, smears the satellites and the splitting cannot be observed. When the anisotropy is zero, the quadrupole coupling constant, $\frac{eqQ}{h}$ is given by $\frac{2I(2I-1)}{3}\Delta\nu$ where $\Delta\nu$ is the separation between the inner pair of satellites. If the anisotropy is small, the quadrupole coupling constant will be somewhat greater than $\frac{2I(2I-1)}{3}\Delta\nu$.

c. Chemical Shift

The magnetic field at the nucleus is not the external magnetic field but contains an additional component caused by the magnetic interaction of the electrons with the nucleus. This additional magnetic field causes a shift in the resonance frequency which is called the chemical shift. The frequency

of the radiation that is absorbed in the transition between two energy levels is given by

$$\nu = \frac{g\mu_N}{h} (H_o+\Delta H) \qquad (2\text{-}16)$$

where H_o is the applied magnetic field, ΔH is the additional magnetic field at the nucleus arising from the motion of electrical charges. This can be expressed as[54]

$$\Delta H = - \sigma \cdot H_o \qquad (2\text{-}17)$$

where σ is the chemical shift tensor. Measurements of σ, therefore, provide valuable information about the charge distribution around the nucleus. Even more information can be obtained by studying the anisotropy of the chemical shift tensor. In order to determine the eigenvalues of σ and the orientation of the three principal axes, the magnetic field must be rotated in three mutually perpendicular planes. However, if the orientation of one of the principal axes is known from symmetry considerations, two rotations, one in the plane perpendicular to the known principal axis, are needed. This is a result of the non-vanishing trace of σ, in contrast with the quadrupole coupling tensor.

Let x,y,z be a coordinate system fixed with respect to the crystal, and let the crystal be rotated around the z axis which is known to be a principal axis. The external magnetic field is applied along the z' axis. The relations between the components of σ in the rotated and laboratory coordinates is given by

$$\sigma'_{zz} = \frac{1}{2}(\sigma_{xx}+\sigma_{yy})+\frac{1}{2}(\sigma_{xx}-\sigma_{yy})\cos 2\theta_z+\sigma_{xy}\sin 2\theta_z \qquad (2\text{-}18)$$

Since

$$\Delta H = -\sigma'_{zz} H_o \qquad (2\text{-}19)$$

$$\frac{\Delta H}{H_o} = -\frac{1}{2}(\sigma_{xx}+\sigma_{yy}) - \frac{1}{2}(\sigma_{xx}-\sigma_{yy})\cos 2\theta_z - \sigma_{xy}\sin 2\theta_z \qquad (2\text{-}20)$$

The expressions for rotation around the other axes can be obtained by cyclic permutations of the indices. Since the z axis is a principal axis, $\sigma_{xz}=\sigma_{yz}=0$ and a rotation around the y axis yields

$$\frac{\Delta H}{H_o} = -\frac{1}{2}(\sigma_{zz}+\sigma_{xx}) - \frac{1}{2}(\sigma_{zz}-\sigma_{xx})\cos 2\theta_y \qquad (2\text{-}21)$$

These two expressions provide five equations for the four unknowns; σ_{xx}, σ_{yy}, σ_{zz} and σ_{xy}. However, these equations are not independent and any four of them can be used to find the components of σ. Diagonalization of this tensor yields the three eigenvalues and the orientations of the other two principal axes.

D. Point Multipole Model

One model of a crystal used in calculating the electric field gradient neglects the overlap of the charge distributions of neighbouring ions and treats each ion as a point charge located at the equilibrium position of its nucleus. This is the point charge model, and the electric field gradient at any site in the crystal can be calculated by summing the contributions from these point charges. The charges may be allowed to spread. If the extended charge distribution is not spherically symmetric there are contri-

contributions from higher electrical multipoles in the calculation of the electric field gradient.

The electrostatic potential ϕ in the vicinity of the nucleus may be expanded in associate Légendre polynomials[55]

$$\phi(\underline{r}) = \sum_{\ell=0}^{\infty} \sum_{m=0}^{\ell} [r^{\ell} P_{\ell}^{m}(\cos\theta)(C_{\ell m}\cos m\phi + d_{\ell m}\sin m\phi)] \quad (2\text{-}22)$$

Terms with $\ell=1$ give the electric field at the nucleus by the following relations

$$\begin{aligned} E_x^{(o)} &= -C_{11} \\ E_y^{(o)} &= d_{11} \\ E_z^{(o)} &= C_{10} \end{aligned} \quad (2\text{-}23)$$

The electric field gradient can be obtained by taking terms with $\ell=2$.

$$\begin{aligned} E_{xx} &= -C_{20} + 6C_{22} \\ E_{yy} &= -C_{20} - 6C_{22} \\ E_{zz} &= 2C_{20} \\ E_{xy} &= 6d_{22} \\ E_{xz} &= 6C_{11} \\ E_{yz} &= 6d_{11} \end{aligned} \quad (2\text{-}24)$$

The field gradient tensor is a sum of two parts. One, caused by point charges, while the second term includes contributions from higher electrical multipole moments. The second part will be limited only to contributions from electric dipole moments, because of the lack of knowledge

of quadrupolar polarizability, although contributions from electric quadrupole moments have been included in a few calculations[56].

In order to calculate the electric dipole moment of an ion, the electric field at this ion has to be known. In order to know the electric field, the electric dipole moments of all the other ions have to be known. A self-consistent result is found by iterations.

If the polar coordinates of the ions are (R_j, θ_j, Φ_j) and they have a charge e_j, the contributions to the electric field from these ions are

$$c_{10}^{(o)} = \sum_j{}' \frac{e_j}{R_j^2} P_1(\cos\theta_j)$$

$$c_{11}^{(o)} - id_{11}^{(o)} = \sum_j{}' \frac{e_j}{R_j^2} P_1^1(\cos\theta_j) e^{-i\Phi_j} \qquad (2\text{-}25)$$

Explicitly

$$c_{10}^{(o)} = \sum_j{}' \frac{e_j}{R_j^3} Z_j$$

$$c_{11}^{(o)} = \sum_j{}' \frac{e_j}{R_j^3} X_j \qquad (2\text{-}26)$$

$$d_{11}^{(o)} = \sum_j{}' \frac{e_j}{R_j^3} Y_j$$

$\underline{E}^{(o)}$ is the electric field gradient due to point charges only. It varies as $1/R^2$, and since the number of ions contributing to the electric field varies as R^2, care has to be taken about the convergence of the sum.

Let $\underline{P}^{(o)}$ be the electric dipole moment of an ion and α its polarizability assumed to be a scalar

$$\underline{P}_j^{(o)} = \alpha \underline{E}_j^{(o)} \tag{2-27}$$

The first iteration of the electric field at a certain ion is defined by

$$\underline{E}^{(1)} = \underline{E}^{(o)} + \sum_j{}' \alpha \left[- \frac{\underline{E}_j^{(o)}}{R_j^3} + 3 \frac{(\underline{E}_j^{(o)} \cdot \underline{R}_j)}{R_j^5} \underline{R}_j \right] \tag{2-28}$$

$\underline{E}^{(1)}$ is the electric field at an ion due to point charges and electric dipole moments of all the other ions.

This procedure can be repeated n times

$$\underline{E}^{(n)} = \underline{E}^{(o)} + \sum_j{}' \alpha \left[- \frac{\underline{E}_j^{(n-1)}}{R_j^3} + 3 \frac{(\underline{E}_j^{(n-1)} \cdot \underline{R}_j)}{R_j^5} \underline{R}_j \right] \tag{2-29}$$

These iterations are repeated until the process converges.

If the electric field gradient is calculated by summing the contributions from the point charges, the coefficients in equation (2-24) are given by

$$c_{20} = \sum_j{}' \frac{e_j}{R_j^3} P_2 (\cos\theta_j) \tag{2-30}$$

$$\frac{1}{2}(c_{2m} - i\, d_{2m}) = \frac{(2-m)!}{(2+m)!} \sum_j{}' \frac{e_j}{R_j^3} P_2^m (\cos\theta_j) e^{-im\Phi_j}$$

If one of the principal axes of the electric field gradient tensor is known and is defined as the Z axis, the components of the field gradient tensor are given by:

$$c_{20} = \frac{1}{2} \sum_j{}' e_j \frac{3Z_j^2 - R_j^2}{R_j^3}$$

$$c_{21} = 0$$

$$d_{21} = 0 \qquad (2\text{-}31)$$

$$c_{22} = \frac{1}{4} \sum_j{}' e_j \frac{X_j^2 - Y_j^2}{R_j^5}$$

$$d_{22} = \frac{1}{2} \sum_j{}' e_j \frac{X_j Y_j}{R_j^5}$$

The above summations converge very rapidly because of the $1/R^3$ dependence.

If contributions from the electric dipole moments are to be included in the electric field gradient tensor, the following equations give the coefficients

$$cP_{20} = \frac{1}{2} \sum_j{}' \left(\frac{\partial}{\partial Z_j}\right)^2 (\underline{P}_j \cdot \nabla_j) \frac{1}{R_j} \qquad (2\text{-}32)$$

$$\frac{1}{2}(cP_{2m} - idP_{2m}) = \frac{1}{(2+m)!} \sum_j{}' \left(\frac{\partial}{\partial X_j} - i \frac{\partial}{\partial Y_j}\right)^{2-m} (\underline{P}_j \cdot \nabla_j) \frac{1}{R_j}$$

where $\underline{P} = \alpha \underline{E}^{(n)}$ is the electric dipole moment of the oxygen. If the Z axis is a principal axis of the quadrupole coupling tensor these equations give

$$cP_{20} = \sum_j{}' \frac{1.5}{R_j^5} \left[\left(1 - 7.5 \frac{Z_j^2}{R_j^2}\right)(\underline{P}_j \cdot \underline{R}_j) + 2P_{z_j} Z_j\right]$$

$$cP_{22} = \frac{1}{12} \sum_j{}' \left[6 \frac{P_{x_j} X_j - P_{x_j} Y_j}{R_j^5} - 15 \frac{\underline{P}_j \cdot \underline{R}_j}{R_j^7} (x_j^2 - y_j^2)\right] \qquad (2\text{-}33)$$

$$dP_{22} = \frac{1}{12} \sum_j{}' \left[6 \frac{P_{x_j} Y_j + P_{y_j} X_j}{R_j^5} - 30 \frac{\underline{P}_j \cdot \underline{R}_j}{R_j^7} X_j Y_j\right]$$

The total field gradient tensor is given by

$$\begin{aligned}\Phi_{zz} &= 2(c_{20} + P_{20}) \\ \Phi_{xx} &= -(c_{20}+cP_{20})+6(c_{22}+cP_{22}) \\ \Phi_{yy} &= -(c_{20}+cP_{20})-6(c_{22}+cP_{22}) \\ \Phi_{xy} &= 6(d_{22} + dP_{22})\end{aligned} \qquad (2\text{-}34)$$

In the above calculations, e_j does not have to be the ionic charge. Screening effects can be taken into account by allowing e_j to be less the ionic charge. According to Pauling, this effective charge is between 0 and 1.

E. Covalent Model

The atomic orbitals of the central and ligand ions can be combined to form molecular orbitals. If the molecular orbitals contain more than one electron, a determinental product of the single electron wavefunctions is the proper wavefunction for the system. Let the wavefunction of the i^{th} ligand be ψ_i^g and the central ion wavefunction $\psi_{\alpha i}^c$. A bonding orbital, ψ_i, can be obtained by taking

$$\psi_i = N_i \left(\psi_i^g + \sum_{\alpha=1}^{n} \lambda_{\alpha i} \psi_{\alpha i}^c\right) \quad i=1....k \qquad (2\text{-}35)$$

N_i is the normalization factor, $\lambda_{\alpha i}$ is the charge transfer coefficient and n is the number of atomic wave functions of the central ion that take part in the bonding. If these atomic orbitals are 3d, 4s and 4p, then n=9.

The number of linear combinations, that can be formed is k where k is equal to the number of ligands that are bonded

to the central ion.

The normalization factor is given by

$$N_i = \{1 + \sum_{\alpha=1}^{n} |\lambda_{\alpha_i}|^2 + \sum_{\alpha=1}^{n} \lambda_{\alpha_i}^* S_{\alpha_i}^{gc} + S_{\alpha_i}^{gc*} \lambda_{\alpha_i}\}^{-\frac{1}{2}}$$

$$\{1 + \sum_{\alpha=1}^{n} |\lambda_{\alpha_i}|^2 + 2 \sum_{\alpha=1}^{n} \mathrm{Re}(\lambda_{\alpha_i}^* S_{\alpha_i}^{gc})\}^{-\frac{1}{2}} \qquad (2\text{-}36)$$

where $S_{\alpha_i}^{gc}$ is the overlap integral between ψ_i^g and $\psi_{\alpha_i}^c$.

$$S_{\alpha_i}^{gc} = \langle \psi_i^g | \psi_{\alpha_i}^c \rangle \qquad (2\text{-}37)$$

Hybridized orbitals are a linear combination of atomic orbitals that reflect the geometry of the environment. Hybridized orbitals can be used for the central ion wavefunctions. The hybridized orbital h_i is defined by

$$\sum_{\alpha=1}^{n} \lambda_{\alpha_i} \psi_{\sigma_i}^c = \lambda_i h_i \quad i=1\ldots k \qquad (2\text{-}38)$$

where h_i is the hybridized orbital of the central ion which is directed toward the ligand i. These hybridized orbitals are orthonormal i.e. $\langle h_i | h_j \rangle = \delta_{ij}$. Equations (2-35) and (2-36) can now be written

$$\psi_i = N_i(\psi_i^g + \lambda_i h_i) \quad i = 1\ldots k \qquad (2\text{-}35a)$$

$$N_i = \{1 + |\lambda_i|^2 + 2\ \mathrm{Re}\ \lambda_i^*\ S_i^{gh}\}^{-\frac{1}{2}} \qquad (2\text{-}36a)$$

where S_i^{gh} is the overlap between hybrid i and ligand i.

In order to avoid calculations of 2 center integrals, the ligand wavefunction may be expanded around the equilibrium position of the central ion. This expansion can be written

as[57]

$$\psi_i^{g}(r,\theta,\phi) = \sum_{\ell,m} \frac{(2L+1)(L-M)!(\ell+M)!}{(2\ell+1)(\ell-M)!(L+M)!}\, \alpha_\ell(gLM|ar)\; Y_\ell^{m}(\theta,\phi)$$

$$\times\, b_{\ell,M,m}(g) \qquad (2\text{-}39)$$

$\alpha_\ell(gLM|ar)$ is the partial radial part of order ℓ of the expansion of the wavefunction with quantum numbers L and M for a ligand which is at a distance a from the central ion. (r,θ,ϕ) are referred to an origin at the central ion. $b_{\ell,M,m}(g)$ are the rotation group elements that are needed to define a unified coordinate system for the k different ligands. Analytical expressions for $\alpha_\ell(gLM|ar)$ have been given by Sharma et al[58].

$$\alpha_\ell(gLM|ar) = B_{L,M,\ell}(ar) \sum_{s=0}^{L+\ell} H_{L,}^{M.S}(ar) \int_{|a-r|}^{a+r} f_{g\ LM}(R)\, R^{-L+2S} \qquad (2\text{-}40)$$

where $f_{g\ LM}(R)$ is defined by

$$\psi^{g} = \frac{f_{gLM}(R)}{R}\; Y_L^{M}(\Theta,\Phi)$$

$$B_{L,M,\ell}(ar) = \begin{cases} \dfrac{2\ell+1}{a^{2-L}} \times \dfrac{(-1)^L}{2^{2L+\ell-M}} \times \left(\dfrac{r}{a}\right)^{M-1} \dfrac{[\cos\frac{1}{2}(\ell+M)\pi]\ (\ell+M-1)!}{[\frac{1}{2}(\ell-M-1)!\,[\frac{1}{2}(\ell+M-1)!} \times \dfrac{(\ell-M)!}{(\ell+M)!} & \ell-M \text{ even} \\ \dfrac{2\ell+1}{a^{2-L}}\, \dfrac{(-1)^L}{2^{2L+\ell-M}} \left(\dfrac{r}{a}\right)^{M-2} \dfrac{[\sin\frac{1}{2}(\ell+M)\pi]}{[\frac{1}{2}(\ell-M-1)]!\,[\frac{1}{2}(\ell+M-1)]!} \left(1+\dfrac{r^2}{a^2}\right) & \ell+M \text{ odd} \end{cases} \qquad (2\text{-}41)$$

$$H_{L,\ell}^{M.S}(ar) = \frac{1}{a^{2s}} \sum_{n,r',q'}^{n_o,r_o',q_o'} C\, C' \left(1-\frac{r^2}{a^2}\right)^{L-r'-M-S+q'} \frac{\left(1+\frac{r^2}{a^2}\right)^{2n-q'}}{(r/a)^{2n}} \qquad (2\text{-}42)$$

n_o = quotient of $\frac{1}{2}(\ell+M)$

r_o' = quotient of $\frac{1}{2}(L-M)$

q_o' = 2n or 2n+1 according if $\ell+M$ is even or odd

$$C = \frac{(-1)^{r'+q'}(2n)!(2L-2r')!}{n!q'!(2n+1-q')!(s-q'-r')!(L-r'-M-S+q')!(L-r')!2^{2n-2r'}} \quad (2\text{-}43)$$

$$C' = \begin{cases} (-\frac{\ell}{2} - \frac{M}{2})_n \times (\frac{1}{2} + \frac{\ell}{2} - \frac{M}{2})_n \times \frac{2n-q'+1}{(\frac{1}{2})_n} & \ell+M \text{ even} \\ (\frac{1}{2} - \frac{\ell}{2} - \frac{M}{2})_n \ (1 + \frac{\ell}{2} - \frac{M}{2})_n (2n+1) & \ell+M \text{ odd} \end{cases} \quad (2\text{-}44)$$

and $(b)_n = 1$ for $n=0$

$$(b)_n = \frac{\Gamma(b+n)}{\Gamma(b)} = b(b+1)(b+2)\ldots(b+n-1)$$

$$b_{\ell,M,m}(g) = (-i)^{M-m} e^{im\gamma_g} e^{iM\alpha_g} B_{\ell,M,m}(-\beta_g) \quad (2\text{-}45)$$

$$B_{\ell,M,m}(\beta_g) = \sum_t (-1)^t \frac{[(L+M)!(L-M)!(\ell+M)!(\ell-M)!]^{\frac{1}{2}}}{(\ell-M-t)!(\ell+m-t)!(t+M-M)!t!} \times \cos^{2\ell-M+m-2t}(\frac{\beta_g}{2}) \times \sin^{M-m+2t}(\frac{\beta_g}{2}) \quad (2\text{-}46)$$

where $(\alpha_g, \beta_g, \gamma_g)$ are the Euler angles that are required for the transformation of the coordinate system.

Expressions for $\alpha_\ell(gLM|ar)$ for L=1, M=0 $\ell \leq 4$ are given in Appendix A. Values of $B_{\ell,o,m}(-\beta_g)$, for $\ell, |m| \leq 4$, and for values of β_g defined in Figure 2 are given in Appendix D.

The electric field gradient tensor operator can be written as[59]

$$\nabla\hat{E} = \frac{e}{r^3}\hat{C}_2 \quad (2\text{-}47)$$

where $\hat{C}_2$ is the spherical tensor operator of order 2 and is defined by the equation

$$\hat{C}_2^q = \sqrt{\frac{4\pi}{5}}\, Y_2^q \tag{2-48}$$

where Y_2^q is the spherical harmonic of the second order.

In Cartesian coordinates, the components of the electric field gradient tensor operator are given by

$$\hat{E}_{zz} = 2\,\frac{e}{r^3}\,\hat{C}_2^{\,o}$$

$$\hat{E}_{xx} = \frac{e}{r^3}\left[-\hat{C}_2^{\,o} + \frac{\sqrt{6}}{2}\,(\hat{C}_2^{\,2} + \hat{C}_2^{\,-2})\right]$$

$$\hat{E}_{yy} = \frac{e}{r^3}\left[-\hat{C}_2^{\,o} - \frac{\sqrt{6}}{2}\,(\hat{C}_2^{\,2} + \hat{C}_2^{\,-2})\right]$$

$$\hat{E}_{xy} = \frac{\sqrt{6}}{2i}\,\frac{e}{r^3}\,(\hat{C}_2^{\,2} + \hat{C}_2^{\,-2}) \tag{2-49}$$

$$\hat{E}_{xz} = -\frac{\sqrt{6}}{2}\,\frac{e}{r^3}\,(\hat{C}_2^{\,1} - \hat{C}_2^{\,-1})$$

$$E_{yz} = -\frac{\sqrt{6}}{2i}\,\frac{e}{r^3}\,(\hat{C}_2^{\,1} + \hat{C}_2^{\,-1})$$

$\nabla\hat{E}$ is a one electron tensor operator, therefore its expectation value is the sum of the expectation values between the one electron wavefunction that makes up the determinental wavefunction.

$$\langle \nabla E \rangle = \sum_{i=1}^{k} \langle \psi_i | \nabla\hat{E} | \psi_i \rangle \tag{2-50}$$

$$\langle \nabla E \rangle = \sum_{i=1}^{k} N_i^{\,2}\, \{\langle \psi_i^{\,g} + \lambda_i h_i | \nabla\hat{E} | \psi_i^{\,g} + \lambda_i h_i \rangle\} \tag{2-51}$$

These expressions can be decomposed into a sum of three components

$$\langle \nabla E \rangle = \langle \nabla E \rangle^{\ell} + \langle \nabla E \rangle^{n \cdot \ell} + \langle \nabla E \rangle^{d} \qquad (2\text{-}52)$$

where

$$\langle \nabla E \rangle^{\ell} = \sum_{i=1}^{k} N_i^2 \{ |\lambda_i|^2 \langle h_i | \nabla E | h_i \rangle \} \qquad (2\text{-}53)$$

This is the local contribution to the electric field gradient tensor and involves only the central ion wavefunctions. For certain configurations of the central ion, this term can be obtained from measurements of atomic hyperfine structure.

$$\langle \nabla E \rangle^{n \cdot \ell} = 2 \sum_{i=1}^{k} N_i^2 \, \mathrm{Re}[\lambda_i \langle \psi_i^{g} | \nabla \hat{E} | h_i \rangle] \qquad (2\text{-}54)$$

This is the nonlocal contribution and involves both the ligand orbitals and the central ion orbitals.

$$\langle \nabla E \rangle^{d} = \sum_{i=1}^{k} N_i^2 \langle \psi_i^{g} | \nabla \hat{E} | \psi_i^{g} \rangle \qquad (2\text{-}55)$$

This is the distant contribution and involves only ligand wavefunctions. The distant contribution is expected to be very small compared to the other terms and will be neglected. For a central ion in an environment with axial symmetry, there is only one nonvanishing component of the field gradient tensor. This component is given by

$$q^{\ell} = 2 \sum_{i=1}^{k} N_i^2 \, |\lambda_i|^2 \langle h_i | \frac{e}{r^3} \hat{C}_2^{o} | h_i \rangle \qquad (2\text{-}56)$$

$$q^{n \cdot \ell} = 4 \sum_{i=1}^{k} N_i^2 \, \mathrm{Re}[\lambda_i \langle \psi_i^{g} | \frac{e}{r^3} \hat{C}_2^{o} | h_i \rangle] \qquad (2\text{-}57)$$

For a central ion in an environment that has no axial symmetry, the matrix elements of $\frac{e}{r^3} C_2^m$ where $m \leq 2$ have to be

calculated. The radial part is calculated numerically with the aid of equations (2-40) and (2-41). The angular part can be obtained from[60]

$$\langle Y_\ell^m | C_2^q | Y_{\ell'}^{m'} \rangle = (-1)^m \begin{pmatrix} \ell & 2 & \ell \\ -m & q & m' \end{pmatrix} \begin{pmatrix} \ell & 2 & \ell' \\ 0 & 0 & 0 \end{pmatrix} \sqrt{(2\ell+1)(2\ell'+1)} \quad (2\text{-}58)$$

where $\begin{pmatrix} \ell_1 & \ell_2 & \ell_2 \\ m_1 & m_2 & m_3 \end{pmatrix}$ is a Wigner 3-j symbol. Inspection of the above expressions and the known properties of the 3-j symbols show that if $\ell+2+\ell'$ is odd the second 3-j symbol vanishes. Hence only matrix elements between states ℓ and ℓ' such that $\ell'+\ell$ is even have to be considered. Since $\ell+2=\ell'$ is a vector summation, ℓ' cannot differ from ℓ by more than 2. The first 3-j symbol vanishes unless $m'+q+m=0$.

E. Hybridized Orbitals

If a vanadium atom is placed in an environment with tetrahedral symmetry, the hybridized orbitals are obtained[61] by taking a mixture of d^3s and p^3s vanadian wavefunctions. For the arrangement of the ligands around the vanadium ion shown in Figure 2-a, the hybridized orbitals are given by

$$\begin{aligned}
h_1 &= \tfrac{1}{2}[4s+\sqrt{\tfrac{3}{8}}\,(4p_x+4p_y+4p_z)+\sqrt{\tfrac{5}{8}}(3d_{xz}+3d_{yz}+3d_{xy})] \\
h_2 &= \tfrac{1}{2}[4s+\sqrt{\tfrac{3}{8}}(-4p_x+4p_y-4p_z)+\sqrt{\tfrac{5}{8}}(3d_{xz}-3d_{yz}-3d_{xy})] \quad (2\text{-}60) \\
h_3 &= \tfrac{1}{2}[4s+\sqrt{\tfrac{3}{8}}(4p_x-4p_y-4p_z)+\sqrt{\tfrac{5}{8}}(-3d_{xz}+3d_{yz}-3d_{xy})] \\
h_4 &= \tfrac{1}{2}[4s+\sqrt{\tfrac{3}{8}}(-4p_x-4p_y+4p_z)+\sqrt{\tfrac{5}{8}}(-3d_{xz}-3d_{yz}+3d_{xy})]
\end{aligned}$$

If the vanadium ion is placed in a five-fold trigonal bi-pyramid coordinate environment, the hybridized orbitals are obtained by mixing a small amount of dsp^3 into d^3sp.

Figure 2

The orientation of the coordinate system used to express the hybridized orbitals of the vanadium ion for tetrahedral coordination (a) and trigonal bipyramid coordination (b). The numbers in parentheses beside each oxygen are the Euler angles that were used in expansion of the ligand wavefunction around the central ion.

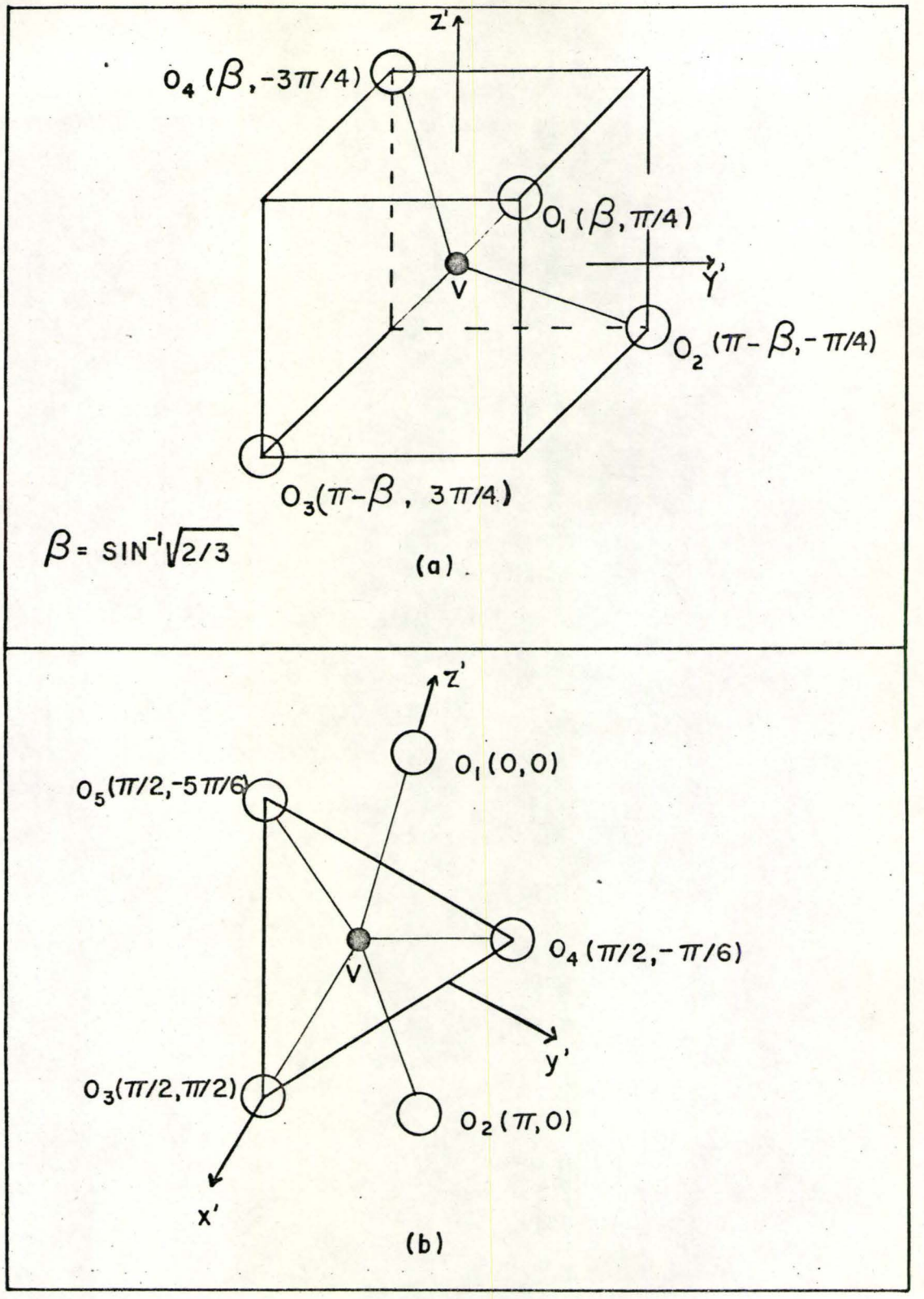
z'
$O_4(\beta, -3\pi/4)$
$O_1(\beta, \pi/4)$
V
Y'
$O_2(\pi-\beta, -\pi/4)$
$O_3(\pi-\beta, 3\pi/4)$
$\beta = \sin^{-1}\sqrt{2/3}$
(a)
z'
$O_1(0,0)$
$O_5(\pi/2, -5\pi/6)$
$O_4(\pi/2, -\pi/6)$
V
y'
$O_3(\pi/2, \pi/2)$
$O_2(\pi, 0)$
x'
(b)

Figure 2

The hybridized orbitals for the arrangement in Figure 2-b is given by:

$$h_1 = \sqrt{\frac{3}{8}} \times 4s + \sqrt{\frac{1}{2}} \times 4p_z + \sqrt{\frac{1}{8}} \times 3d_{z^2}$$

$$h_2 = \sqrt{\frac{3}{8}} \times 4s - \sqrt{\frac{1}{2}} \times 4p_z - \sqrt{\frac{1}{8}} \times 3d_{z^2}$$

$$h_3 = \sqrt{\frac{1}{12}} \times 4s - \frac{1}{2} \times 3d_{z^2} + \sqrt{\frac{2}{3}} [0.316 \times 4p_x + 0.948 \times 3d_{x^2-y^2}] \quad (2\text{-}60)$$

$$h_y = \sqrt{\frac{1}{12}} \times 4s - \frac{1}{2} \times 3d_{z^2} - \sqrt{\frac{1}{6}} [0.316 \times 4p_x + 0.948 \times 3d_{x^2-y^2}]$$

$$- \sqrt{\frac{1}{2}} [0.316 \times 4p_y - 0.948 \times 3d_{xy}]$$

$$h_5 = \sqrt{\frac{1}{12}} \times 4s - \frac{1}{2} \times 3d_{z^2} - \sqrt{\frac{1}{6}} [0.316 \times 4p_x + 0.948 \times 3d_{x^2-y^2}$$

$$+ \sqrt{\frac{1}{2}} [0.316 \times 4p_y - 0.948 \times 3d_{xy}]$$

F. The Antishielding Factor

The electric field gradient at the nucleus of an ion in a crystal is proportional to the electric field gradient of the environment of the ion. This constant of proportionality is called the antishielding factor and it arises from the quadrupolar polarizability of the electrons around the nucleus. Another way to look at the effect is an induced quadrupole moment, in the charge distribution around the nucleus,which is proportional to the quadrupole moment of the nucleus. A quantum mechanical treatment[67] shows that the quadrupole coupling tensor is multiplied by a factor of $1-\gamma_\infty$ where γ_∞ is the antishielding factor. This antishielding factor is composed of a sum of

two parts, a radial part and an angular part. The angular part can be considered to be a result of the quadrupolar field of the nucleus. This field varies as $(3\cos^2\theta-1)/r^3$. In a shell of radius r, this potential has positive and negative values, so that the electrons will move from regions of negative potential to regions of positive potential. The radial part arises from the movement of the electrons toward the nucleus in regions of positive potential and from the nucleus in regions of negative potentials.

Thus a charge distribution which originally was spherically symmetric will become distorted and contribute to the measured quadrupole coupling constant. There is no way of measuring the antishielding factor and it has to be calculated. Sternheimer[63-68] calculated values of γ_∞ for atoms with closed shell configurations by solving the Schrödinger equation numerically. Das and Bersohn[69] used a variational method to obtain numerical values for γ_∞. The two ways of computing γ_∞ are consistent and a general result of the calculations is, that for the same closed shell configuration, γ_∞ is a monotonic decreasing function of Z, the atomic number. This is because the electrons are more tightly bound to the nucleus for higher Z, and hence less susceptible to polarization. Makhanek[70] used a Fermi-Thomas model to calculate γ_∞ for Cs^-, K^+, Ca^{2+}, Sc^{3+} and Ti^{4+} which are isoelectronic with V^{5+}. Therefore these results

were extrapolated to V^{5+}, the ion which is considered in this work. However, the Fermi-Thomas model tends to overestimate γ_∞ because it considers the electrons to be more free than they really are. Sternheimer[68] estimates that the antishielding factors, calculated by the Fermi-Thomas model, are 50% larger than the actual values. The value of γ_∞ that was extrapolated from Makhanek's calculation is -4.5. Based on Steinheimer's estimates, a value of -3.5 was used in this work.

CHAPTER III

EXPERIMENTAL METHODS

A. APPARATUS

All the nuclear magnetic resonance data were taken at 300°K with a Varian variable frequency nuclear magnetic resonance spectrometer. This spectrometer employs the crossed coil technique. This technique allows the use of either the absorption or the dispersion mode of measurement. In order to detect the resonance line, the frequency was fixed while the magnetic field was swept at a constant rate. In addition the magnetic field was modulated at a low frequency, and the resulting low frequency signal was amplified by a narrow band amplifier and then detected with a phase sensitive detector. The integration time of the phase sensitive detector was variable. The choice of sweep rate and integration time are not independent, since their product has to be much less than the linewidth of the detected resonance. Broad resonance lines were recorded with the spectrometer operating in the dispersion mode while narrow resonance lines were recorded with the absorption mode.

The magnetic susceptibility data were taken with a commercial vibrating sample magnetometer. This technique

involved vibration of the sample perpendicular to the applied magnetic field. The resulting oscillating dipolar field was detected by pickup coils. The magnitude of the signal induced in the pickup coils was proportional to the magnetic moment of the sample. At the same time, a reference signal was generated at the vibration frequency. The magnitude of the reference signal was varied to produce a null between the reference and the sample signals. This "nulling" technique insured that the measured result was independent of the vibration frequency and amplitude. Data for the magnetic susceptibility were taken over a temperature range from 4.2°K to 300°K, while the anisotropy of the magnetic susceptibility was measured at 300°K.

B. SAMPLES

1. Sodium orthovanadate dodecahydrate ($Na_3VO_3 \cdot 12H_2O$)

Single crystals of sodium orthovanadate dodecahydrate were grown from an aqueous solution of sodium orthovanadate. The solution was allowed to become saturated by slow evaporation of the water at a constant temperature of approximately 40°C. The size of the crystal that was used in the nuclear magnetic resonance measurements was $12 \times 6 \times 3$ mm^3. Initially, the crystals were transparent, but they became cloudy under prolonged exposure to the atmosphere. The reason is probably the loss of water of hydration. Data were taken on an unoriented crystal.

2. Calcium Orthovanadate [$Ca_3(VO_4)_2$]

Single crystals of calcium orthovanadate were obtained from the Defence Research Board in Ottawa through the kindness of Drs. Cox and Chambers. They were grown there by the Kyropoulos technique, and have a cylindrical shape. The size was approximately 25 mm long by 10 mm in diameter. One of the crystals was doped with Eu^{3+} ions for an electron paramagnetic resonance experiment whereas the other crystal had no intentional impurities. The undoped crystal was oriented with the aid of a precession camera using Mo radiation. Data were also taken on the γ-irradiated unoriented doped crystal.

3. Vanadinite [$Pb_5Cl(VO_4)_3$]

Crystals of vanadinite, a naturally occurring mineral, were purchased from the Southeast Scientific Company in Arizona. The crystals were yellow-red in colour and had the shape of a rectangular prism with approximate dimensions of $10 \times 6 \times 3$ mm^3. Crystals that appeared to be twinned were rejected. Data were taken on an unoriented crystal.

4. Descloizite [$Pb(Zn,Cu)OHVO_4$]

Crystals of descloizite, a naturally occurring mineral, were also purchased from the Southeast Scientific Company in Arizona. The crystals are black and had the shape of a rectangular prism with approximate dimensions of $10 \times 4 \times 4$ mm^3. No effort was made to check the crystals

or orient them.

5. Cadmium Divanadate [$Cd_2V_2O_7$]

Data were taken on a polycrystalline sample because of the difficulty in growing a single crystal that is large enough for nuclear magnetic resonance measurements. The polycrystalline sample was obtained by reacting stochiometric amounts of vanadium pentoxide with cadmium oxide, and allowing the cadmium oxide to dissolve and react in the liquid vanadium pentoxide. The product was then slowly cooled. The sample was reground and remelted. This procedure was continued until a homogenous brown-black powder was obtained. An x-ray powder pattern showed it to be cadmium divanadate.

6. Zirconium Divanadate [ZrV_2O_7]

Data were taken on a polycrystalline sample because of the difficulties in growing large single crystals. Zirconium divanadate melts incongruently. The polycrystalline sample was obtained by reacting stochiometric amounts of zirconium oxide and vanadium pentoxide. The reaction was allowed to take place just above the melting point of vanadium pentoxide. The product was reground and then reheated to the same temperature. This procedure was continued until a homogenous black powder was obtained. The powder was examined by x-ray diffraction methods and the resulting powder

powder pattern was compared with that of powdered zirconium diphosphate, which is reported to be isostructural[47] with zirconium divanadate.

7. Potassium Metavanadate [KVO_3]

A single crystal of potassium metavanadate was grown by the Bridgman technique. Stochiometric amounts of potassium carbonate and vanadium pentoxide were reacted at about 750°C, and then lowered through a constant temperature gradient at a rate of 1 mm/hr. The crystal that was used in the nuclear magnetic resonance measurements had a reddish-brown colour, and had the shape of rectangular prism with dimensions $8 \times 5 \times 3$ mm^3. The crystal was checked for perfection by examination of the diffraction pattern arising from Mo x-rays that had been transmitted through the crystal. Alignment was performed with precession cameras using Mo radiation.

8. Vanadium Pentoxide [V_2O_5]

A single crystal of vanadium pentoxide was grown from powdered vanadium pentoxide by the Kyropoulos method. A seed crystal was obtained from a previous trial at growing a large single crystal by the Bridgman technique. Considerable difficulties were experienced in obtaining volume growth on the {010} plane, which is a natural cleavage plane. The crystal was brown and had the dimensions $11 \times 6 \times 1$ mm^3. The perfection of the crystal was checked

by an x-ray technique that involved transmission of the beam through the crystal. Alignment of the crystal was performed with Mo radiation using Weissenberg and precession cameras.

C. EXPERIMENTAL PROCEDURE

Data were taken at a constant frequency appropriate to the sample. The integrating time was in the range from 1 to 10 sec and depended on the signal to noise ratio. The rotation pattern data were taken at 300^{o}K over an angular range of 180^{o} at intervals of 12^{o} in every case except for the magnetic susceptibility data. The susceptibility data were taken over an angular range of 360^{o} at intervals of 15^{o}.

CHAPTER IV

RESULTS

This chapter contains the results of the experiments and the calculations. Part A contains the results of the nuclear magnetic resonance studies of the quadrupolar interaction and the chemical shift. In addition, the magnetic susceptibility results for vanadium pentoxide are given. Parts B and C contain the results of the calculations using the point multipole and the covalent models.

A. EXPERIMENTAL RESULTS

1. Sodium Orthovanadate Dodecahydrate

Figures 3 and 4 show a reproduction of the recorder trace of the V^{51} and Na^{23} resonance lines in an unoriented single crystal of sodium orthovanadate dodecahydrate. The resonance lines are unsplit and have a line width (full width at half maximum) of approximately 0.25 gauss. The chemical shift of the Na^{23} resonance line, relative to Na^{23} resonance line in an aqueous solution of sodium metavanadate was isotropic and had the value 1.5 gauss.

2. Calcium Orthovanadate

Figure 5 shows a recorder trace of the V^{51} resonance line in the γ-irradiated single crystal of calcium orthovanadate. The resonance pattern consists

Figure 3

The recorder trace of the absorption mode of the Na^{23} resonance line in sodium orthovanadate dodecahydrate. The data were taken at 8 MHz, with a magnetic field sweep of 0.25 gauss per minute and an integration line of 1 sec.

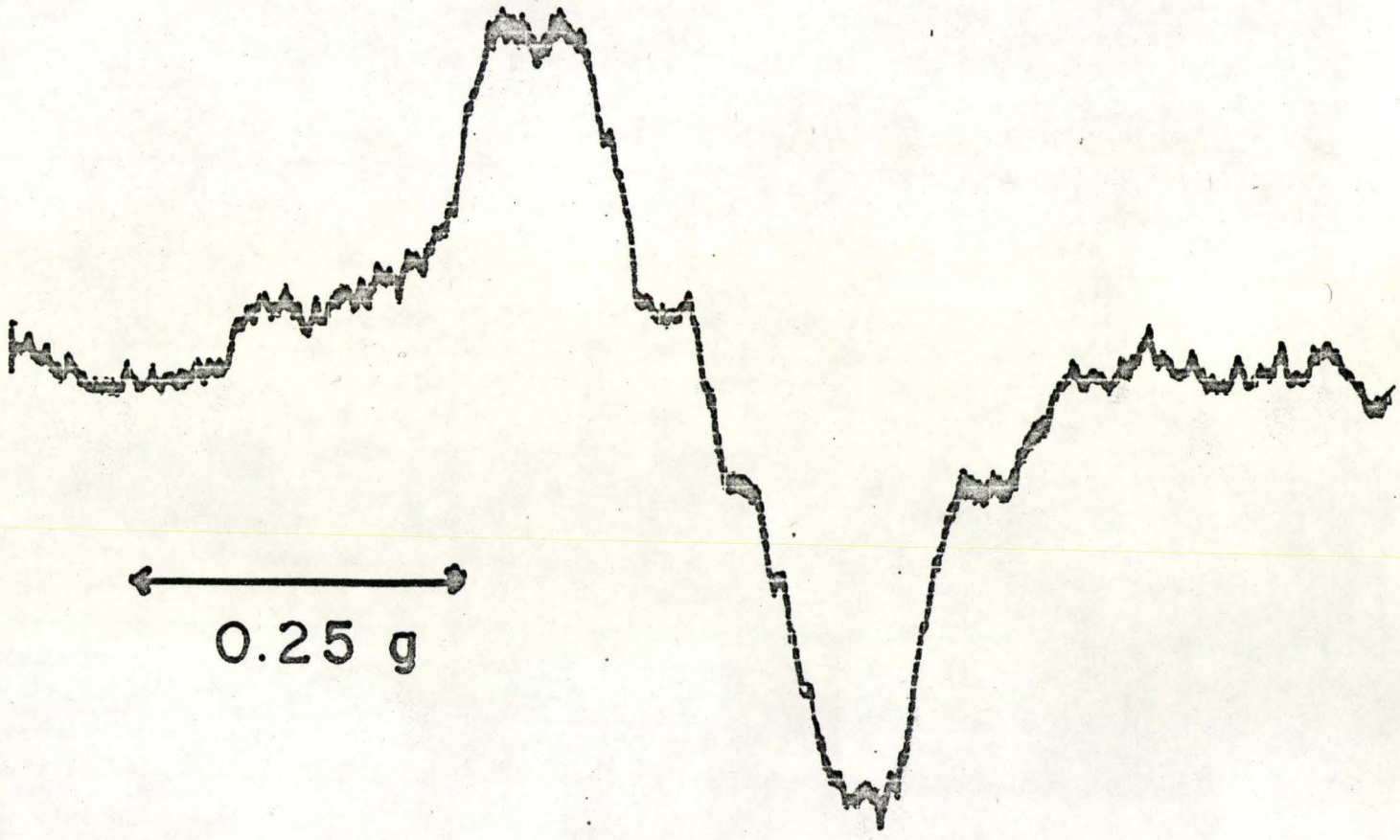

Na^{23} IN $Na_3VO_4 \cdot 12H_2O$

Figure 3

Figure 4

A trace recorder of the absorption mode of the V^{51} resonance line in sodium orthovanadate dodecahydrate. These data were taken at 8 MHz. The magnetic field was swept at 0.5 gauss per minute with an integration time of 1 sec.

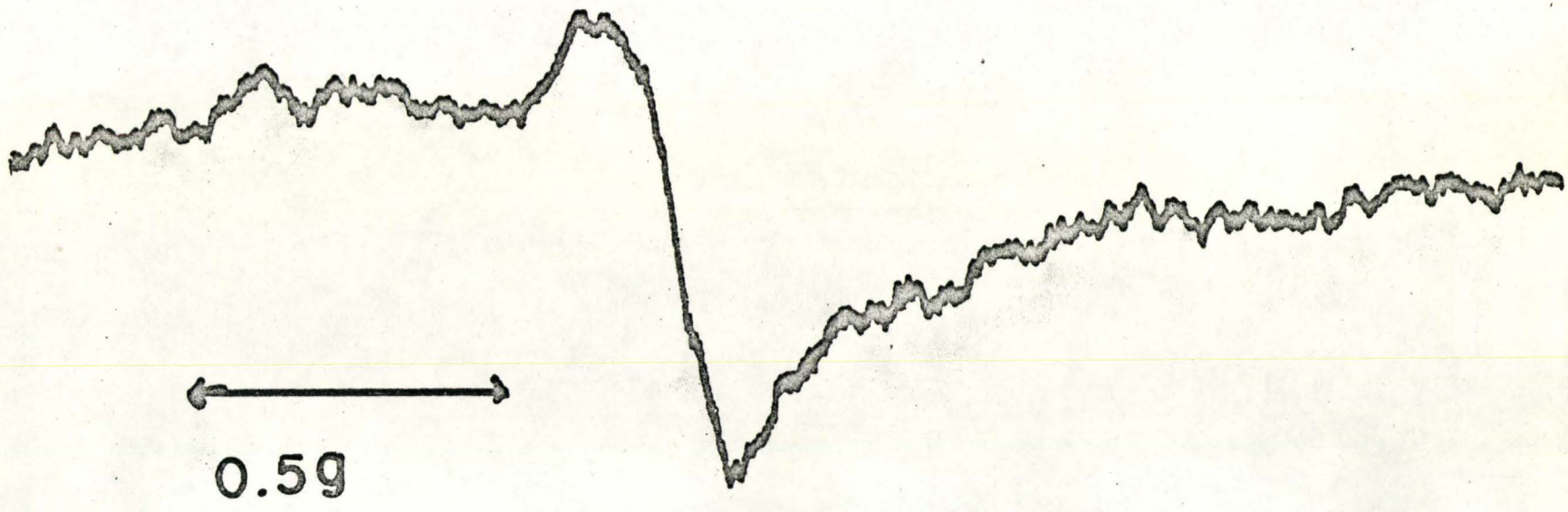

V^{5+} IN $Na_3VO_4 \cdot 12H_2O$

Figure 4

Figure 5

The dispersion mode of the V^{51} resonance line in γ irradiated calcium orthovanadate. The data were taken at 11.190 MHz, with a magnetic field sweep of 50 gauss per minute and integration time of 3 sec.

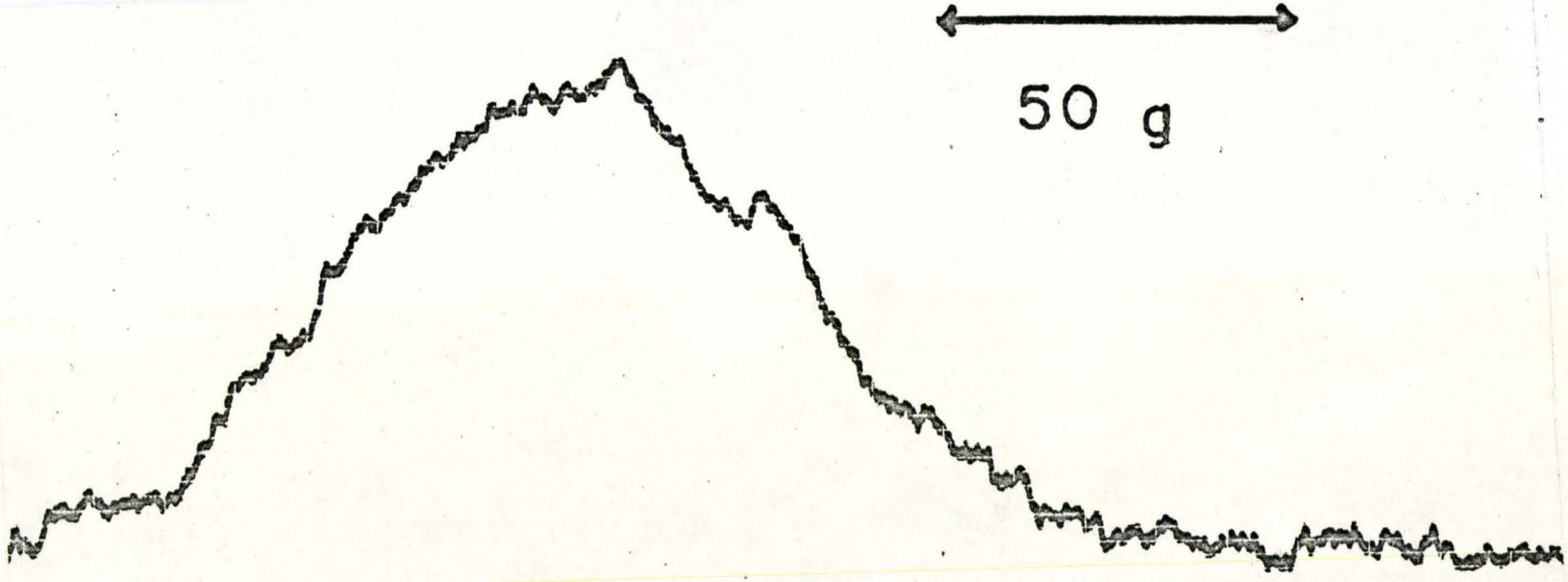

V^{51} IN $Ca_3(VO_4)_2$

Figure 5

of a single line with a width of approximately 90 gauss, which is independent of orientation. The upper limit of the V^{51} quadrupole coupling constant is 425(10) kHz.

3. Vanadinite and Descloizite

V^{51} resonance lines were observed in the two minerals,vanadinite and descloizite. The recorder traces of these resonance lines are in figures 6 and 7. No splitting of the resonance line was observed in either case. The line width of the V^{51} resonance lines is 5 gauss in vanadinite and 20 gauss in descloizite. These numbers give an upper limit of 27(10) kHz and 109(10) kHz for the V^{51} quadrupole coupling constants in vanadinite and descloizite respectively.

4. Cadmium Divanadate

The V^{51} resonance line was observed in a polycrystalline sample, and the recorder trace of the resonance is shown in Figure 8. Two pairs of satellites can be seen, while the third pair is not observed because of the noise. The separation between the satellites is 56(4) kHz . By assuming $\eta=0$, the value of 1.58(11) MHz can be assigned to the V^{51} quadrupole coupling constant in cadmium divanadate.

5. Zirconium Divanadate

A recorder trace of the V^{51} resonance line in a polycrystalline sample of zirconium divanadate is shown in Figure 9. There is a splitting of the central resonance line. Only the inner pair of satellites are observed.

Figure 6

The dispersion mode of the V^{51} resonance line in vanadinite. The frequency is 16.000 MHz and the magnetic field was swept at 10 gauss per minute. The integration time is 3 sec.

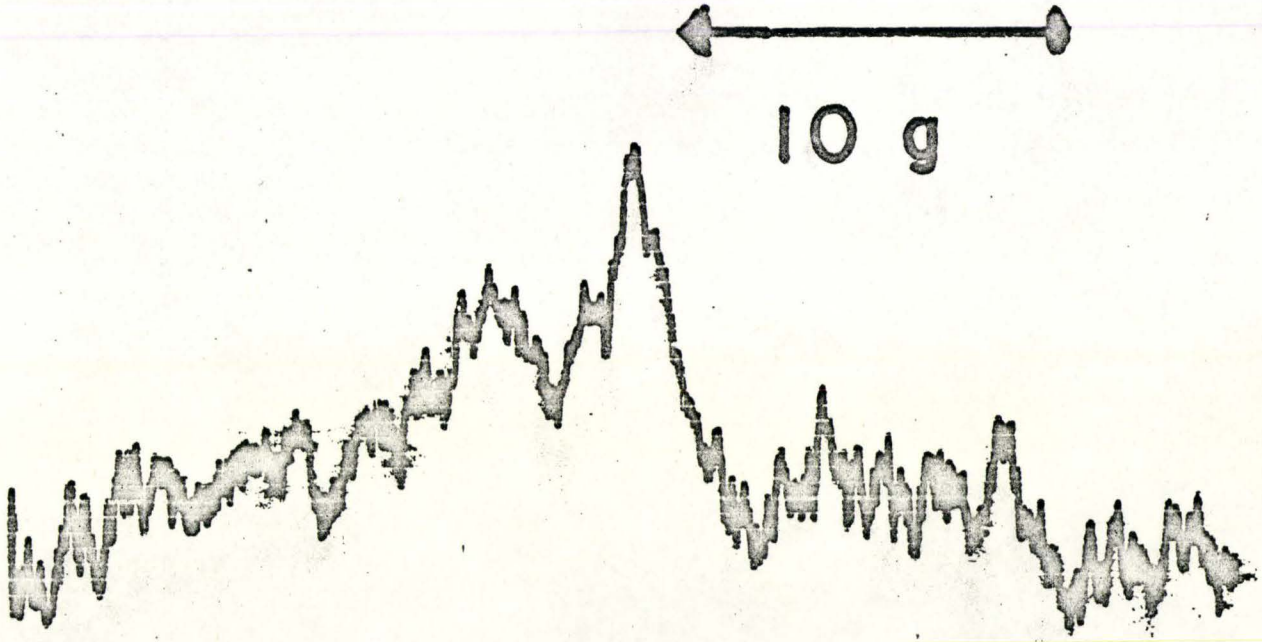

V^{5+} IN VANADINITE

Figure 6

Figure 7

The dispersion mode of the V^{51} resonance line in descloizite. The data were taken at 16.000 MHz, with a magnetic field sweep of 10 gauss per minute and an integration time of 3 sec.

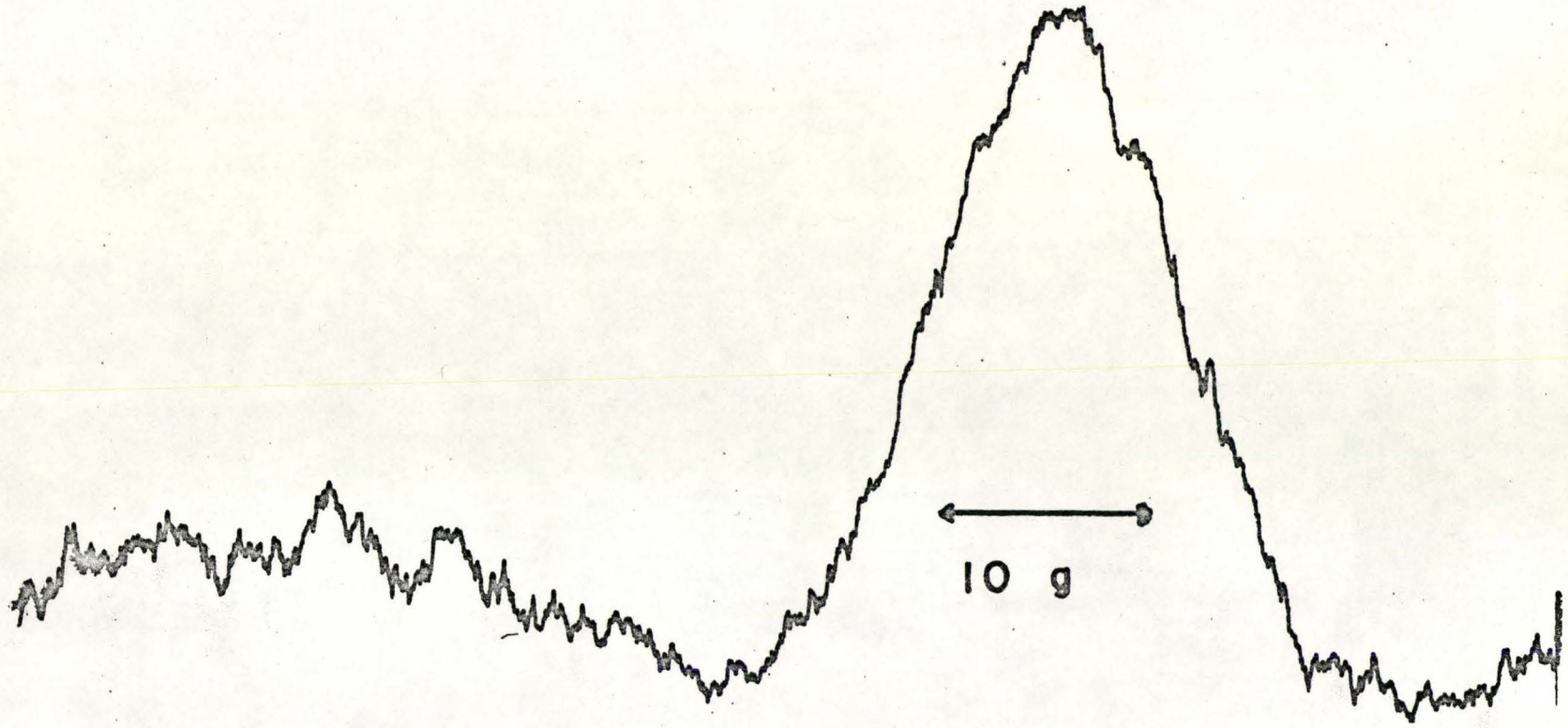

V^{51} IN DESCLOIZITE

Figure 7

Figure 8

V^{51} resonance line in polycrystalline cadmium divanadate The pairs of satellites can be seen and are indicated by the arrows. The strong resonance line between the two right satellites is the resonance line of Al^{27} nuclei in the magnetic resonance apparatus. The data were taken at 11.190 MHz, with a magnetic field sweep of 20 gauss per minute and an integration time of 3 sec.

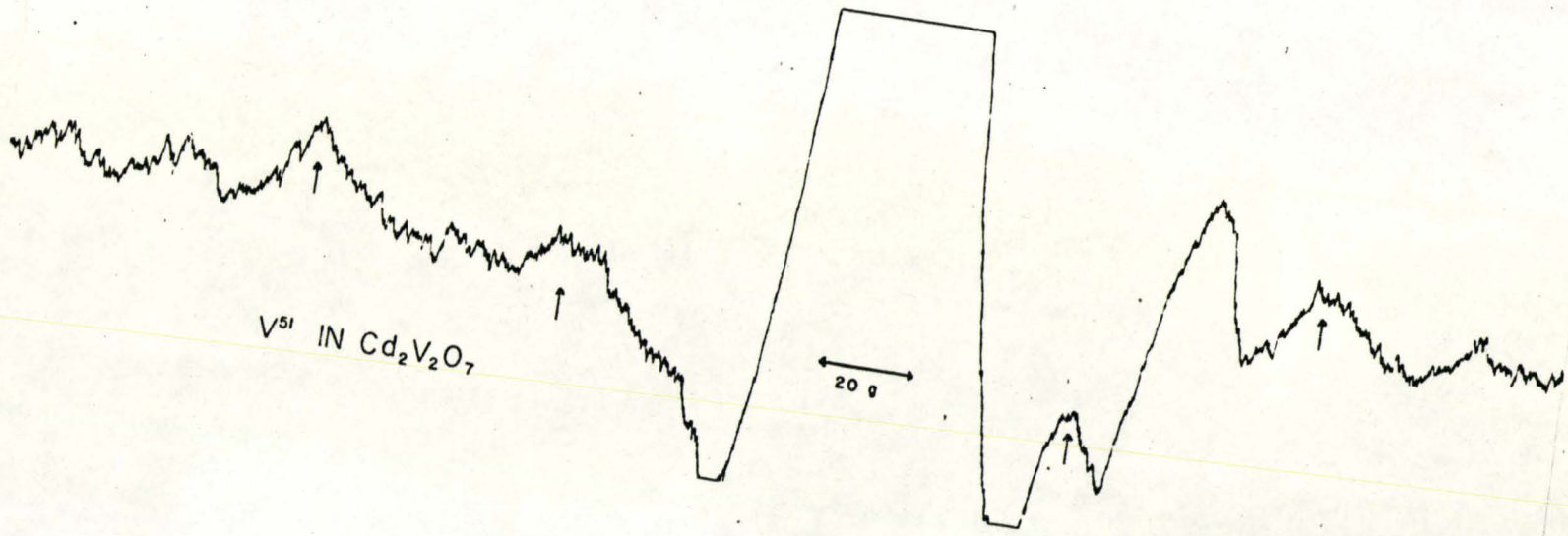

Figure 8

Figure 9

The V^{51} resonance line in polycrystalline zirconium divanadate. The two arrows show the two visible satellites. The narrow line to the right is the resonance line of the Al^{27} nuclei in the nuclear magnetic resonance apparatus. Data were taken at a constant frequency of 16.000 MHz, with a magnetic field sweep of 50 gauss per minute and an integration time of 3 sec.

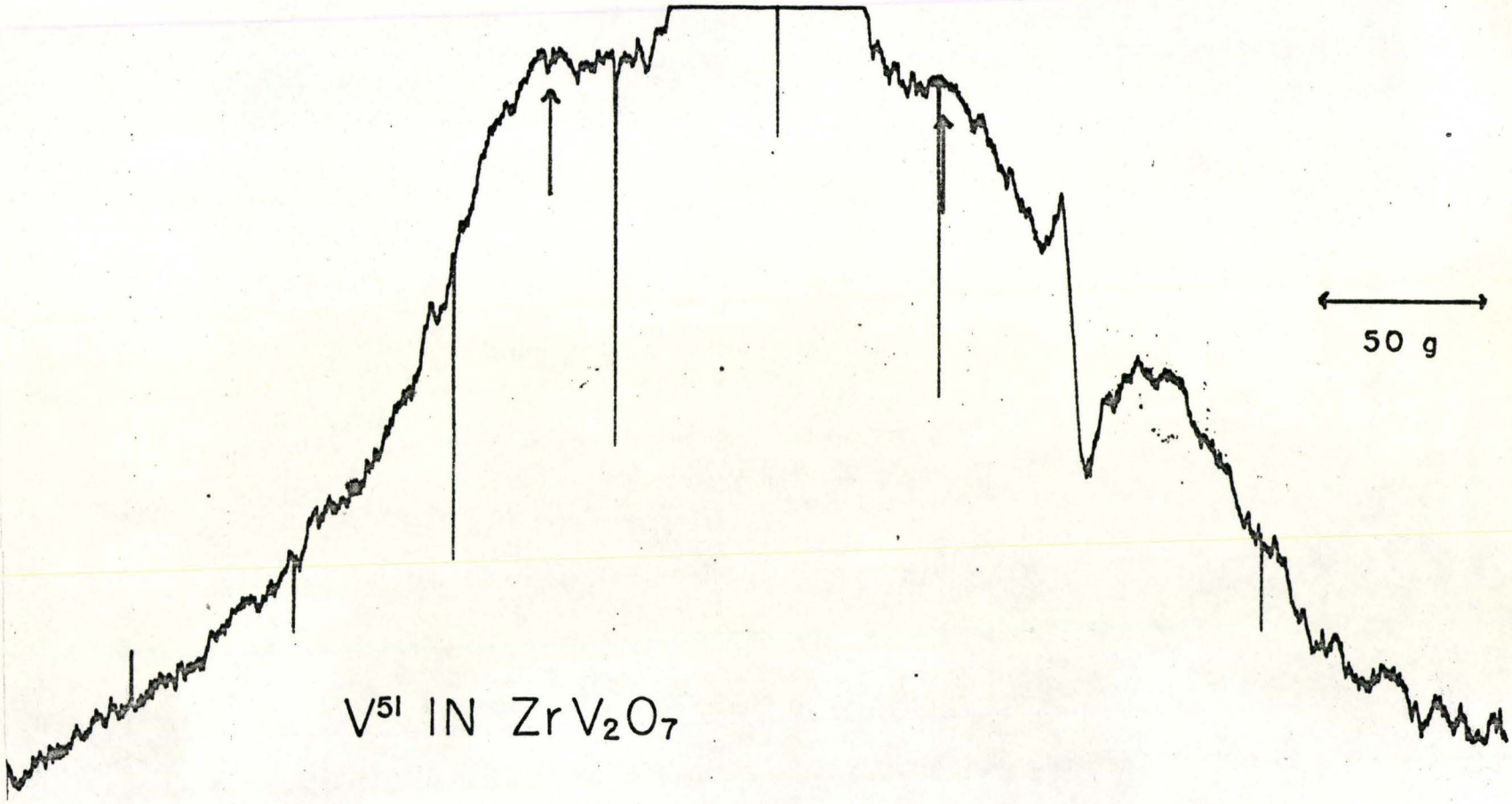

Figure 9

The separation between the satellites is 67(5) kHz. The crystal structure implies that $\eta=0$ and therefore the V^{51} quadrupole coupling constant in zirconium divanadate is 1.88(14) MHz.

6. Potassium Metavanadate

The quadrupolar interaction splits the V^{51} resonance line in potassium metavanadate. A typical recorder trace of the V^{51} resonance line in a single crystal of potassium metavanadate is shown in Figure 10. This is a spectrum in which the magnetic field is perpendicular to the crystallographic a axis. Only one magnetic site is seen. The angular dependences of the splitting of the inner pair of satellites for the magnetic field perpendicular to both the a and the c crystallographic axes are shown in Figure 11. The c axis rotation pattern shows two magnetic sites, which superimpose when the magnetic field is along the a and b crystallographic axes.

The results of the two rotation patterns are consistent, and the computed least squares fit is

c axis rotation

Site one; $\Delta\nu = 294(6) + 354(5)\cos 2[\theta-38.1(15)]$ kHz

Site two; $\Delta\nu = 250(7) + 350(1)\cos 2[\theta+39.5(15)]$ kHz

a axis rotation

$\Delta\nu = -172(2) + 355(1)\cos 2[\theta-0.00(1)]$ kHz

The numbers in parentheses are the standard deviations obtained from the computed least square fit. These results

Figure 10

V^{51} resonance lines in potassium metavanadate. The magnetic field is in the bc plane. The arrows show two pairs of satellites. The narrow line to the right of the central resonance line is the resonance line of the Al^{27} nuclei in the nuclear magnetic resonance apparatus. The data were taken at 15.375 MHz with a magnetic field sweep of 100 gauss per minute and an integration time of 3 sec.

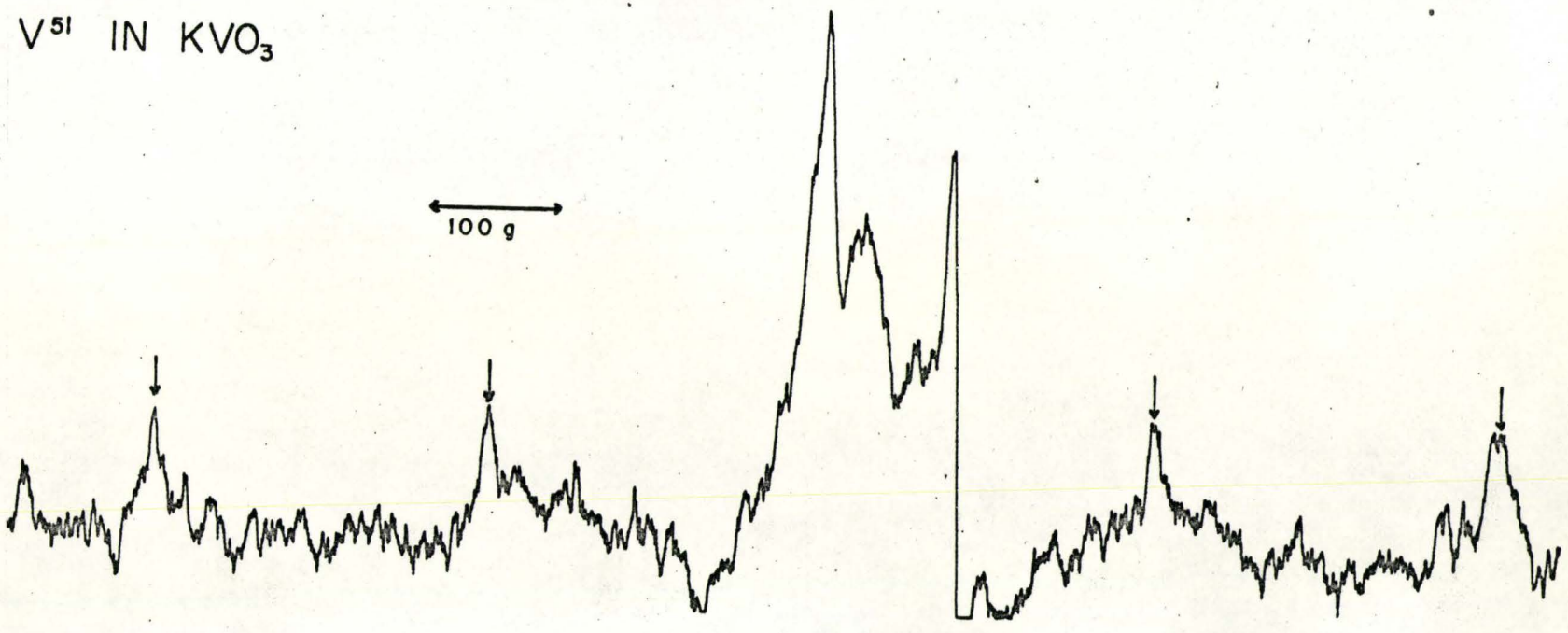

Figure 10

Figure 11

Splitting of the innermost pair of satellites of the V^{51} resonance line in potassium metavanadate. The field is in a plane perpendicular to the crystallographic a and c axes. The error bars are the experimental points. The solid curves are the least square fits and give

Site one; $\Delta\nu = 249(6) + 354(5)\cos 2[\theta - 38.1(1.5)]$ kHz

Site two; $\Delta\nu = 250(7) + 350(1)\cos 2[\theta + 39.5(1.5)]$ kHz

a axis rotation

$$\Delta\nu = -172(2) + 355(1)\cos 2\theta \text{ kHz}$$

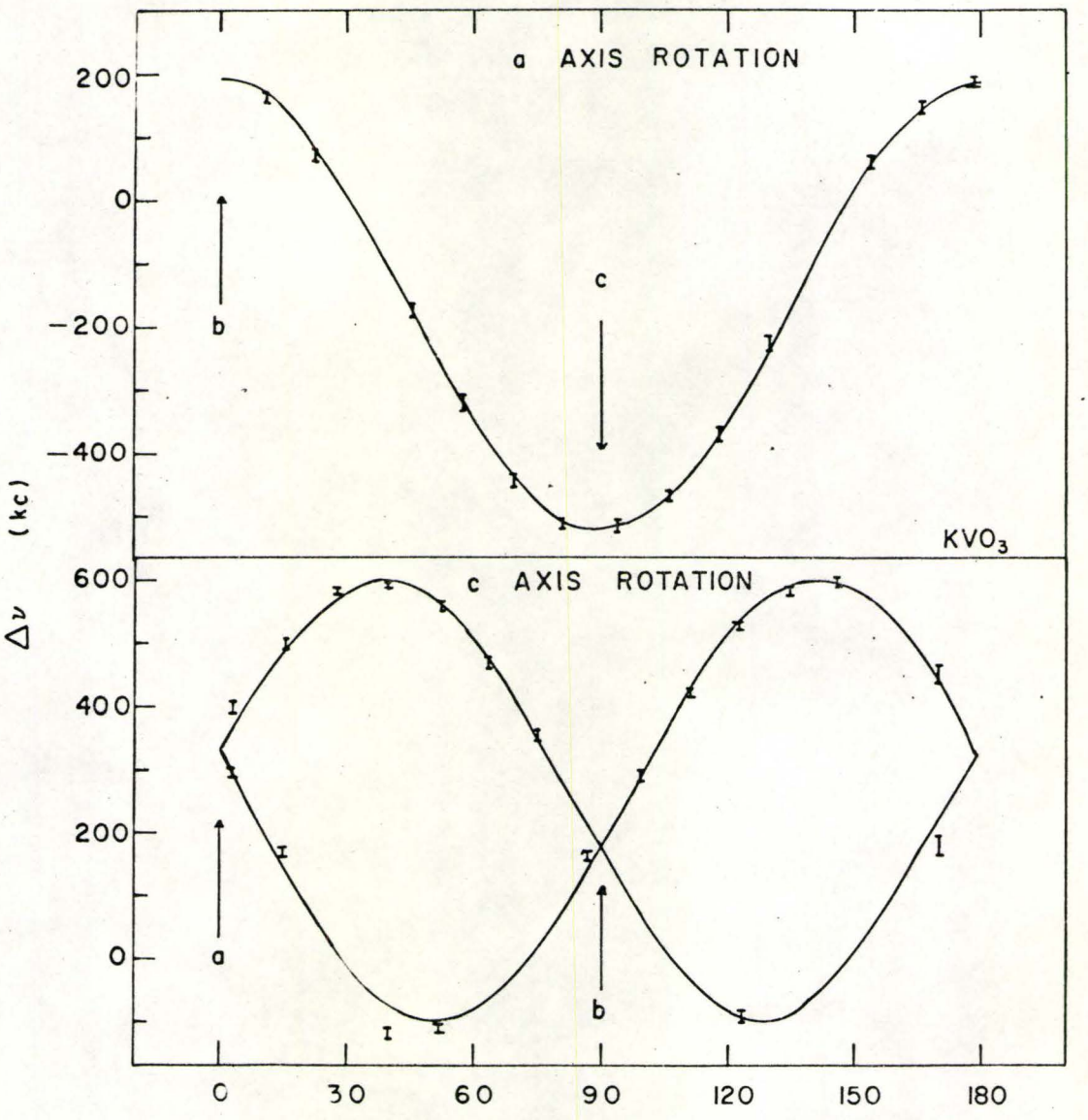
a AXIS ROTATION
200
0
-200
-400
b
c
KVO3
c AXIS ROTATION
600
400
200
0
a
b
Δν (kc)
0
30
60
90
120
150
180

Figure 11

give the value 4.22(15)MHz for the V^{51} quadrupole coupling constant in potassium metavanadate and an anisotropy factor η of 0.65(15).

The X principal axis is along the crystallographic c axis, while the Z principal axis is at an angle of $\pm$ 39(2)° from the crystallographic a axis in the ab plane. The ambiguity in the orientation of the z principal axis arises from the two magnetic sites which are present when the magnetic field is perpendicular to the crystallographic c axis.

The V^{51} resonance lines in potassium metavanadate are very broad, approximately 15 gauss. A possible explanation is an interaction of the V^{51} nucleus with the electronic magnetic moments of V^{4+} and V^{3+} ions in the sample caused by non-stochiometry of the sample.

7. Vanadium Pentoxide

The V^{51} resonance line in vanadium pentoxide splits because of the quadrupolar interaction. A typical recorder trace is shown in Figure 12, where the magnetic field is perpendicular to the crystallographic c axis. Two magnetic sites can be seen. However, one of them is poorly resolved from the central resonance line in this orientation.

Two rotational patterns were recorded. In one, the magnetic field was perpendicular to the crystallographic c axis, and a second was taken when the magnetic field was perpendicular to the crystallographic a axis. The angular dependence of the inner pair of satellites for each of the

Figure 12

A typical recorder trace of the V^{51} resonances in vanadium pentoxide. The field is perpendicular to the c axis. The seven arrows indicate the V^{51} lines from one site. The lines caused by the other site are poorly resolved from the central line in this orientation. The data were taken at 16.000 MHz with a magnetic field sweep of 20 gauss per minute and an integration time of 3 sec.

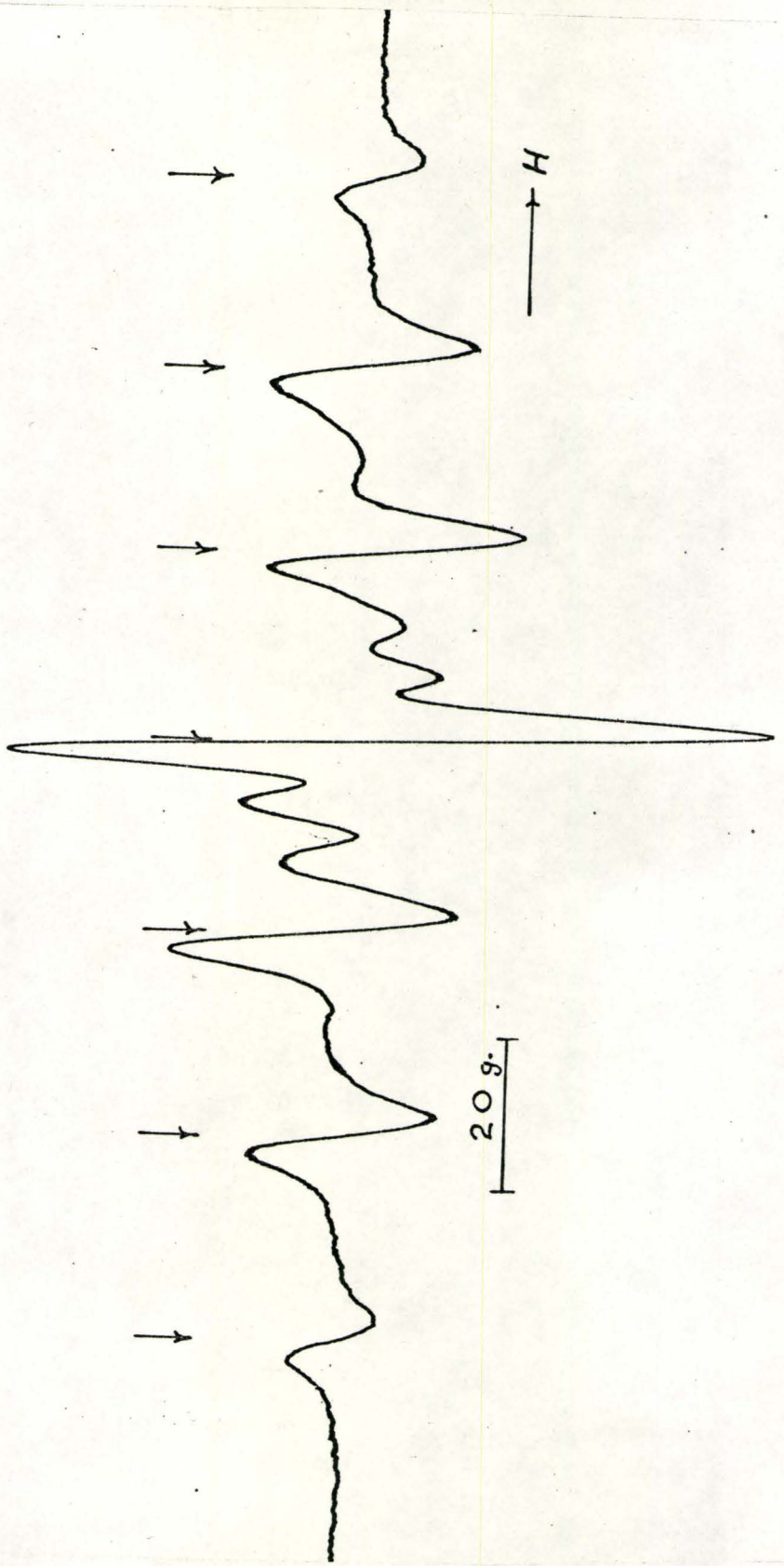

Figure 12

rotation patterns is shown in Figures 13 and 14. The computed least squares fit for these two rotation patterns is given by the following expressions

c axis rotation

Site one; $\Delta\nu = 27.6(4) + 87.5(5)\cos 2[\theta - 1.2(2)]$ kHz

site two; $\Delta\nu = 27.5(4) + 87.1(4)\cos 2[\theta - 87.6(2)]$ kHz

a axis rotation

$\Delta\nu = -11.3(13) + 46.0(1)\cos 2[\theta - 23.6(1)]$ kHz

The numbers in parentheses are the standard deviations obtained from the least square fit.

The two rotation patterns are consistent and show that one of the principal axes coincides with the crystallographic c axis within 0.5^{o}. Coincidence of the axes would imply that the space group of vanadium pentoxide is Pmnm.

Since the crystallographic c axis is a principal axis, the first rotation pattern is sufficient to determine the quadrupole coupling constant of V^{51} in vanadium pentoxide. $\frac{eqQ}{h}$ is 805(6) kHz and the anisotropy factor η is 0.04(1). The Y principal axis is found to coincide with the crystallographic c axis, while the Z principal axis is at an angle of $\pm$ 44.4(4) from the crystallographic a axis in the ab plane. The orientation of the Z principal axis is shown in Figure 15.

The shift of the central V^{51} resonance line is a sum of two terms. One is the chemical shift, and is proportional to H_o, the applied magnetic field. The second term is proportional to $1/H_o$ and is caused by the quadrupolar interaction

Figure 13

Separation of the innermost satellites of the V^{51} resonance line in vanadium pentoxide, as a function of the rotation angle around the c crystallographic axis. The arrows indicate when the magnetic field is along the a and b crystallographic axes. The solid curves are the least square fits

Site one; $\Delta\nu = 27.6(4) - 87.5(5)\cos 2[\theta - 1.2(2)]$

Site two; $\Delta\nu = 27.5(4) + 871.(4)\cos 2[\theta - 87.6(2)]$

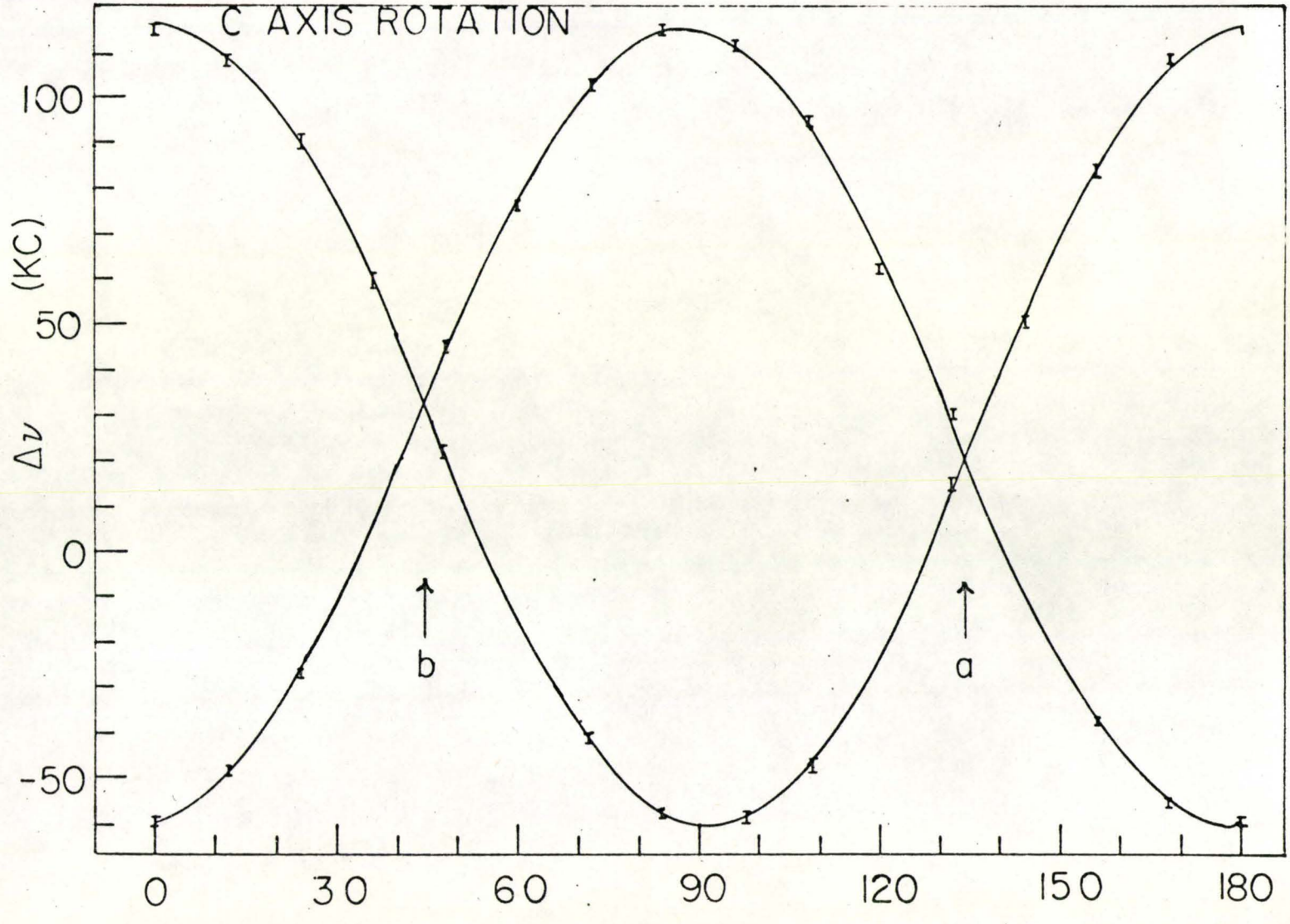

Figure 13

Figure 14

Separation of the innermost satellites of the V^{51} resonance line in vanadium pentoxide for rotation around the a axis. The solid curve is

$$\Delta\nu = -11.3(13) + 46.0(1)\cos 2[\theta + 23.6(1))]\text{kHz}.$$

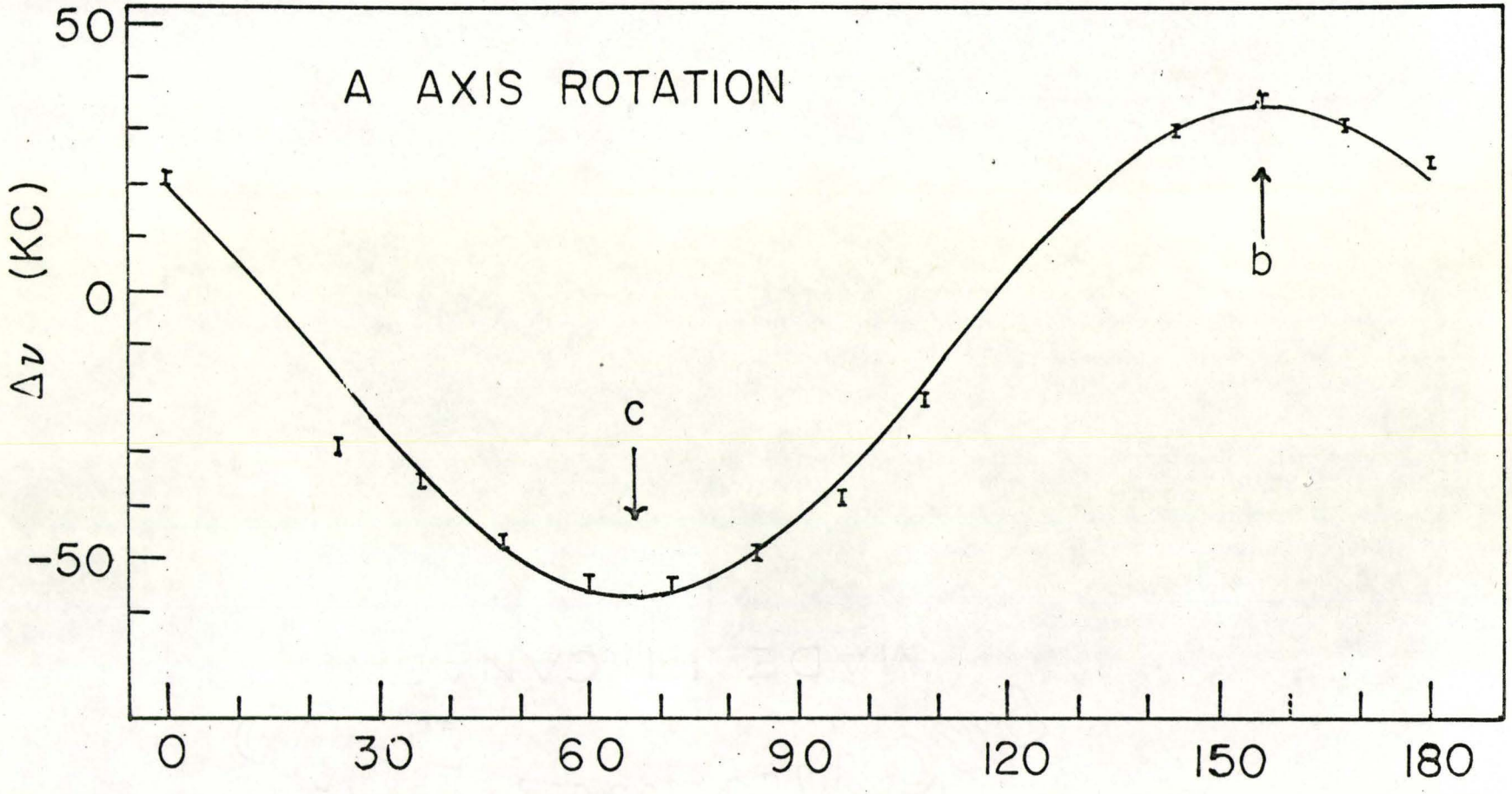

Figure 14

Figure 15

Environment of the V^{5+} ion in vanadium pentoxide, projected in the ab plane. The open circles are oxygen ions and the small full circle is the vanadium ion. The arrows are the two principal axes of the quadrupole coupling tensor in this plane.

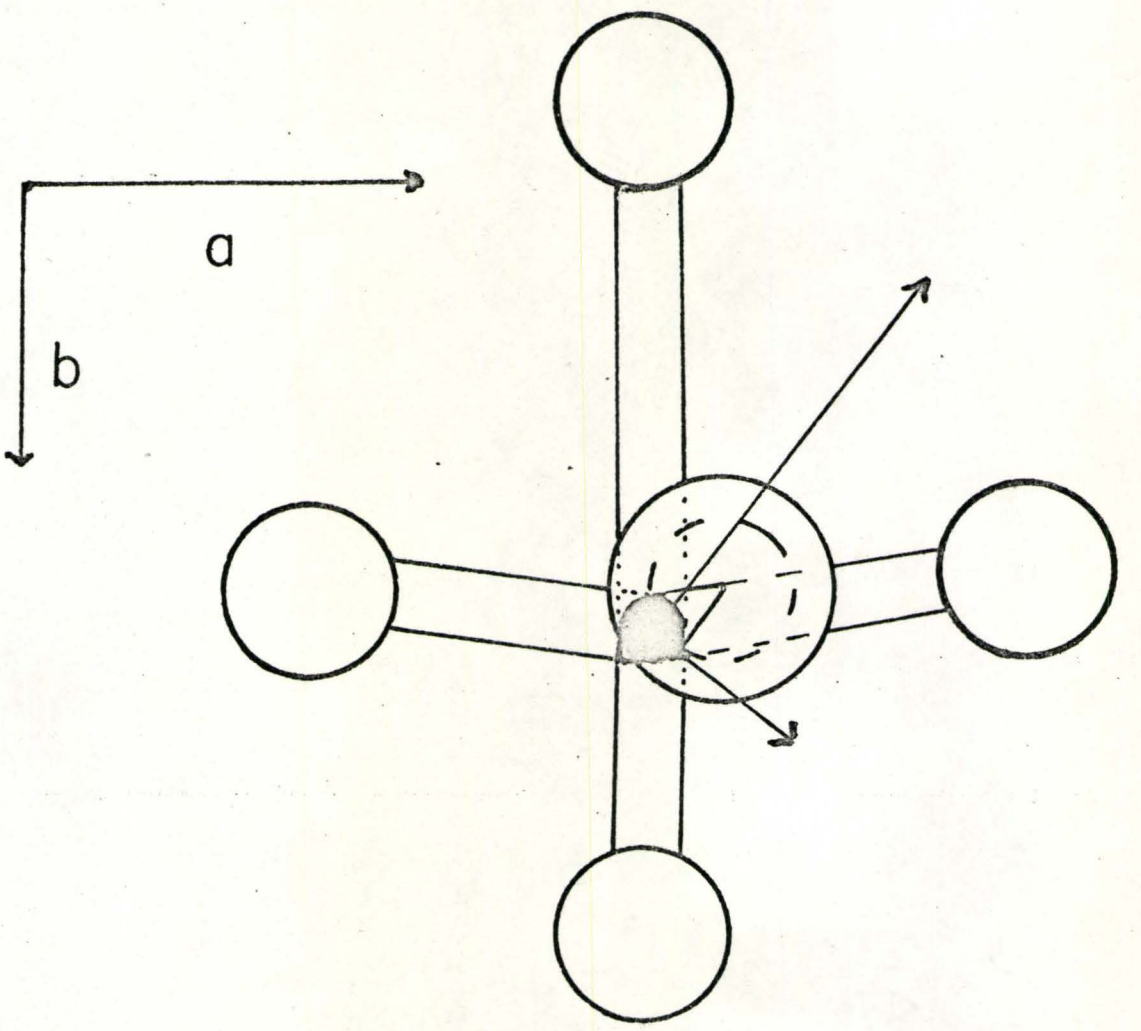

Figure 15

in second order.

Figure 16 shows the shift of V^{51} resonance line in vanadium pentoxide relative to a V^{51} resonance line in an aqueous solution of sodium orthovanadate as a function of the applied magnetic field. The bars show the total shift, while the triangles show the total shift minus the second order quadrupolar contribution. The error bars were excluded from the triangles for the sake of clarity. The corrected values lie on a straight line that can be extrapolated to the origin, as would be expected from a pure chemical shift contribution. Data for the anisotropy of the chemical shift tensor were taken at a constant frequency of 16.000 MHz and the quadrupolar contribution to the shift was neglected. Rotation patterns were taken in which the magnetic field was perpendicular to the crystallographic a and c axes. These two rotation patterns are shown in Figure 17. The computed least square fit gives the following results.

For the c axis rotation

$$\Delta H = 3.3(2) + 5.9(4)\cos 2[\theta - 45.7(19)] \text{ gauss}$$

For the a axis rotation

$$\Delta H = 2.6(2) + 6.9(2)\cos 2[\theta - 62.3(26)] \text{ gauss}$$

The three eigenvalues of the chemical shift tensor are obtained from these expressions by the use of equations (2-20) and (2-21) given in Chapter II. The three eigenvalues are $\sigma_{xx} = -1.8(4) \times 10^{-4}$, $\sigma_{yy} = 6.5(3) \times 10^{-4}$, $\sigma_{zz} = -3.0(3) \times 10^{-4}$

Figure 16

Shift of the central line of the V^{51} resonance pattern in vanadium pentoxide, relative to a solution of sodium orthovanadate. The vertical bars are the experimental data. The triangles give the result of subtracting the second order quadrupole shift from the experimental points.

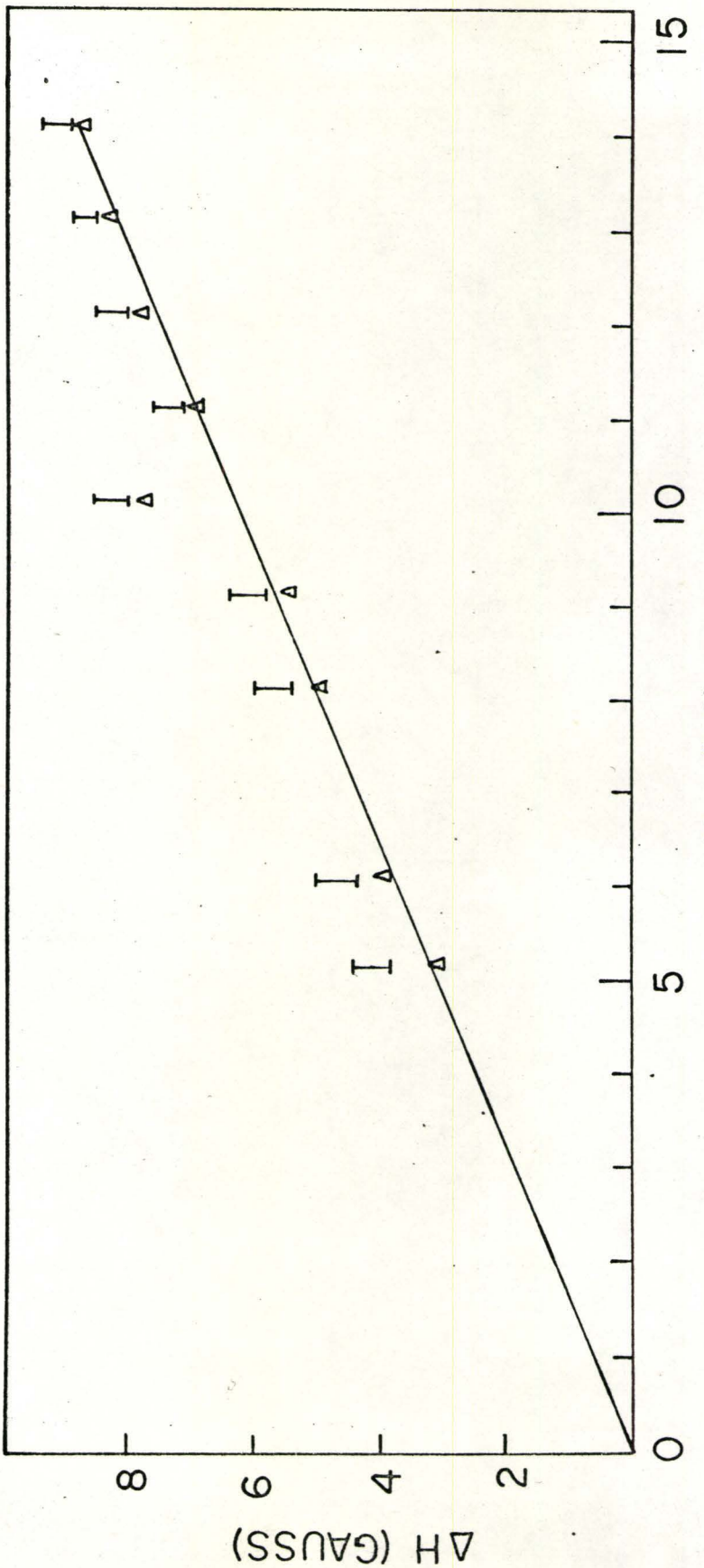

Figure 16

Figure 17

Chemical shift of the central resonance line of V^{51} in vanadium pentoxide for rotation around the a axis (upper) and c axis (lower). The least square fits are

a axis rotation; $\Delta H = 2.6(2)+6.9(2)\cos 2[\theta-45.7(19)]$ gauss

c axis rotation; $\Delta H = 3.3(2)+5.9(4)\cos 2[\theta+62.3(26)]$

The data were taken at 16.000 MHz.

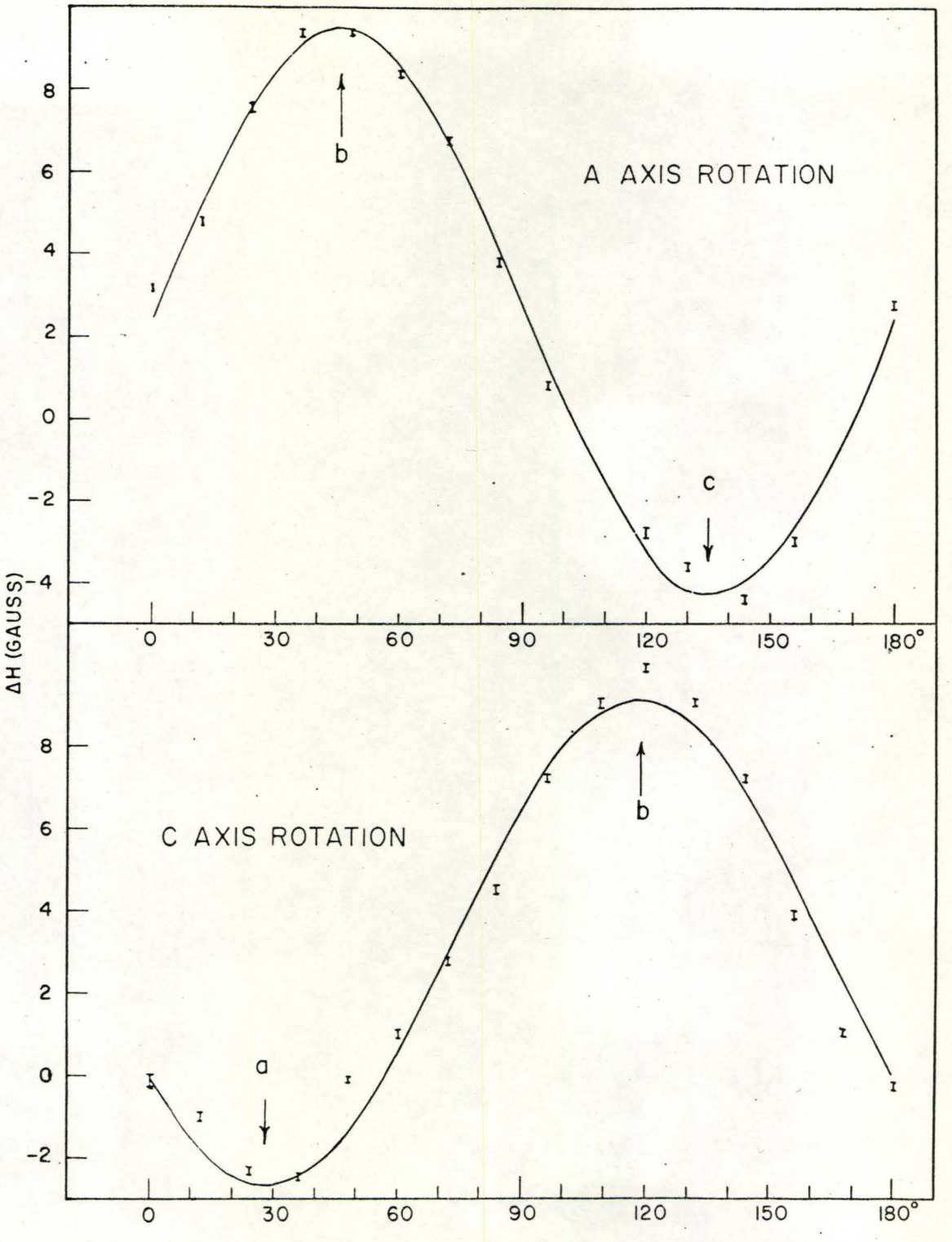
A AXIS ROTATION
C AXIS ROTATION
ΔH (GAUSS)
8
6
4
2
0
-2
-4
0
30
60
90
120
150
180°
a
b
c

Figure 17

TABLE 2

Summary of the experimental values of the quadrupole coupling constants and the electric field gradients

Compound	Nucleus	$\frac{eqQ}{h}$(MHz)	η	$q \times 10^{-14}$ (e.s.u) [a]
$Na_2VO_4 \cdot 16H_2O$	Na^{23}	<0.001	-	<0.0006
$Na_3VO_4 \cdot 16H_2O$	V^{51}	<0.001	-	<0.0006
$Ca_3(VO_4)_2$	V^{51}	<0.425(10)	-	<0.260(6)
Descloizite	V^{51}	<0.109(10)	-	<0.067(6)
Vanadinite	V^{51}	<0.027(10)	-	<0.017(6)
$Cd_2V_2O_7$	V^{51}	1.58(6)	0[b]	0.97(4)
ZrV_2O_7	V^{51}	1.88(14)	0[b]	1.16(8)
KVO_3	V^{51}	4.22(15)	0.65(15)	2.60(9)
V_2O_5	V^{51}	0.802(6)	0.04(1)	0.495(4)

[a] based on $\gamma_\infty = -3.5$

[b] assumed value.

The Z principal axis of the chemical shift tensor is constrained to be along the crystallographic c axis. The X and Y principal axes coincide with the crystallographic a and b axes within an experimental error of 2.0°.

There are two conflicting reports about the magnetic susceptibility of vanadium pentoxide. It was measured again. The susceptibility was found to be paramagnetic and temperature independent from $4.2^{\circ}K$ to $300^{\circ}K$. The anisotropy of the magnetic susceptibility at $300^{\circ}K$ for the magnetic field perpendicular to the crystallographic c axis is shown in Figure 18. The computed least square fit to the experimental data is given by

$$\chi = 0.62(1) + 0.31(3)\cos 2[\theta + 71.7(30)]$$

in arbitrary units.

B. POINT MULTIPOLE MODEL

1. Cadmium Divanadate

The space group of cadmium divanadate shows that the vanadium ions are situated on a mirror plane perpendicular to the crystallographic b axis. If the electric field gradient is defined in a coordinate system such that the x axis coincides with the crystallographic a axis, y with the crystallographic b axis and z with the crystallographic c^{*} axis, then the E_{xy} and E_{yz} components vanish. Summations for the other components included contributions from the 5632 nearest ions. The charge of the cadmium ion was fixed at a value of +2.0, while the charge on the oxygen ions was varied from -2.0 to

Figure 18

The magnetic susceptibility of vanadium pentoxide (in arbitrary units) for an applied magnetic field perpendicular to the crystallographic c axis. The solid line is

$$\chi = 0.62(1) + 0.31(3)\cos 2[\theta + 71.7(30)] \text{ arbitrary units}$$

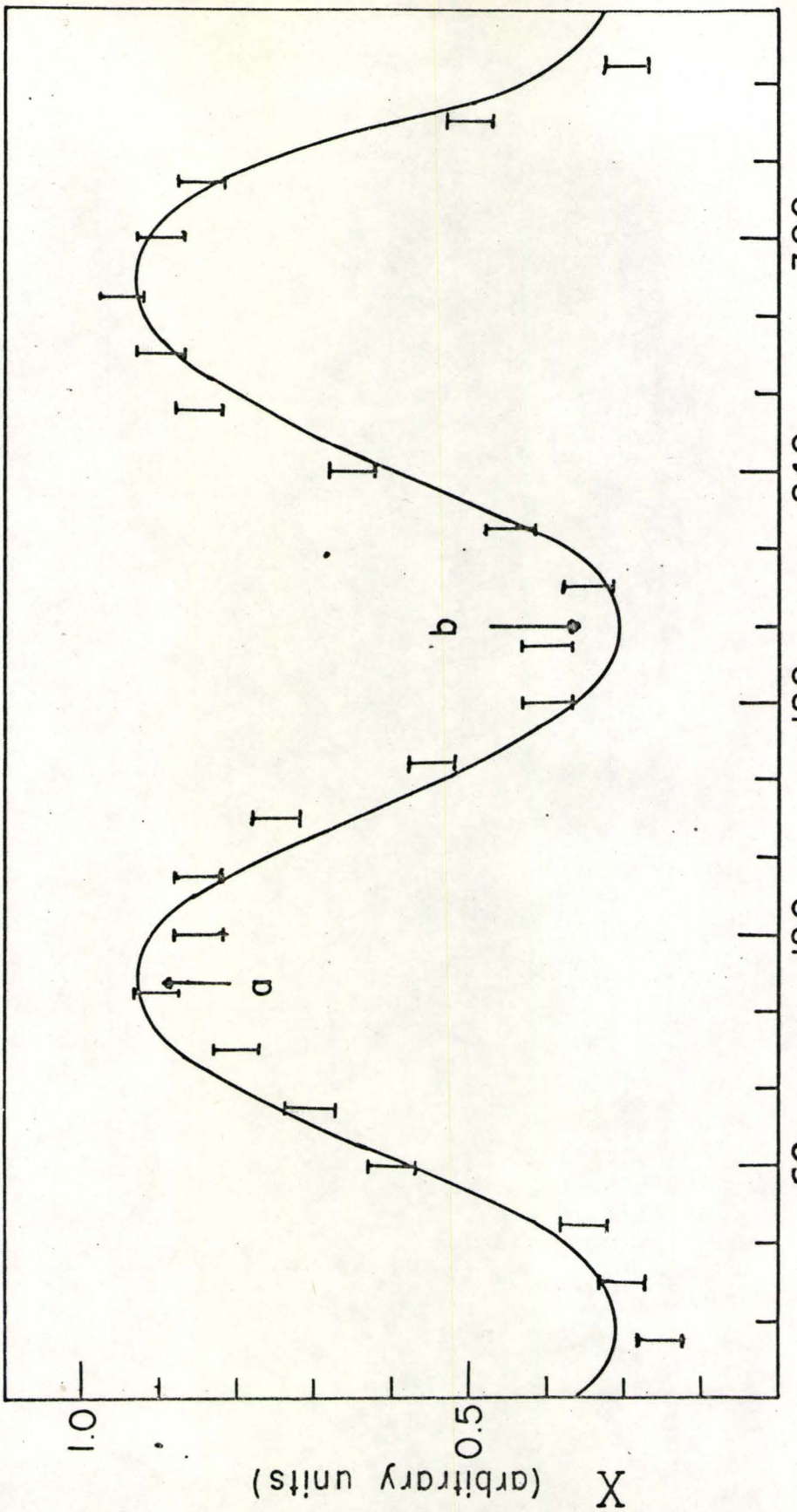

Figure 18

-1.0. The charge on the vanadium is determined by the requirement that the crystal be neutral. The position of the ions in the unit cell are given in Table 3, and the results for different effective charges are given in Table 4.

2. Potassium Metavanadate

The space group of potassium metavanadate is Pabm. In this space group the vanadium ion is situated on a mirror plane perpendicular to the crystallographic c axis. In a coordinate system in which the x, y and z axes are parallel to the crystallographic a, b and c axes respectively, the components E_{xz} and E_{yz} of the field gradient tensor vanish. Contributions from the 13,824 nearest ions were included in the calculations of the electric field gradient at the vanadium site. The effective charges on the oxygen ions were varied between -0.5 and -2.0. The charge on the potassium ion was fixed at +1.0. The positions of the ions in the unit cell are given in Table 5 and the results for the various effective charges are given in Table 6.

3. Vanadium Pentoxide

The experimental results of the quadrupole coupling tensor verified the space group of vanadium pentoxide to be Pmnm. In a coordinate system, xyz, in which the axes are parallel to the crystallographic a, b and c axes respectively, the components E_{xz}, and E_{yz} of the electric field gradient tensor vanish. The non-zero components of the electric field gradient tensor included contributions from point charges

TABLE 3

The fractional coordinates of the atoms in the unit cell of cadmium divanadate. The enumeration of the oxygens follows figure 2-a

	x/a	y/b	z/c
Cd	0.0000	0.3051	0.5000
	0.5000	0.8051	0.5000
	0.0000	0.6949	0.5000
	0.5000	0.1949	0.5000
V	0.2264	0.0000	0.9089
	0.7264	0.5000	0.9089
	0.7736	0.0000	0.0911
	0.2736	0.5000	0.0911
O_1	0.2372	0.1568	0.7198
	0.7372	0.6568	0.7198
	-0.2372	-0.1568	-0.7198
	0.2628	0.3432	-0.7198
	0.2372	-0.1568	0.7198
	0.7372	0.3432	0.7198
	-0.2372	0.6568	-0.7198
	0.2628	0.6568	-0.7198
O_2	0.3877	0.0000	0.2131
	0.8877	0.5000	0.2131
	0.6123	0.0000	0.7869
	0.1123	0.5000	0.7869
O_3	0.0000	0.0000	0.0000
	0.5000	0.5000	0.0000

TABLE 4

The results of the point charge calculations of the field gradient tensor at the vanadium site in calcium divanadate

Charge on V	Charge on O	η	$q \times 10^{-14}$ e.s.u.
+ 5.00	-2.00	0.84	0.95
+ 3.25	-1.50	0.32	0.72
+ 1.50	-1.00	0.69	0.41

TABLE 5

The fractional coordinates of the atoms in the unit cell of potassium metavanadate. The enumeration of the oxygens follows figure 2-a

	x/a	y/b	z/c
K	0.9371	0.3948	0.2500
	0.0629	0.6052	0.7500
	0.0629	0.8948	0.2500
	0.9371	0.1052	0.7500
O_1	0.1600	0.1480	0.2500
	0.8400	0.8520	0.7500
	0.8400	0.6480	0.2500
	0.1600	0.3520	0.7500
O_2	0.5870	0.2500	0.0000
	0.4130	0.7500	0.0000
	0.5870	0.2500	0.5000
	0.4130	0.7500	0.5000
O_3	0.6060	0.0230	0.2500
	0.3940	0.9770	0.7500
	0.3940	0.5230	0.2500
	0.6060	0.4770	0.7500

TABLE 6

The results of a point charge calculations of the field gradient tensor at the vanadium site in potassium metavanadate

Charge on V	Charge on O	δ[1]	η	$q \times 10^{-14}$ e.s.u.
+ 5.0	- 2.0	- 9.4	0.36	2.0
+ 3.5	- 1.5	-12.5	0.26	1.4
+ 2.0	- 1.0	-23.6	0.03	0.8
+ 0.5	- 0.5	20.1	0.4	0.3

[1] δ is the angle between the Z principal axis and the crystallographic a axis in the ab plane.

and from the electric dipole moments on the oxygen ions.

Contributions from the 7840 nearest ions were included in the point charge calculations. The positions of the ions in the unit cell are given in Table 7 and the results of the point charge calculations for various effective charges are given in Table 8. The dipolar contributions to the field gradient were calculated by using equation (2-33). The dipole moments were calculated by using equation (2-27) with a a value of the electric polarizability of 2.63 $\mathring{A}^{(71)}$. The electric field was calculated by using equations (2-29) and (2-26).

A very slow convergence of the sum in equation (2-26) was achieved by excluding all contributions to the electric field from ions that are related by symmetry operations and have a zero total contribution to the electric field. Even then contributions from the 64,064 nearest ions were needed. Thirteen iterations were needed for the calculation of the total electric field at the oxygen site. The sum of the point charge and electric dipole contributions are given in Table 8. The dipolar contributions were based on a charge of +5 for the vanadium ion and -2 for the oxygen ions. Only polarization at the oxygen ions was considered.

C. COVALENT MODEL

In the calculations of the radial part of the various expectation values, $\alpha_\ell(gLM|ar)$ is needed. This is the partial radial part of order ℓ of the expansion of the ligand wavefunction around the central ion. The values

TABLE 7

The fractional coordinates of the atoms in the unit cell of vanadium pentoxide. The enumeration of the oxygens follows figure 2-b

	x/a	y/b	z/c
V	0.1487	0.1086	0.0000
	0.8513	0.1086	0.0000
	0.3513	0.8914	0.5000
	0.6487	0.8914	0.5000
O_1, O_2 and O_5	0.1808	0.0026	0.5000
	0.8192	0.0026	0.5000
	0.3192	0.9974	0.0000
	0.6808	0.9974	0.0000
O_3	1.0000	0.9969	0.0000
	0.5000	0.0031	0.5000
O_4	0.1460	0.4713	0.0000
	0.8540	0.4713	0.0000
	0.3540	0.5287	0.5000
	0.6460	0.5287	0.5000

TABLE 8

The results of the point multipole calculations of the field gradient tensor at the vanadium site of vanadium pentoxide

Charge on V	Charge on O	δ[1]	η	$q \times 10^{-14}$ e.s.u.
+ 5	- 2.0	-12.5°	0.05	2.43
+ 4	- 1.6	-12.5°	0.05	1.95
+ 3	- 1.2	-12.5°	0.05	1.46
+ 1	- 0.4	-12.5°	0.05	0.49
+ 3.875	- 1.75[2] - 2.0[2] - 1.0[2]	1.15°	0.28	1.30
Total[3]		21.17°	0.38	55.2

[1] δ is the angle between the Z principal axis and the crystallographic a axis in the ab plane.

[2] Three charges belonging to three inequivalent oxygens in the unit cell.

[3] The field gradient due to point charges and dipole moments.

of $\alpha_\ell(gLM|ar)$ for L = 1 M = 0 $\ell \leq 4$ are given in Appendix A. The calculations of the expectation values of $\frac{1}{r^3}$ and the overlap integrals were done numerically on an IBM 7040 computer using a double precision technique. A double precision technique was used because the calculations involve the differences of large numbers. Appendix B shows the variation of the expectation values of $\frac{1}{r^3}$ as the central ion-ligand distance is increased. Also shown in Appendix B are the magnitudes of the average values of $\frac{1}{r^3}$ for the values of ℓ from 0 to 4. Each term is reduced by approximately an order of magnitude as ℓ increases, and therefore, the most important term is given by ℓ=0. All the calculations used vanadium 3d and 4s Hartree-Fock[12] wavefunctions and 4p Slater orbitals. The oxygen was considered as singly ionized and only $2p_z$ Hartree-Fock wavefunctions were used. Appendix C gives the values of $\langle Y_\ell^m | C_2^q | Y_{\ell'}^{m'} \rangle$ that were needed for the angular part of the integrations. The rotation group elements for the Euler angles defined in Figure 2 are given in Appendix D.

1. Cadmium Divanadate

The anion in cadmium divanadate is a $V_2O_7^{4-}$ group, which is composed of two VO_4 groups sharing one oxygen. Referring to Figure 2-a, O_3 is the shared oxygen. There is also a mirror plane defined by O_3-O_2-V. The z axis of the field gradient tensor was chosen to be along the V-O_3-V

chain and the x axis is perpendicular to the mirror plane. The vanadium-oxygen bond distances for cadmium divanadate are given by[46]

$$V\text{-}O_3 = 1.764(4)\,\text{Å}$$
$$V\text{-}O_4 = V\text{-}O_1 = 1.672(32)\,\text{Å}$$
$$V\text{-}O_2 = 1.717(16)\,\text{Å}\ .$$

The overlap integrals and the expectation values of $\frac{1}{r^3}$ for ligands at the above distances from the central ion are given in Tables 9 and 10.

A VO_4 group was considered in this model . It was treated as a slightly distorted tetrahedron. As only radial distortions are considered and the charge transfer coefficient is assumed to be independent of the bond length the local contributions vanish. In atomic units, the contributions from the non-local terms to the field gradient tensor are given by:

Contributions from O_1 and O_4,

$$\frac{\lambda}{1+\lambda^2-0.236\lambda}\begin{pmatrix} 2.181 & 0 & 0 \\ 0 & -3.216 & 2.547 \\ 0 & 2.547 & 1.035 \end{pmatrix}$$

Contributions from O_2

$$\frac{\lambda}{1+\lambda^2-0.270\lambda}\begin{pmatrix} -0.990 & 0 & 0 \\ 0 & 1.512 & -1.167 \\ 0 & -1.167 & -0.522 \end{pmatrix}$$

TABLE 9

Overlap integrals for the various ligand-central ion distances in cadmium divanadate

	4s	4p	3d
	a = 3.161 a.u.		
$\ell=0$	-0.546	-	-
$\ell=1$	-	0.340	-
$\ell=2$	-	-	-0.107
	a = 3.246 a.u.		
$\ell=0$	-0.543	-	-
$\ell=1$	-	0.304	-
$\ell=2$	-	-	-0.105
	a = 3.335 a.u.		
$\ell=0$	-0.535	-	-
$\ell=1$	-	0.257	-
$\ell=2$	-	-	-0.104

TABLE 10

The matrix elements of $\frac{1}{r^3}$ for the various ligand-central ion distances in cadmium divanadate

	a = 3.161 a.u.		
	4s	4p	3d
ℓ=0	-	-	-0.876
ℓ=1	-	-0.012	-
ℓ=2	-0.014		-0.037
ℓ=3	-	-0.010	-
ℓ=4	-	-	-0.007
	a = 3.246 a.u.		
	4s	4p	3d
ℓ=0	-	-	-0.813
ℓ=1	-	-0.011	-
ℓ=2	-0.014	-	-0.034
ℓ=3	-	-0.010	-
ℓ=4	-	-	-0.006
	a = 3.335 a.u.		
	4s	4p	3d
ℓ=0	-	-	-0.753
ℓ=1	-	-0.011	-
ℓ=2	-0.013	-	-0.031
ℓ=3	-	-0.011	-
ℓ=4	-	-	-0.005

Contributions from O_3

$$\frac{\lambda}{1+\lambda^2-0.302\lambda}\begin{pmatrix} -0.918 & 0 & 0 \\ 0 & 1.406 & -1.707 \\ 0 & -1.707 & -0.488 \end{pmatrix} .$$

Diagonalization of the sum of these contributions was done using λ as a parameter. A plot of q, the largest eigenvalue of the electric field gradient tensor vs λ is shown in Figure 19. For an antishielding factor of -3.5, the measured q was $0.97(4)\times10^{14}$ c.g.s. The experimental and calculated values agree if λ, the charge transfer coefficient has the value 0.07.

2. Potassium Metavanadate

Potassium metavanadate has VO_4 groups which share two corner oxygens to form a chain through the crystal which is parallel to the crystallographic c axis. Referring to Figure 2, the shared oxygens are O_2 and O_3. The isolated oxygen and the vanadium ions are situated on a mirror plane which relates the two shared oxygens. The vanadium-oxygen bond lengths are given by[34]

$$V\text{-}O_2 = V\text{-}O_3 = 1.81(1)\text{Å}$$
$$V\text{-}O_1 = V\text{-}O_4 = 1.65(1)\text{Å} .$$

The overlap integrals and the expectation values of $\frac{1}{r^3}$ for these ligand-central ion distances are given in Tables 11 and 12.

The z axis of the electric field gradient tensor was chosen to be perpendicular to the mirror plane with the x

TABLE 11

Overlap integrals for the various ligand-central ion distances in potassium metavanadates

	a = 3.119 a.u.		
	4s	4p	3d
ℓ=0	-0.544	-	-
ℓ=1	-	0.356	-
ℓ=2	-	-	-0.108
	a = 3.425 a.u.		
	4s	4p	3d
ℓ=0	-0.522	-	-
ℓ=1	-	0.196	-
ℓ=2	-	-	-0.103

TABLE 12

The matrix elements of $\frac{1}{r^3}$ for the various ligand-central ion distances in potassium metavanadate

	a = 3.421 a.u.		
	4s	4p	3d
ℓ=0	-	-	-0.697
ℓ=1	-	-0.012	-
ℓ=2	-0.013	-	-0.028
ℓ=3	-	-0.013	-
ℓ=4	-	-	-0.005
	a = 3.119 a.u.		
	4s	4p	3d
ℓ=0	-	-	-0.915
ℓ=1	-	-0.012	-
ℓ=2	-0.014	-	-0.039
ℓ=3	-	-0.011	-
ℓ=4	-	-	-0.007

axis along the z' axis in Figure 2-a.Again, only an isolated VO_4 group in the shape of a slightly distorted tetrahedron was considered. In atomic units, the nonlocal contributions are given by:

Contributions from O_1 and O_4

$$\frac{\lambda}{1+\lambda^2-0.218\lambda} \begin{pmatrix} -1.107 & 1.635 & 0 \\ 1.635 & -0.013 & 0 \\ 0 & 0 & 1.120 \end{pmatrix}$$

Contributions from O_2 and O_3

$$\frac{\lambda}{1+\ ^2-0.360\lambda} \begin{pmatrix} 0.856 & -1.369 & 0 \\ -1.369 & -0.014 & 0 \\ 0 & 0 & -0.842 \end{pmatrix}$$

A plot of q vs λ is given in Figure 19. The experimental and calculated values agree if λ=0.23. For this value of λ, the anisotropy factor η is 0.37 compared with a measured anisotropy of 0.65. The X principal axis is at 33^o from the y' axis in Figure 2-a compared with a measured principal axis approximately along y'.

3. Vanadium Pentoxide

Vanadium pentoxide has VO_5 groups in the shape of a distorted trigonal bipyramid which shares corner oxygens and an edge of the trigonal bypyramid to form a continuous sheet. This sheet is approximately parallel to

Figure 19

A plot of the largest calculated eigenvalues of the field gradient tensor vs the charge transfer coefficient λ for cadmium divanadate and potassium metavanadate.

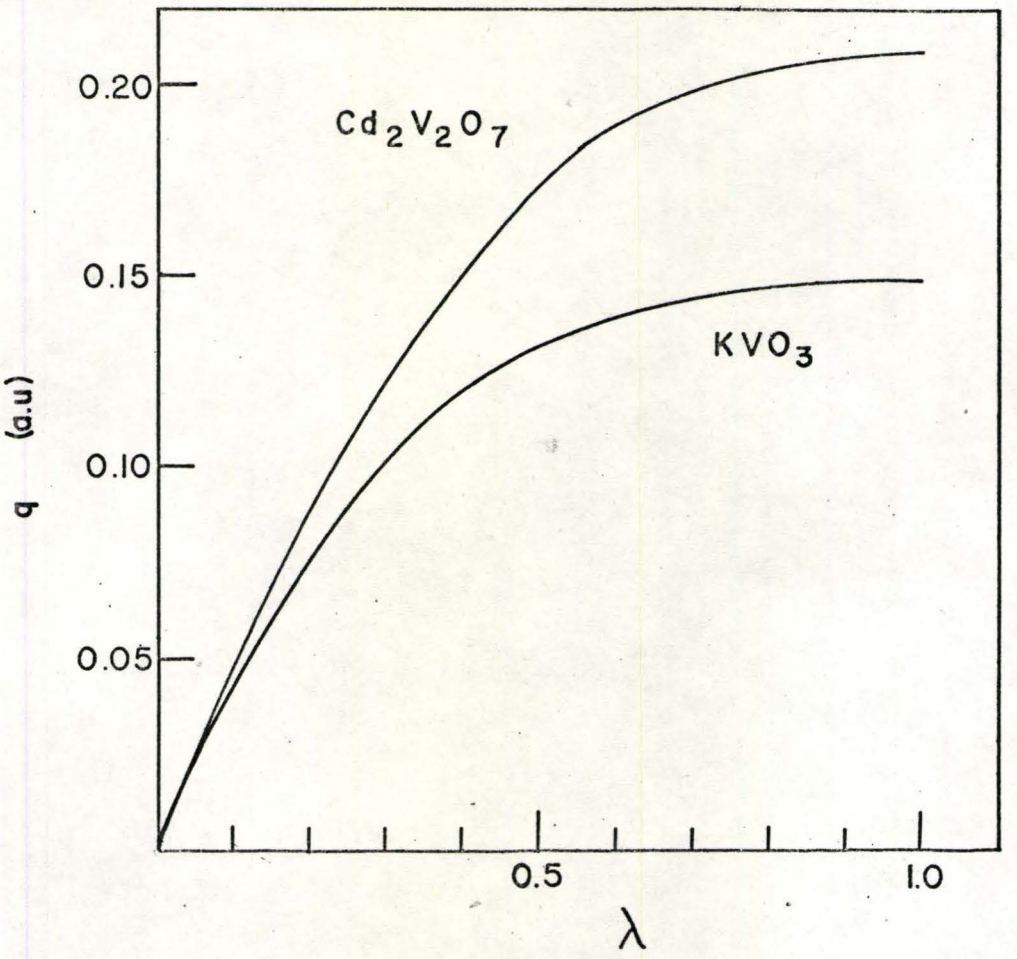

Figure 19

TABLE 13

The matrix elements of $\frac{1}{r^3}$ for the local term in vanadium pentoxide

	4s	4p	3d
4s	-	-	-
4p	-	0.014	-
3d	-0.002	-	3.084

TABLE 14

Overlap integrals for the various ligand-central ion distances in vanadium pentoxide

a = 2.987 a.u.

	4s	4p	3d
ℓ=0	-0.523	-	-
ℓ=1	-	0.386	-
ℓ=2	-	-	-0.113

a = 3.365 a.u.

	4s	4p	3d
ℓ=0	-0.531	-	-
ℓ=1	-	0.238	-
ℓ=2	-	-	-0.104

a = 3.554 a.u.

	4s	4p	3d
ℓ=1	-0.501	-	-
ℓ=1	-	0.090	-
ℓ=2	-	-	-0.100

a = 3.819 a.u.

	4s	4p	3d
ℓ=0	-0.464	-	-
ℓ=1	-	-0.126	-
ℓ=2	-	-	-0.092

TABLE 15

The matrix elements of $\frac{1}{r^3}$ for the various ligand-central ion distances in vanadium pentoxide

	4s	4p	3d
	a = 2.987 a.u.		
ℓ=0	-	-	-1.022
ℓ=1	-	-0.013	-
ℓ=2	-0.012	-	-0.044
ℓ=3	-	-0.012	-
ℓ=4	-	-	-0.008
	a = 3.365 a.u.		
ℓ=0	-	-	-0.734
ℓ=1	-	-0.012	-
ℓ=2	-0.013	-	-0.030
ℓ=3	-	-0.012	-
ℓ=4	-	-	-0.005
	a = 3.554 a.u.		
ℓ=0	-	-	-0.625
ℓ=1	-	-0.013	-
ℓ=2	-0.012	-	-0.025
ℓ=3	-	-0.018	-
ℓ=4	-	-	-0.004
	a = 3.819 a.u.		
ℓ=0	-	-	-0.502
ℓ=1	-	-0.016	-
ℓ=2	-0.010	-	-0.019
ℓ=3	-	-0.028	-
ℓ=4	-	-	-0.003

the crystallographic b axis. Referring to Figure 2-b the x'y' plane is a mirror plane. The Z principal axis of the field gradient tensor is therefore constrained to be perpendicular to this plane. The vanadium-oxygen distances are given by[35]

$$V\text{-}O_1 = V\text{-}O_2 = 1.878(2)\ \text{Å}$$
$$V\text{-}O_3 = 1.780(2)\ \text{Å}$$
$$V\text{-}O_4 = 1.585(4)\ \text{Å}$$
$$V\text{-}O_5 = 2.021(3)\ \text{Å}$$

The expectation values of $\frac{1}{r^3}$ and the overlap integrals for these ligand-central ion distances are given in Tables 13, 14 and 15. In the calculations, the VO_5 group was treated as a discrete slightly distorted trigonal bipyramid. The local terms do not vanish, but have axial symmetry. As the non-local terms do not have axial symmetry, the electric field gradient tensor will not be axially symmetry. In atomic units the contributions from the different ligands are given by:

Contributions from O_1 and O_2

$$\frac{\lambda^2}{1+\lambda^2-0.557\lambda}\begin{pmatrix} -0.227 & 0 & 0 \\ 0 & -0.227 & 0 \\ 0 & 0 & 0.454 \end{pmatrix} +$$

$$\frac{\lambda}{1+\lambda^2-0.557\lambda}\begin{pmatrix} 0.450 & 0 & 0 \\ 0 & 0.450 & 0 \\ 0 & 0 & -0.900 \end{pmatrix}$$

Contributions from O_2

$$\frac{\lambda^2}{1+\lambda^2-0.324\lambda}\begin{pmatrix}-0.749 & 0 & 0\\ 0 & -0.749 & 0\\ 0 & 0 & 1.498\end{pmatrix} +$$

$$\frac{\lambda}{1+\lambda^2-0.324\lambda}\begin{pmatrix}-0.803 & 0 & 0\\ 0 & 0.015 & 0\\ 0 & 0 & -0.688\end{pmatrix}$$

Contributions from O_4

$$\frac{\lambda^2}{1+\lambda^2-0.386\lambda}\begin{pmatrix}-0.749 & 0 & 0\\ 0 & -0.749 & 0\\ 0 & 0 & 1.498\end{pmatrix} +$$

$$\frac{\lambda}{1+\lambda^2-0.386\lambda}\begin{pmatrix}-0.113 & 1.102 & 0\\ 1.102 & -0.752 & 0\\ 0 & 0 & 0.865\end{pmatrix}$$

Contributions from O_5

$$\frac{\lambda^2}{1+\lambda^2-0.479\lambda}\begin{pmatrix}-0.749 & 0 & 0\\ 0 & -0.749 & 0\\ 0 & 0 & 1.498\end{pmatrix} +$$

$$\frac{\lambda}{1+\lambda^2-0.479\lambda}\begin{pmatrix}-0.084 & -0.443 & 0\\ -0.443 & -0.292 & 0\\ 0 & 0 & 0.476\end{pmatrix}$$

The calculated value of $\mathfrak{q}$ agrees with the measured value if $\lambda = 0.03$. For this value of λ , $\eta = 1$ compared

with a measured value of 0.04 and the z principal axis is at 45° from the y' axis, compared with the experimental value of 43° from the y axis.

CHAPTER V

DISCUSSION

A. ORTHOVANADATES

Most of the orthovanadates, with a known crystal structure, have the vanadium ion in almost perfect tetrahedral symmetry. Therefore the V^{51} quadrupole coupling constants in these compounds are expected to be very small.

1. Sodium Orthovanadate Dodecahydrate

The upper limit of the V^{51} and Na^{23} quadrupole coupling constants in sodium orthovanadate dodecahydrate were determined from the linewidth of the unsplit resonance lines. There are two contributions to the linewidth, dipolar interaction and unresolved quadrupolar splitting. The dipolar contribution can not be calculated since the details of the crystal structure are unknown. The upper limit was obtained by attributing all of the linewidth to the unresolved quadrupolar splitting. The space group of sodium orthovanadate dodecahydrate, if centrosymmetric, requires the vanadium ion to be in a special position on a three-fold axis. Therefore, the anisotropy factor η is zero. As the vanadium environment is an almost perfect tetrahedron, it is not surprising that the quadrupole coupling constant of V^{51} in sodium orthovanadate dodeca-

hydrate is very small, less than 1.5 kHz. However, in this space group, the sodium ions are in a general position[41], with no nontrivial point symmetry element. Therefore, it is surprising to observe a lack of splitting of the Na^{23} resonance line in sodium orthovanadate dodecahydrate. If the point symmetry was octahedral or tetrahedral, there would be no splitting, but this explanation is incompatible with the space group assignment. In order to examine the possibility that the satellites are very weak and cannot be seen, the chemical shift of the Na^{23} resonance line was measured. If the sodium ions are in a tetrahedral or octahedral environment, the chemical shift tensor is isotropic. The chemical shift measurements tend to support the hypotheses that the Na^{23} ions in sodium orthovanadate dodecahydrate are in a pseudo cubic environment. It will be interesting to check this conclusion when the structure of this crystal is determined.

2. Calcium Orthovanadate

There are two possibilities for the space group of calcium orthovanadate , Cc or C2/c[43]. If the space group is Cc, there are 4 crystallographically inequivalent sites and 16 inequivalent magnetic sites. If the space group is C2/c, the number of inequivalent sites is reduced by a factor of 2.

The V^{51} resonance line in calcium orthovanadate is unsplit, broad and independent of the orientation of the

magnetic field. Therefore, the broad line is probably caused by a superposition of the resonance patterns of the inequivalent sites. The upper limit is obtained by attributing the linewidth to an unresolved quadrupolar splitting. The non-zero quadrupolar interaction is expected for both space groups.

The small V^{51} quadrupole coupling constants in vanadinite, descloizite, sodium orthovanadate dodecahydrate and calcium orthovanadate are correlated with the crystal structures. The compounds with almost perfect tetrahedral symmetry have very small coupling constants. Therefore, the large value of the V^{51} quadrupole coupling constant obtained by Saraswati [33] for a polycrystalline sample of $Na_3VO_4 \cdot 14H_2O$ is questionable.

B. DIVANADATES

Zirconium and cadmium divanadates have a linear V-O-V group, where the central oxygen is shared by two VO_4 groups. In zirconium divanadate, this linear group is along a three fold axis. Hence the assumption that $\eta=0$, that was made earlier for this compound is valid. In cadmium divanadate the V-O-V group is not along a three fold axis, but it can be considered as a pseudo three fold axis. Therefore, η is not zero but is expected to be small. Therefore the V^{51} quadrupole coupling constant of cadmium divanadate, given in Table 2, is a lower limit.

The V-O-V group in the divanadates is really not

linear. X-ray diffraction data show that a high thermal motion or positional superstructure is associated with the bridging oxygen of this group. It is not known at present which is the correct interpretation. However, a single crystal nuclear magnetic resonance technique could resolve this ambiguity.

As expected, the V^{51} quadrupole coupling constants in the divanadates are larger than the V^{51} quadrupole coupling constants in the orthovanadates. This is expected as the V^{51} ions are in a more distorted tetrahedron and the quadrupole coupling constants will show a strong correlation with the deviations from tetrahedral symmetry. The V^{51} quadrupole coupling constants for divanadates are expected to be between 1.5 and 2.0 MHz. These values are to be compared with the reported value of 3.1 MHz[33] obtained from the linewidth of the V^{51} central resonance line in a polycrystalline sample.

C. METAVANADATES

The V^{51} quadrupole coupling constant in potassium metavanadate is the largest value measured in this work. This result is expected since the tetrahedral environment around the vanadium is more distorted than in the divanadates or the orthovanadates.

The V^{51} resonance line in potassium metavanadate is very broad. The estimated dipolar broadening can not explain this linewidth. The probable reason is an interaction with

electronic magnetic dipole moments of V^{4+} ions, which are present in the nonstochiometric sample.

There are two previously reported values of V^{51} quadrupole coupling constants in metavanadates[33]. The V^{51} quadrupole coupling constant in ammonium metavanadate, which is isostructural with potassium metavanadate, is 3.04 MHz. The V^{51} nucleus in ferroelectric sodium metavanadate, which is not isostructural with the above compounds, has a quadrupole coupling constant of 3.4 MHz. The method used by Saraswati[33] to obtain these values, an analysis of the central resonance linewidth, is subject to large errors, unless extreme care is taken to avoid other effects that contribute to the linewidth. These effects are paramagnetic impurities and chemical shift of inequivalent magnetic sites.

D. VANADIUM PENTOXIDE

The environment of the vanadium ion in vanadium pentoxide is a distorted trigonal bipyramid. Therefore, the V^{51} quadrupole coupling constant is expected to be larger than the V^{51} quadrupole coupling constant in the orthovanadates, divanadates or metavanadates. It is therefore surprising to measure a smaller value.

The V^{51} quadrupole coupling constant has been reported three times[33,36,37]. All the results were obtained from polycrystalline samples. Therefore the reported values are smaller than the value obtained in this work because η, the anisotropy factor, is not zero.

For reasonable values of the magnetic field, the second order quadrupolar effect is very small. However, the V^{51} quadrupole coupling constant is not small enough to cause overlap between the central resonance line and the satellites. These features make the vanadium pentoxide a good sample for a study of the anisotropy of the chemical shift tensor.

The chemical shift tensor of the V^{51} resonance line has been reported for a polycrystalline sample of vanadium pentoxide, relative to the V^{51} resonance line in an aqueous solution of sodium orthovanadate[37]. The reported results do not agree in either sign or magnitude with the present data, obtained from a single crystal sample. The discrepancy could not arise from the use of two different reference samples because the chemical shift between the V^{51} resonance lines in these solutions is 0.3×10^{-4}, too small to explain the discrepancy. The expected resonance pattern of the V^{51} resonance in a polycrystalline sample of vanadium pentoxide was calculated, using the procedure outlined in Appendix E. These calculations are based on the single crsytal results. In order to simplify the calculations, the chemical shift tensor was replaced by an axially symmetric tensor with $\sigma_{\parallel} = \sigma_{yy} = 6.5 \times 10^{-4}$ and $\sigma_{\perp} = -2.4 \times 10^{-4}$ where $\sigma_{\perp}$ is the average of σ_{xx} and σ_{zz}. For reasonable values of the single crystal linewidth, the shift of the maximum of the resonance pattern, from the Larmor frequency, agrees with the experimental values in sign and magnitude. A recorder trace of the

Figure 20

The shift of the V^{51} resonance line in polycrystalline vanadium pentoxide relative to the V^{51} resonance line in an aqueous solution of sodium orthovanadate. The broad line at lower fields is the resonance line of the powder. The narrow line is the resonance in the solution.

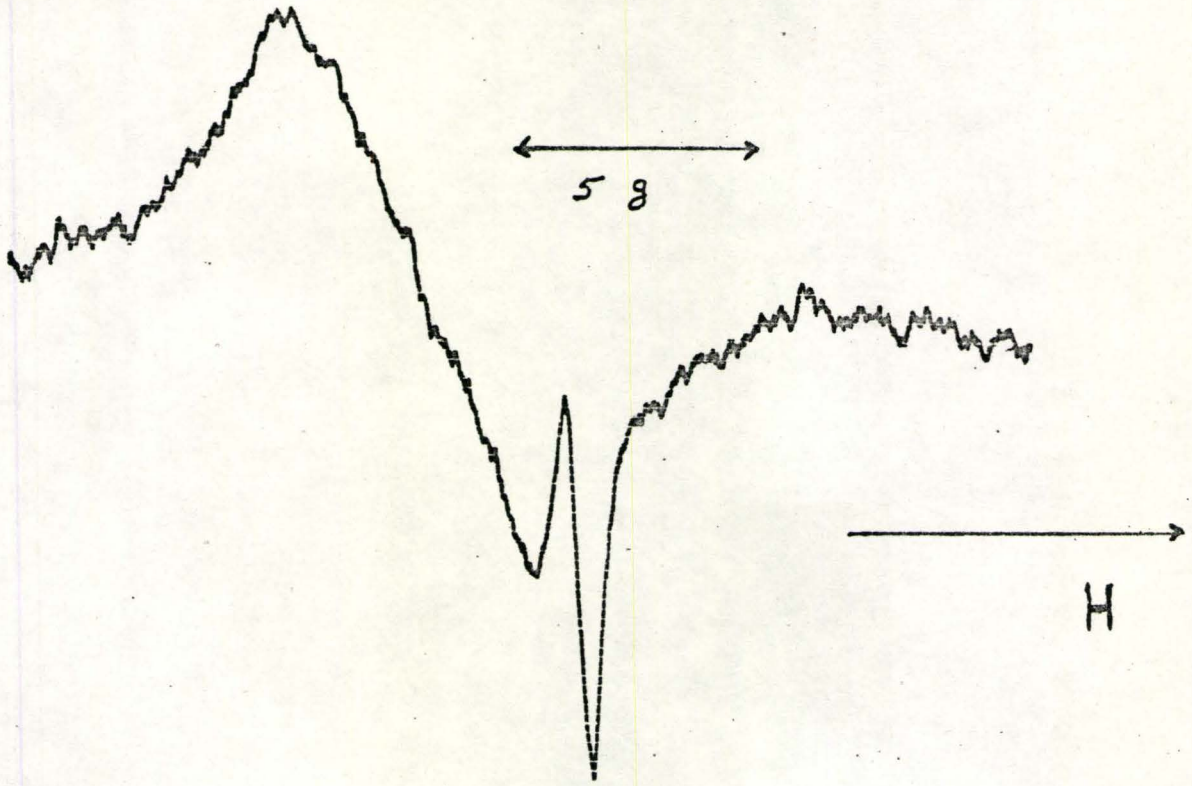

Figure 20

Figure 21

The synthesized lineshape of V^{51} resonance line in a polycrystalline sample of vanadium pentoxide. The calculations are based on the single crystal chemical shift data at an external magnetic field of 14.250 kilogauss. The non-normalized lineshapes are given for various values of the single crystal linewidth.

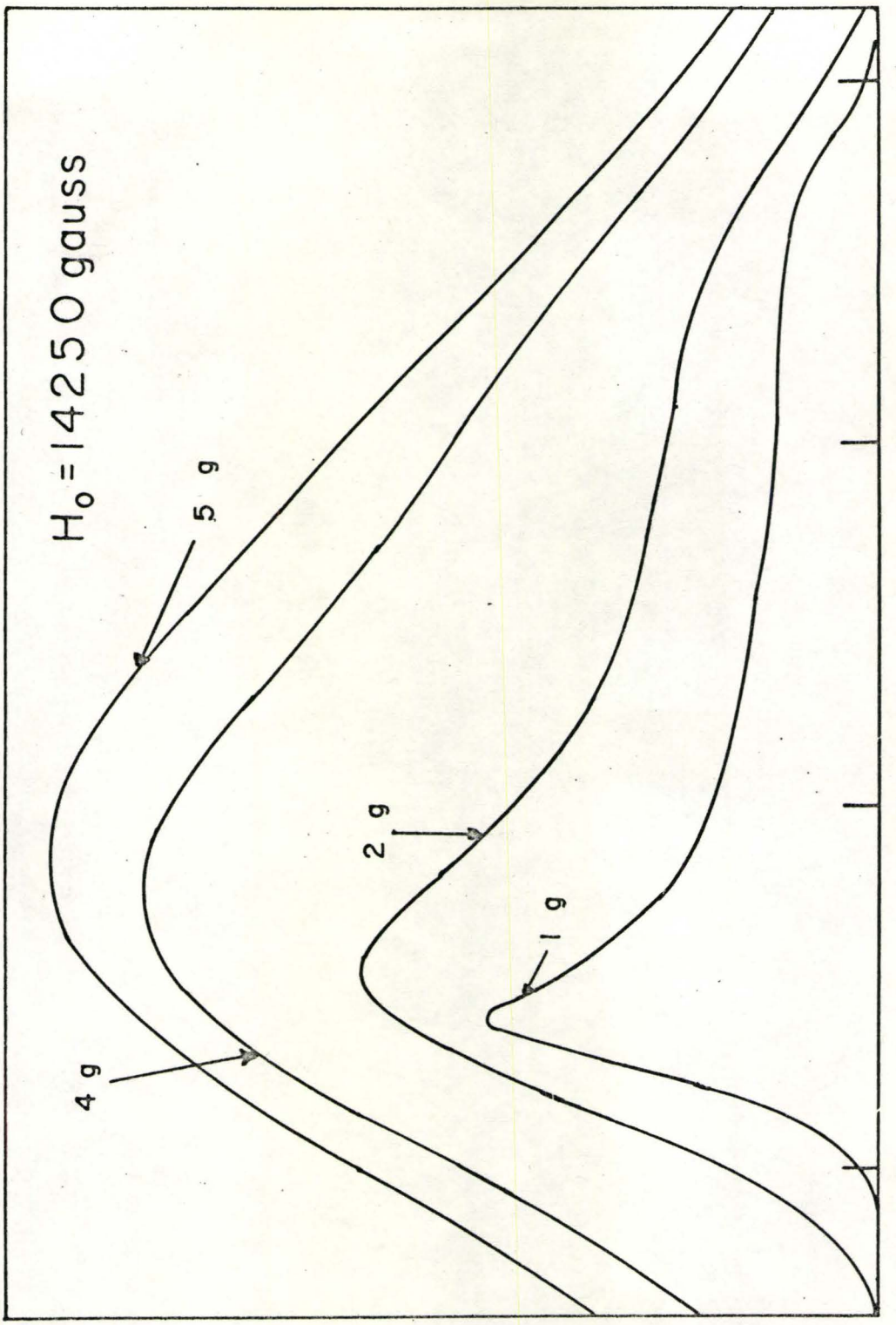

Figure 21

chemical shift of the V^{51} resonance line in vanadium pentoxide relative to the V^{51} resonance line in an aqueous solution of sodium metavanadate is shown in Figure 20. The synthesized V^{51} resonance line shape for polycrystalline vanadium pentoxide is shown in Figure 21 for a few values of the assumed single crystal linewidth.

The anisotropic paramagnetic part of the chemical shift can be correlated with the Van Vleek term of the magnetic susceptibility. The large value of the chemical shift implies that the susceptibility will have a large temperature independent paramagnetic contribution. Since there were two contradictory measurements of the magnetic susceptibility, it was measured again. It was found, as expected, to be paramagnetic and temperature independent over a temperature range of $4.2^{\circ}K$ to $300^{\circ}K$. The large values of the chemical shift and the magnetic susceptibility suggest a low lying excited magnetic state in vanadium pentoxide. Infrared spectra of polycrystalline vanadium pentoxide indicate an excited state at 0.4 eV[73]. However, it is not possible to assign this state to either a vibrational excited state or an electronic excited state without further studies.

E. POINT MULTIPOLE MODEL

The point multipole model confirms the expected order of the values of the V^{51} quadrupole coupling constants in the divanadates, metavanadates and vanadium pentoxide.

By referring to Tables 2, 4, 6 and 8 it is found that the point charge model overestimates the V^{51} quadrupole coupling constant in vanadium pentoxide, agrees with the experimental value for cadmium divanadate and underestimates the value for potassium metavanadate. These results are based on charges of +5.0 on the vanadium ion and -2.0 for the oxygen ion. The antishielding factor was assumed to be -3.5.

In order to achieve better agreement between the calculated and measured values of the V^{51} quadrupole coupling constant in vanadium pentoxide, contributions from dipole moments were included in the electric field gradient. They increase the value by a factor of 20. The importance of the contributions from the dipole moments agrees with the conclusion of Sharma and Das[18] and Taylor and Das[56]. The calculated contributions from the electric dipole moments are uncertain because of the uncertainty in the value of the dipole polarizability. However, inclusion of the dipole contributions increases the discrepancy between the measured and calculated coupling constant of V^{51} in vanadium pentoxide. These contributions were not considered for the metavanadate and divanadate calculations because of the lack of knowledge of the dipole polarizability.

The above results show that this oversimplified model can not be applied to vanadium-oxygen compounds. The vanadium pentoxide case shows that contributions from electric dipole

moments are very important. Therefore, whenever this model is applied, these contributions must be included if the crystal contains highly polarizable ions situated on sites with no inversion symmetry.

F. COVALENT MODEL

Another approach to the problem of calculating the electric field gradient in a crystal is given by the covalent model. This model permits the charge distribution to be diffuse. It also permits an overlap of the charge distributions of neighbouring ions. The inclusion of the overlap effect demands that, in contrast to the point multipole model, the environment be treated quantum mechanically. The symmetry of the environment is taken into account by the choice of wavefunctions, i.e. by using hybridized orbitals.

The covalent model was applied to the calculations of the electric field gradient in cadmium divanadate, potassium metavanadate and vanadium pentoxide. The following approximations were made .

a) Only σ bonding orbitals were considered. Each σ orbital can accept two electrons which have opposite spins.

b) All the electrons that were not in the σ bonding orbitals were treated as being in non-bonding orbitals.

c) The charge transfer coefficient, λ, was treated as being independent of the ligand-central ion distance.

d) Distortion of the idealized symmetry was taken into

account only for the non-local terms.

e) The oxygens were considered as singly ionized and only $2p_z$ wavefunctions were included.

f) The vanadium 4p orbitals were taken as Slater type orbitals because of the non-existence of vanadium 4p Hartree-Fock wavefunctions.

g) No "distant" contributions were included.

Kimball[74] showed that for a tetrahedral d^3s configuration which was the one used in the calculations, the other d^2 orbitals are available for strong π bonding orbitals. For the d^3sp trigonal bipyramid configuration, d^2 orbitals are again available for strong π bonding orbitals. Ballhausen and Gray[75] calculated λ for a vanadyl ion by considering the molecular orbitals of the ion. They included π bonding orbitals in their calculations. It is therefore surprising to find agreement between their value of λ and the value of λ obtained for potassium metavanadate and cadmium divanadate. A possible answer is provided by considering the relation between the bond order and bond distance for vanadium-oxygen compound provided by Evans[34]. This relation is plotted in Figure 22. The plot shows that an oxygen at 1.58 $\mathring{A}$ from the vanadium, the closest vanadium-oxygen distance in vanadium pentoxide, is doubly bonded to the vanadium. Therefore π bonding orbitals must be included in the calculations of the field gradient in vanadium pentoxide. On the other hand, for the closest vanadium-oxygen distance in potassium

Figure 22

Relation between bond number and bond length given by Evans[34] for vanadium-oxygen bonds in different vanadium-oxygen compounds.

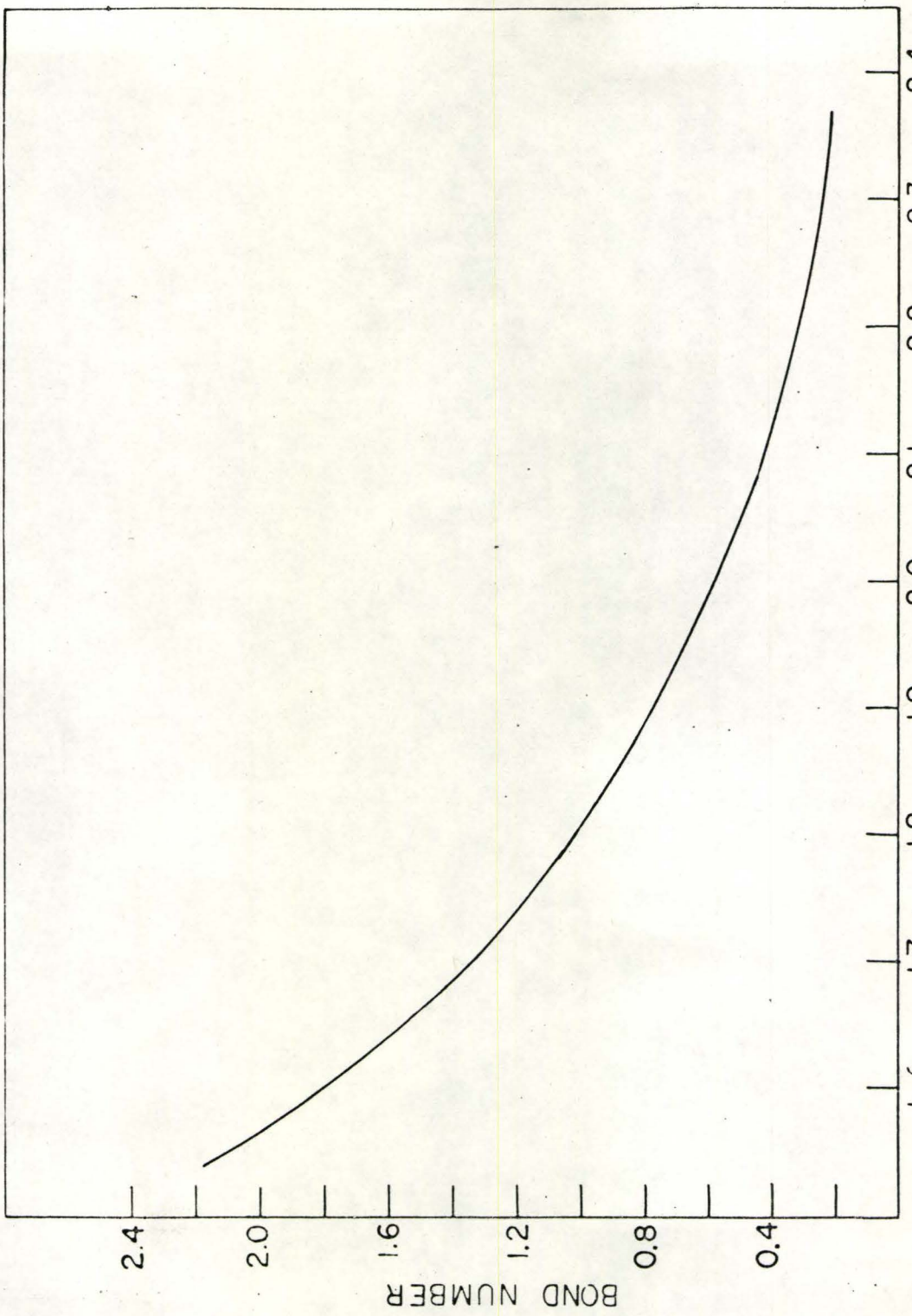
BOND NUMBER
2.4
2.0
1.6
1.2
0.8
0.4
1.6
1.7
1.8
1.9
2.0
2.1
2.2
2.3
2.4
BOND LENGTH (Å)

Figure 22

metavanadate and cadmium divanadate the bond order is only 1.5, and the exclusion of π orbitals is a better approximation.

The error in the calculation was not increased by a significant amount by approximations e and f. The expectation value of $\frac{1}{r^3}$ calculated for a neutral oxygen Hartree-Fock $2p_z$ wavefunction as a function of the bond length is shown in Figure 24. The value is reduced by approximately 25% compared with the use of Hartree-Fock singly ionized oxygen $2p_z$ wavefunctions. This is expected since the charge distribution of a singly ionized oxygen is more spread out than the charge distribution of neutral oxygen. Following Ballhausen and Gray[73], the expectation value of $\frac{1}{r^3}$ was calculated when the vanadium 4p wavefunction had the same radial dependence as the vanadium 4s orbitals. The new value differs from the value obtained by using Slater type orbitals by approximately 30%. However, no serious error was caused since both results are much smaller than the value obtained from the vanadium 3d orbitals.

A possible explanation for the small value of the V^{51} quadrupole coupling constant in vanadium pentoxide is provided by the covalent model. Some of the local and non-local contributions have opposite signs and therefore cancel. A check of this possibility will be provided by measuring the V^{51} quadrupole coupling constant in hydrated potassium metavanadate, which also has a sheet of distorted trigonal

bipyramids.

A better check of the validity of this model can be provided by considering the V_2O_7 polyion of the divanadate. Hybridized orbitals can be constructed to obey the symmetry of that group. There is not much variation in the vanadium-oxygen distances in this group so that the assumption that λ is constant is a valid assumption, and not like in the case of vanadium pentoxide when the bond distance varies by as much as 30%.

CHAPTER VI

CONCLUSIONS

The V^{51} quadrupole coupling constants were measured for different vanadium-oxygen compounds. It was found that the V^{51} quadrupole coupling constant increased as the tetrahedron around the vanadium is distorted. Vanadium pentoxide is an exception, and showed a surprisingly small quadrupole coupling constant. The point multipole model is incapable of explaining the quadrupole coupling constants in the above compounds. The covalent model provides an explanation of the small value of the V^{51} quadrupole coupling constant in vanadium pentoxide.

The chemical shift tensor of the V^{51} resonance line was determined for a single crystal sample of vanadium pentoxide. The large eigenvalues are consistent with the large temperature paramagnetic term in the magnetic susceptibility tensor.

There is no apparent correlation between the principal axes of the chemical shift tensor and quadrupole coupling tensor in V_2O_5.

APPENDIX A

The different values of $\alpha_{\ell}(gLM|ar)$, which were defined in equation (2-40) are given for $\ell \leq 4$, L = 1, M = 0 and a singly ionized oxygen ion as a ligand.

$$\alpha_o(o10|ar) = -\frac{0.5}{r}\left[\left(1 - \frac{r^2}{a^2}\right) \times X_o - \frac{1}{a^2} \times X_1\right]$$

$$\alpha_1(o10|ar) = -\frac{0.75a}{r^2}\left[1 + \frac{r^2}{a^2}\right]\left[\left(1 - \frac{r^2}{a^2}\right) \times X_o + 2r^2 \times \frac{1}{a^4\left(1+\frac{r^2}{a^2}\right)} \times X_1 + \frac{1}{a^4\left(1+\frac{r^2}{a^2}\right)} \times X_2\right]$$

$$\alpha_2(o10|ar) = \frac{5}{16r}\left[0.5\left(1 - \frac{r^2}{a^2} + 3\frac{a^2}{r^2} + 3\frac{r^4}{a^4}\right) \times X_o - \frac{1}{a^2}\left(1 - 1.5\frac{a^2}{r^2} + 4.5\frac{r^2}{a^2}\right) \times X_1 + \frac{1}{a^4}\left(1.5\frac{a^2}{r^2} + 4.5\right) \times X_2 - \frac{1.5}{a^4 r^2} \times X_3\right]$$

$$\alpha_3(o10|ar) = \frac{21a}{16r^2} \times \left(1 + \frac{r^2}{a^2}\right)\left[1.25\frac{r^4}{a^4} + 0.75 - 0.75\frac{r^2}{a^2} - 1.25\frac{a^2}{r^2}\right) \times X_o + \frac{1}{a^2\left(1+\frac{r^2}{a^2}\right)}\left(2.5\frac{a^2}{r^2} - 5\frac{r^4}{a^4} - 3.5\frac{r^2}{a^2}\right) \times X_1 + \frac{1}{a^2 r^2\left(1+\frac{r^2}{a^2}\right)}\left(7.5\frac{r^4}{a^4} + 5.5\frac{r^2}{a^2}\right) \times X_2$$

$$- \frac{1}{a^4 r^2 (1+\frac{r^2}{a^2})} (2.5 + 5 \frac{r^2}{a^2}) \times X_3 + \frac{1.25}{a^6 r^2 (1+\frac{r^2}{a^2})} \times X_4]$$

$$\alpha_4(\text{o10|ar}) = \frac{9}{512a^6r^5} [(-35a^{10} + 15a^8r^2 + 2a^6r^4 - 2a^4r^6 - 15a^2r^8 + 35r^{10}) \times X_o - (105a^8 + 20a^6r^2 - 18a^2r^4 - 60a^2r^6 - 175r^8) \times X_1 + (-70a^6 - 90a^4r^2 - 270a^2r^4 - 350r^6) \times X_2 + (70a^4 - 300a^2r^2 - 350r^4) \times X_3 + (105a^2 + 175r^2) \times X_4 - 35 \times X_5]$$

where

$$X_o = \sum_k \int_{|a-r|}^{|a+r|} f_{21}{}^k(R)\, R^{-1}\, dR$$

$$X_1 = \sum_k \int_{|a-r|}^{|a+r|} f_{21}{}^k(R)\, R\, dR$$

$$X_2 = \sum_k \int_{|a-r|}^{|a+r|} f_{21}{}^k(R)\, R^3\, dR$$

$$X_3 = \sum_k \int_{|a-r|}^{|a+r|} f_{21}{}^k(R)\, R^5\, dR$$

$$X_4 = \sum_k \int_{|a-r|}^{|a+r|} f_{21}{}^k(R)\ R^7\ dR$$

$$X_5 = \sum_k \int_{|a-r|}^{|a+r|} f_{21}{}^k\ (R)\ R^9\ dR$$

and the ligand wavefunction is given by

$$\sum_k \frac{f_{21}{}^k(R)}{R}\ Y_1{}^o\ (\Theta,\Phi)$$

and k is the number of Slater type wavefunctions that are needed to form a Hartree-Fock wavefunction.

APPENDIX B

Figures 23, 24 and 25 show the convergence of $\langle \frac{1}{R^3} \rangle$ as the distance of the ligand from the central ion is increased. The decrease of the value of the expectation value of $\frac{1}{R^3}$, for a given ligand as ℓ is increased is apparent.

Figure 23

$\langle 3d|\frac{1}{R^3}|\alpha_o(gl0|aR)\rangle$ as a function of the ligand-central ion distance for singly ionized oxygen (upper curve) and neutral oxygen (lower curve).

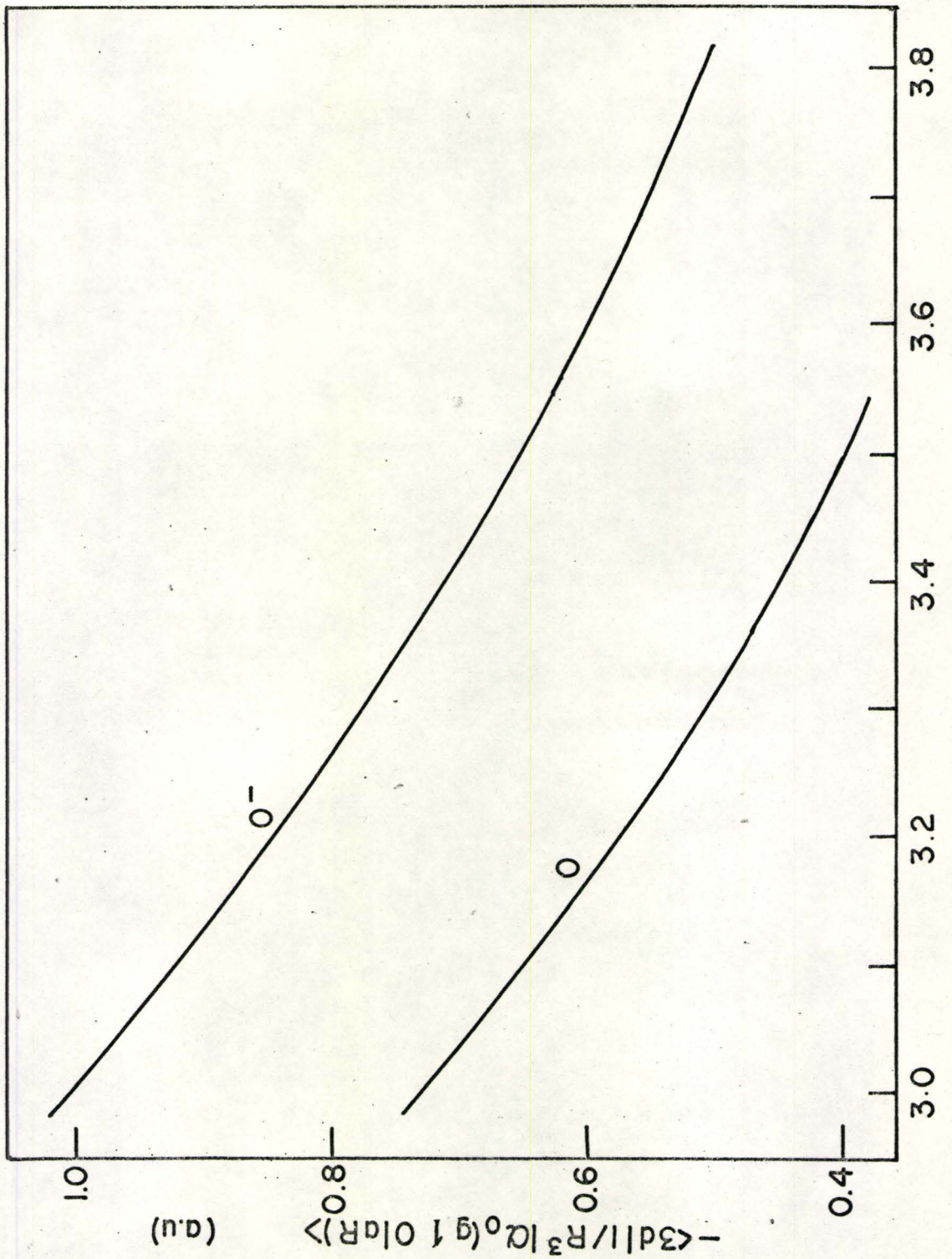
1.0
0.8
0.6
0.4
3.0
3.2
3.4
3.6
3.8
a (a.u)
$-\langle 3d|1/R^3|\alpha_0(g\ 1\ 0|\alpha R)\rangle$ (a.u)
0
0⁻

Figure 23

Figure 24

$\langle 3d|\frac{1}{R^3}|\alpha_2(g10|aR)\rangle$ and $\langle 4s|\frac{1}{R^3})\ \alpha_2(g10|aR)\rangle$ as a function of the ligand-central ion distance.

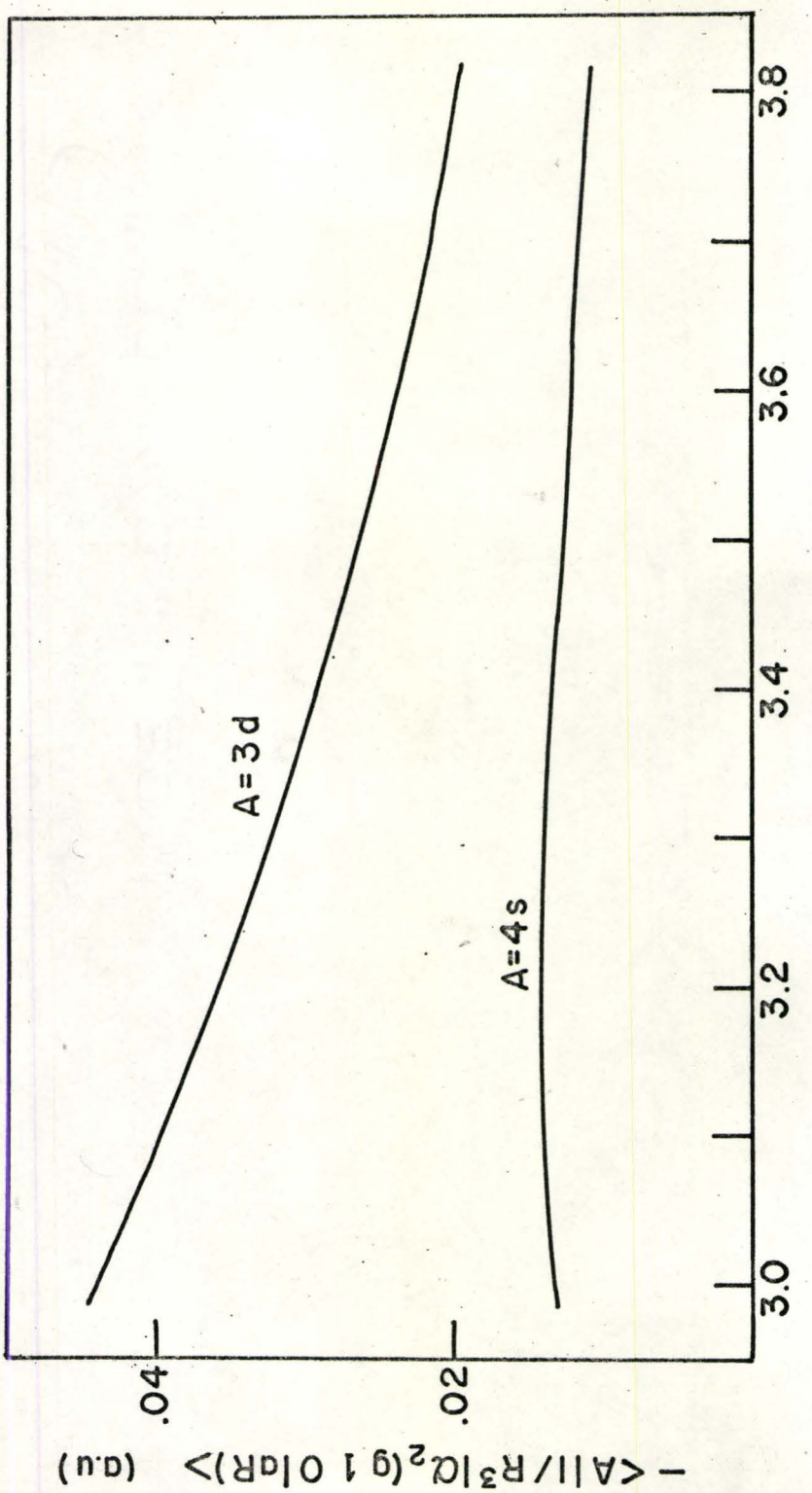

Figure 24

Figure 25

$\langle 3d|\frac{1}{R^3}|\alpha_4(gl0|aR)\rangle$ as a function of the ligand-central ion distance.

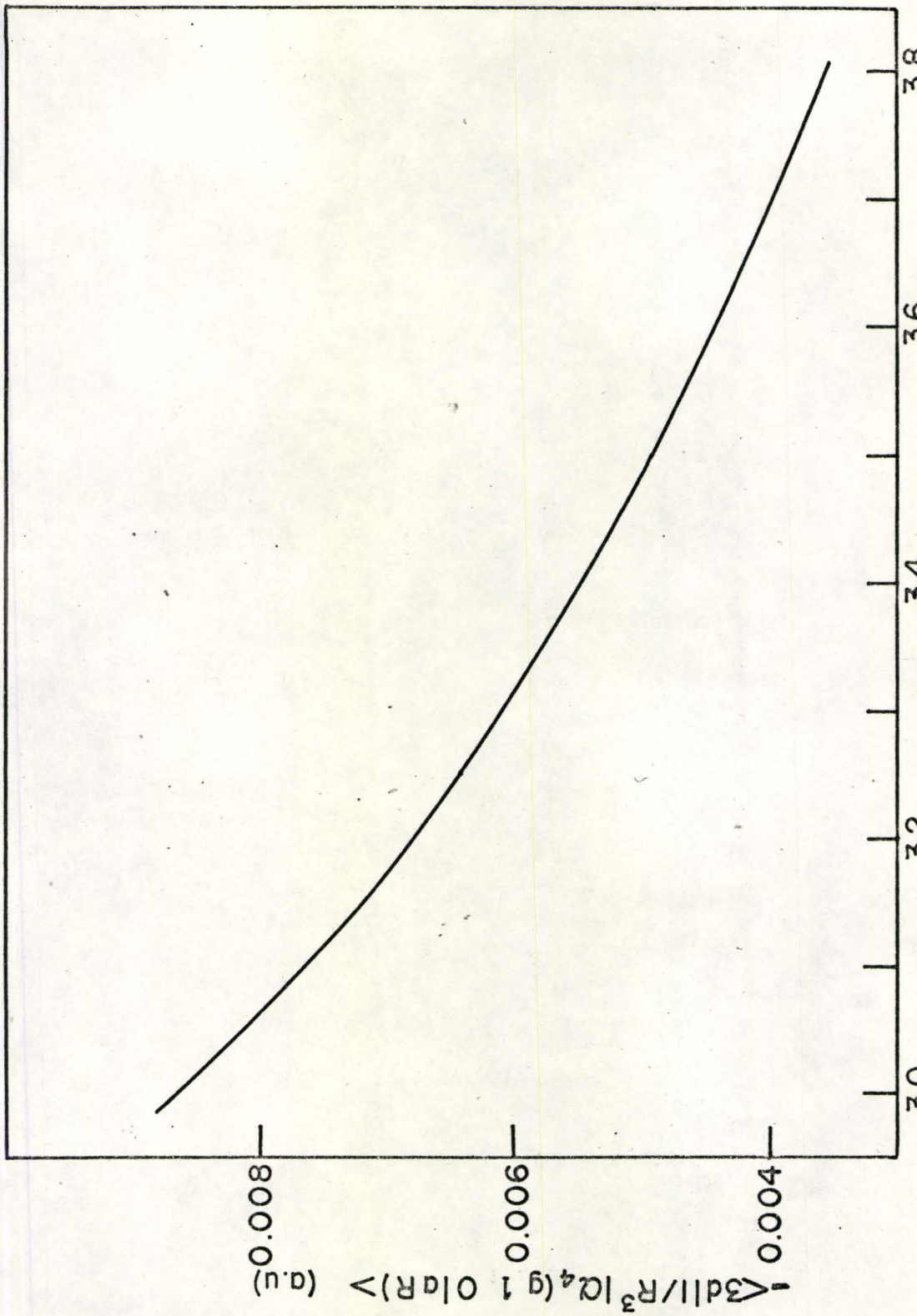

Figure 25

APPENDIX C

The angular part of the expectation values of ∇E, the field gradient, is given by $\langle Y_{\ell'}^{m'} | C_2^q | Y_\ell^m \rangle$. The values of these matrix elements, for $\ell, \ell', |m|, |m''| \leq 4$ are given in this appendix.

$$\langle Y_0^0 | C_2^0 | Y_2^0 \rangle = \sqrt{\frac{1}{5}}$$

$$\langle Y_2^0 | C_2^0 | Y_2^0 \rangle = \frac{2}{7}$$

$$\langle Y_2^1 | C_2^0 | Y_2^1 \rangle = \frac{1}{7}$$

$$\langle Y_2^2 | C_2^0 | Y_2^2 \rangle = -\frac{2}{7}$$

$$\langle Y_2^0 | C_2^0 | Y_4^0 \rangle = \frac{6\sqrt{5}}{35}$$

$$\langle Y_2^2 | C_2^0 | Y_4^2 \rangle = \sqrt{\frac{3}{7}}$$

$$\langle Y_2^1 | C_2^0 | Y_4^1 \rangle = \sqrt{\frac{6}{7}}$$

$$\langle Y_1^0 | C_2^0 | Y_1^0 \rangle = \sqrt{\frac{2}{5}}$$

$$\langle Y_1^1 | C_2^0 | Y_1^1 \rangle = -\frac{1}{5}$$

$$\langle Y_1^0 | C_2^0 | Y_3^0 \rangle = \frac{3}{5}\sqrt{\frac{3}{7}}$$

$$\langle Y_0^0 | C_2^1 | Y_2^{-1} \rangle = -\sqrt{\frac{1}{5}}$$

$$\langle Y_1^0 | C_2^1 | Y_1^{-1} \rangle = -\frac{\sqrt{3}}{5}$$

$$\langle Y_0^0 | C_2^2 | Y_2^{-2} \rangle = \sqrt{\frac{1}{5}}$$

$$\langle Y_2^2 | C_2^2 | Y_2^0 \rangle = -\frac{2}{7}$$

$$\langle Y_2^2 | C_2^2 | Y_4^0 \rangle = \sqrt{\frac{1}{245}}$$

$$\langle Y_2^0 | C_2^2 | Y_4^{-2} \rangle = \sqrt{\frac{3}{7}}$$

$$\langle Y_2^{-1} | C_2^2 | Y_4^{-3} \rangle = \sqrt{\frac{1}{7}}$$

$$\langle Y_2^{-1} | C_2^2 | Y_4^{-4} \rangle = \sqrt{\frac{2}{7}}$$

$$\langle Y_1^0 | C_2^2 | Y_3^{-2} \rangle = \sqrt{\frac{3}{35}}$$

$$\langle Y_1^{-1} | C_2^2 | Y_3^{-3} \rangle = \sqrt{\frac{9}{35}}$$

$$\langle Y_2^1 | C_2^2 | Y_4^{-1} \rangle = \frac{1}{7}$$

$$\langle Y_1^1 | C_2^2 | Y_3^{-1} \rangle = \sqrt{\frac{3}{175}}$$

$$\langle Y_2^1 | C_2^2 | Y_2^{-1} \rangle = -\frac{\sqrt{6}}{7}$$

$$\langle Y_1^1 | C_2^2 | Y_1^{-1} \rangle = -\frac{\sqrt{6}}{5}$$

$$\langle Y_1^{-1} | C_2^1 | Y_3^{-2} \rangle = -\sqrt{\frac{6}{35}}$$

$$\langle Y_2^1 | C_2^1 | Y_2^0 \rangle = \frac{1}{7}$$

$$\langle Y_1^{\,0}|C_2^{\,1}|Y_3^{\,-1}\rangle = -\frac{4}{5}\sqrt{\frac{3}{14}}$$

$$\langle Y_1^{\,1}|C_2^{\,1}|Y_1^{\,0}\rangle = \frac{\sqrt{3}}{5}$$

$$\langle Y_2^{\,-2}|C_2^{\,1}|Y_4^{\,-3}\rangle = -\sqrt{\frac{1}{7}}$$

$$\langle Y_1^{\,1}|C_2^{\,1}|Y_3^{\,0}\rangle = -\frac{3}{5}\sqrt{\frac{1}{7}}$$

$$\langle Y_2^{\,1}|C_2^{\,-1}|Y_2^{\,2}\rangle = -\frac{\sqrt{6}}{7}$$

$$\langle Y_2^{\,1}|C_2^{\,1}|Y_4^{\,0}\rangle = -\frac{4}{7}\sqrt{\frac{1}{5}}$$

$$\langle Y_2^{\,2}|C_2^{\,1}|Y_4^{\,1}\rangle = -\frac{1}{7}$$

$$\langle Y_2^{\,-1}|C_2^{\,1}|Y_4^{\,-2}\rangle = -\frac{2\sqrt{2}}{7}$$

APPENDIX D

Rotational group elements for angles used in the calculations.

$\Theta = \frac{\pi}{2}$

$B_{100} = 0.0$	$B_{200} = -0.5$	$B_{300} = 0.0$	$B_{400} = 0.375$
$B_{101} = \frac{1}{\sqrt{2}}$	$B_{201} = 0.0$	$B_{301} = -0.433$	$B_{401} = 0.0$
	$B_{202} = 0.612$	$B_{302} = 0.0$	$B_{402} = -0.395$
		$B_{303} = -0.559$	$B_{403} = 0.0$
			$B_{404} = 0.523$

$\Theta = \sin^{-1} \sqrt{\frac{2}{3}}$

$B_{100} = 0.578$	$B_{200} = 0.0$	$B_{300} = -0.385$	$B_{400} = -0.389$
$B_{101} = -0.578$	$B_{201} = 0.577$	$B_{301} = 0.236$	$B_{401} = -0.176$
	$B_{202} = 0.408$	$B_{302} = 0.527$	$B_{402} = 0.351$
		$B_{303} = 0.304$	$B_{403} = 0.465$
			$B_{404} = 0.232$

The values for the other angles can be obtained by the following relation

$$B_{\ell 0 m}(\pi-\Theta) = (-1)^{\ell+m} B_{\ell 0 m}(\Theta)$$

APPENDIX E

The chemical shift tensor of the V^{51} resonance line in a polycrystalline sample of vanadium pentoxide has been reported[37]. These values did not agree with the present values either in sign or magnitude. In order to check these results, the data obtained from a single crystal sample can be used to obtain the line shape of the V^{51} resonance line in a polycrystalline sample.

Equation (2-26) can be written

$$\frac{\Delta H}{H_o} = -[\tfrac{1}{2}(\sigma_{xx} + \sigma_{yy}) + \tfrac{1}{2}(\sigma_{xx} - \sigma_{yy})(\cos^2\theta - \sin^2\theta)]$$

$$= [\tfrac{1}{2}\sigma_{xx}(1 + \cos^2\theta - \sin^2\theta) + \tfrac{1}{2}\sigma_{yy}(1 - \cos^2\theta + \sin^2\theta)]$$

$$\frac{\Delta H}{H_o} = -\sigma_{yy} - (\sigma_{xx} - \sigma_{yy})\cos^2\theta \qquad \text{(E-1)}$$

The term σ_{xy} is zero because the three eigenvalues of σ are used.

σ is considered as an axially symmetric tensor. Therefore σ_{xx} is being replaced by $\frac{1}{2}(\sigma_{xx} + \sigma_{zz})$

$$\frac{\Delta H}{H_o} = A + (B-A)\cos^2\theta \qquad \text{(E-2)}$$

where

$$A = -\sigma_{yy} \qquad B = -\tfrac{1}{2}(\sigma_{xx} + \sigma_{zz})$$

The total magnetic field at the nucleus is defined as

$$H = H_o + \Delta H$$

$$H = H_o[1 + A + (B-A)\cos^2\theta] \qquad \text{(E-3)}$$

Let $\frac{dN}{dH}$ be the number of nuclei in a polycrystalline sample that are subjected to a magnetic field between H and ΔH.

$$\frac{dN}{dH} = \frac{dN}{d(\cos\ )} \quad \frac{d(\cos\ )}{dH}$$

$$dN = \frac{N}{4\pi} \; 2\pi\sin\theta \; d\theta = -\frac{N}{2} d(\cos\theta)$$

$$\frac{dN}{d(\cos\theta)} = -\frac{N}{2} \quad . \qquad \text{(E-4)}$$

From equation (E-3)

$$\frac{1}{H_o} = 2(B-A)\cos\theta \frac{d(\cos\theta)}{dH}$$

$$\frac{d(\cos\theta)}{dH} = \frac{1}{2\ H_o(B-A)\cos\theta} \qquad \text{(E-5)}$$

$$1 + A \leqslant \frac{H}{H_o} \leqslant 1 + B$$

$$\frac{dN}{dH} = \frac{N}{4} \frac{1}{(B-A)^{\frac{1}{2}}} \quad \frac{1}{\sqrt{\frac{H}{H_o} - A - 1}} \qquad \text{(E-6)}$$

This will be the lineshape of a resonance in a polycrystalline sample if the single crystal resonance line is a δ-function. For a more realistic situation, the line-width of the single crystal resonance line must be taken

into account. In order to simplify the calculations, it is assumed that the single resonance line shape is gaussian

$$\frac{dN}{dH} = \frac{N}{4} \frac{1}{(B-A)^{\frac{1}{2}}} \int_{o}^{\infty} \frac{1}{\sqrt{\frac{H}{H_o} - A - 1}} e^{-\left(\frac{H-h}{\Gamma}\right)^2} dh$$

Γ is the linewidth of the single crystal resonance line.

A plot of $\frac{dN}{dH}$ vs H for a given H_o and Γ gives the resonance line shape in a polycrystalline sample.

REFERENCES

1. R. V. Pound, Phys. Rev. 73, 1247 (1948).
2. R. V. Pound, ibid. 79, 685 (1950).
3. H. G. Dehmlet and H. Krüger, Naturwissenschaften 37 111 (1950).
4. H. G. Dehmlet and K. Krüger, Z. Physik 129 , 401 (1950).
5. E. F. Carr and C. Kikuchi, Phys. Rev. 78, 1470 (1950).
6. G. M. Volkoff, H. E. Petch and D. W. L. Smellie, Can. J. Phys. 30, 270 (1952).
7. R. Bersohn, J. Chem. Phys. 20, 1505 (1952).
8. G. M. Volkoff, Can. J. Phys. 31, 820 (1953).
9. H. E. Petch, N. G. Cranna and G. M. Volkoff, ibid. 31, 837 (1953).
10. C. H. Townes and B. P. Dailey, J. Chem. Phys. 17, 782 (1949).
11. B. P. Dailey and C. H. Townes, ibid. 23, 118 (1955).
12. D. Nakamura, Y. Kurita, K. Ito and M. Kubo, J. Am. Chem. Soc. 82, 5783 (1960).
13. K. Ito, D. Nakamura, Y. Kurita, K. Ito and M. Kubo, ibid. 83, 4526 (1961).
14. D. Nakamura and M. Kubo, J. Phys. Chem. 68, 2986 (1964).
15. R. Ikeda, D. Nakamura and M. Kubo, ibid. 69, 2101 (1965).

16. R.Bersohn, J. Chem. Phys. 29, 326 (1958).

17. L. Pauling, The Nature of the Chemical Bond (Cornell University Press, N. Y. 1960) 3rd ed.

18. R. R. Sharma and T. P. Das, J. Chem. Phys. 41, 3581 (1964).

19. N. F. Ramsey, Phys. Rev. 77, 567 (1950).

20. N. F. Ramsey, ibid. 78, 699 (1950).

21. N. F. Ramsey, ibid. 83, 540 (1951).

22. N. F. Ramsey, ibid. . 86, 243 (1952).

23. A. Saika and P. C. Slichter, J. Chem. Phys. 22, 26 (1954).

24. M. Karplus and T. P. Das, ibid. 34, 1683 (1961).

25. R. Bramley, B. N. Figgis and R. S. Nyholm, J. Chem. Soc. (A), 861 (1967).

26. N. Bloembergen and T. J. Roland, Phys. Rev. 97, 1679 (1955).

27. E. R. Andrew and D. P. Tunstall, Proc. Phys. Soc. (London) 81, 986 (1963).

28. H. S. Gutowsky and D. E.Woessner, Phys. Rev. 104 , 843 (1956).

29. P. C. Lauterbur, Phys. Rev. Letters 1, 343 (1958).

30. J. S. Griffith and L. E. Orgel, Trans. Faraday Soc. 53, 601 (1957).

31. W. J. Child, Phys. Rev. 156, 71 (1967).

32. C. L. Christ, J. R. Clark and H. T. Evans, Jr., Acta Cryst. 7, 801 (1954).

33. V. Saraswati, J. Phys. Soc. Japan 23, 761 (1967).

34. H. T. Evans Jr., Z. Krist 114, 257 (1960).

35. H. G. Bachmann, F. R. Ahmed and W.H. Barnes, Z. Krist. 115, 110 (1961).

36. H. Nagasaw, S. K. Takeshita and Y. Tomono, J. Phys. Soc. Japan, 19, 764 (1964).

37. J. L. Ragle, J. Chem. Phys. 35, 753 (1961).

38. W. Klemm and E. Hoschek, Z. Anorg. Allegm. Chem. 226, 359 (1936).

39. K. Kosuge, T. Takada and S. Kachi, J. Phys. Soc. Japan 18, 318 (1963).

40. G. L. Clark and S. T. Gross, Z. Krist. 98, 107 (1937).

41. C. Calvo, Private communication.

42. C. D. Cox and T. Surek, J. Can. Ceramic Soc. 35 (1965).

43. C. Calvo, private communication.

44. S. B. Hendricks, M. E. Jefferson and V. M. Mosley, Z. Krist. 76, 352 (1931).

45. H. G. Bachmann, Acta Cryst. 6, 102 (1953).

46. D. K. L. Au and C. Calvo, Can. J. Chem. 45, 2297 (1967).

47. G. Peyronel, Gazz. Chim. Ital. 72, 83 (1942).

48. C. H. Townes, A. N. Holden and F. R. Merritt, Phys. Rev. 74, 1113 (1948).

49. W. Gordy, J. W. Simmons and A. G. Smith, ibid. 74, 243 (1948).

50. B. P. Dailey, K. Rusinow, R. Shulman and C. H. Townes, Phys. Rev. 74, 1245 (1948).

51. C. H. Townes, F. R. Merritt and B. D. Wright ibid. 73, 1338 (1948).

52. G. E. Patterson, P. M. Bridenbaugh and P. Green, J. Chem. Phys. 46, 4009 (1967).

53. T. P. Das and E. L. Hahn, Solid State Phys. 5, Supplement.

54. C. P. Slichter, "Principles of Magnetic Resonance" (Harper and Row 1963).

55. J. Kanamori, T. Moriya, K. Motizuki and T. Nagamiya, J. Phys. Soc. Japan 10, 93 (1955).

56. T. T. Taylor and T. P. Das, Phys. Rev. 133, A1327 (1964).

57. Per-Olov Löwdin, Advan. Phys. 5 (1956).

58. R. R. Sharma, T. P. Das and R. Orbach, Phys. Rev. 155, 338 (1967).

59. A. R. Edmonds, "Angular Momenta in Quantum Mechanic" (Princeton University Press, 1960).

60. B. R. Judd, "Operator Technique in Atomic Spectra" (McGraw-Hill, 1962).

61. G. Pilcher and H. A. Skinner, J. Inorg. Nucl. Chem. 7, 8 (1958).

62. M. H. Cohen and F. Reif, Solid State Phys. 5, 436 (1957).

63. R. M. Sternheimer, Phys. Rev. 80, 102 (1950).

64. R. M. Sternheimer, ibid. 84, 244 (1951).

65. R. M. Sternheimer and H. M. Foley, ibid. 92, 1460 (1953).

66. H. M. Foley, R. M. Sternheimer and D. Tycko, ibid. 93, 734 (1954).

67. R. M. Sternheimer and H. M. Foley, ibid. 102 , 731 (1956).

68. R. M. Sternheimer, ibid. 146, 140 (1966).

69. T. P. Das and R. Bersohn, ibid. 102, 733 (1956).

70. A. C. Makhanek, Opt. Spectry. 14, 241 (1963). [Opt. i. Spektroskopiya 14, 449 (1963)].

71. J. R. Tessman, A. H. Kahn and W. Shockley, Phys. Rev. 92, 890 (1953).

72. E. Clementi, IBM Journal of Research and Development 9, 2 (1965) (Supplement).

73. J. Boros, Z. Physik 126, 721 (1949).

74. G. E. Kimball, J. Chem. Phys. 8, 188 (1940).

75. C. J. Ballhausen and H. B. Gray, Inorg. Chem. 1, 111 (1962).